UNIVERSITÀ DEGLI STUDI DI PADOVA

UNIVERSITA' DEGLI STUDI DI PADOVA

DIPARTIMENTO DI TECNICA E GESTIONE DEI SISTEMI INDUSTRIALI

Corso di Laurea Magistrale in Ingegneria dell'Innovazione del Prodotto

Correlazione tra parametri di processo e proprietà meccaniche in una lega 42000 da fonderia pressocolata in semi-solido

Relatori: Ch. mo Prof. Franco Bonollo

Ch. mo Prof. Anders Wollmar Jarfors

Correlatore: Ing. Ziyu Li

Laureando: Magrin Vittorio

Matricola: 2017831

Anno Accademico 2021/2022

Ringraziamenti

Il più grande ringraziamento è dedicato ai miei genitori, Eleonora e Giuseppe. In questi anni mi hanno sempre sostenuto e guidato nelle scelte più importanti. Grazie a loro sono diventato la persona che sono oggi. Mi hanno insegnato ad essere una persona responsabile e a non arrendermi mai nei momenti più difficili. Da loro ho sempre cercato di ispirarmi, cogliendo gli insegnamenti di vita ed ereditandone le loro passioni e conoscenze.

Voglio menzionare anche i miei nonni Antonio e Caterina, che sono stati per me speciali e il loro volermi bene sarà per me indimenticabile.
Un sincero grazie anche a mia sorella Micol, che è stata per me quasi una seconda mamma nel periodo di infanzia. Ringrazio anche i miei fratelli Carlo ed Elisa per il bene che mi vogliono nonostante il tempo condiviso assieme non sia ancora tantissimo.

Un grande ringraziamento è dedicato al mio gruppo di amici, di cui fanno parte Francesco, Elisa, Giovanna, Patriche, Alberto, Gianpiero, Angelica, Elena, Luca, Federico. La nostra amicizia è nata fin dai primi anni delle scuole di infanzia, e da lì non ci siamo più persi di vista. Assieme abbiamo passato i nostri anni di adolescenza e di gioventù, in cui abbiamo vissuto momenti memorabili, e abbiamo condiviso i nostri problemi e dubbi di gioventù, dandoci sempre una mano reciproca per superarli nel migliore dei modi. Mi ritengo molto fortunato ad avere un gruppo di amici così unito e sincero, non sarebbe stato possibile raggiungere questo traguardo senza di loro.

Desidero ringraziare il professor Bonollo per la sua comprensività e disponibilità dimostratami in questi mesi, anche durante il periodo di scambio. I suoi consigli e indicazioni sono stati un'ispirazione per me e sono risultati fondamentali per raggiungere risultati rilevanti e di interesse rispetto alla letteratura già presente sugli argomenti trattati.

During my study program I was offered the opportunity to go abroad and live an Erasmus experience in Sweden. I was welcome in the Materials and Manufacturing research team, which gave me everything I need to do a great job and treated me like I was one of their students. I want to thank my thesis supervisor Anders, who guided me from the very first day and made possible this thesis work.

A special thank also for my co-supervisor and true friend Ziyu, an excellent PhD student and human being, which make me bond with the working environment and was a great example on demonstrating me that hard work and commitment is a guarantee of success and satisfactions.
I want to give credits to the company ComptechAB and all its members. Their experience on slurry making and hi-integrated die casting were key to the completion of this thesis work on the times established. It was a pleasure to work and discuss with them.

I also want to give a big thanks to the friends I had a pleasure to met and share good non-working times: Adyasha, Matteo, Ramon, Ricardo, Bilal, Daniele, Deepak, Maxime, Noelie, Roman, Davide, Bin, Gayathri, Dmitri, Arne and Kelvin. It was hard to imagine I could meet such good people in this experience.

"When I was sixteen, my father said, "You can do anything you want with your life, you just need the will to work hard and get it." - That's when I decided when I die, all of you remember me for the life I live(d), not the money I made."

Avicii

Riassunto

Analisi della letteratura

La pressocolata (anche detta colata ad alta pressione) è un processo utilizzato nella produzione delle leghe d'alluminio da fonderia.

Si compone di tre fasi principali: nella prima, il metallo liquido viene versato nella camera di iniezione, che viene poi riempita tramite un movimento a velocità costante dello stantuffo di iniezione. Nella seconda fase, lo stantuffo di iniezione viene accelerato fino ad una velocità di stampaggio (velocità di seconda fase) e la cavità dello stampo viene riempita in pochi centesimi di secondo (per evitare la pre-solidificazione del fuso con conseguente non riempimento di alcune porzioni dello stampo). Nella terza fase, lo stantuffo viene rallentato fino a fermarsi in una posizione finale e mantiene una pressione di intensificazione per alcuni secondi, in modo da compattare il più possibile il getto e avere meno porosità interne.

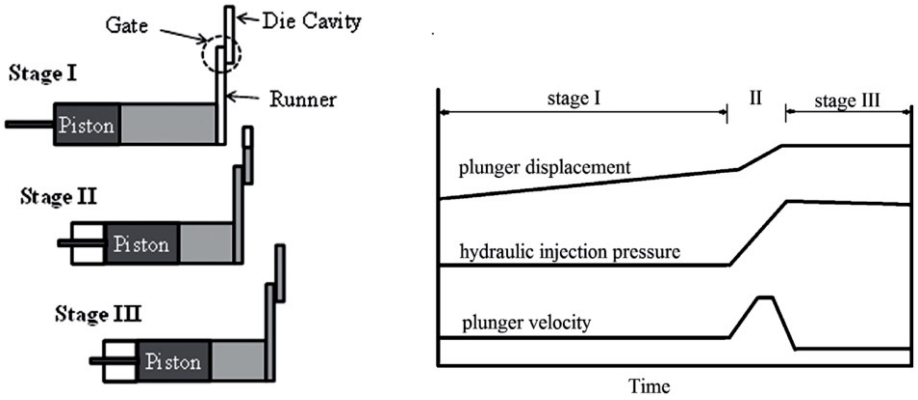

Figura 1: Le tre fasi principali della pressocolata

Tale processo ha una velocità di produzione di 150-250 cicli all'ora (il tempo ciclo totale si aggira generalmente attorno ai 40/50 secondi), è possibile formare prodotti con pesi compresi tra 0,1 e 30 Kg, con spessori di parete compresi tra 1 e 15 mm, mantenendo buone tolleranze geometriche e dimensionali. Prevede degli elevati costi di investimento iniziale, quindi diventa conveniente per quantità elevate di produzione, superiori a 5000/10000 getti all'anno. Queste caratteristiche lo rendono uno dei processi fondiari più popolari.

Nonostante le sue caratteristiche versatili, gli alti tassi di produzione e la alta diffusione di utilizzo, la pressocolata è un processo noto per generare difetti, che possono influire creando fino al 10% di percentuale di scarto rispetto alla produzione totale. Il processo è stato ritenuto "generatore di difetti" e allo stesso tempo contraddittorio, poiché l'industria richiede una qualità dei getti sempre più alta, ma questa viene influenzata negativamente dall'alta percentuale di pezzi scartati generata dal processo.

L'industria si pone due obiettivi: il primo è migliorare la qualità dei getti generando meno percentuali di scarto; e il secondo, conseguenza del primo, è valutare la qualità dei getti nel modo più rapido e più rappresentativo possibile.

Per migliorare la qualità di un processo di pressocolata standard, sono stati studiati molti processi innovativi. Uno di questi è la colata in semi-solido. Tale processo si basa su un'agitazione meccanica del bagno liquido di alluminio ad una temperatura di 1-2°C al di sopra della temperatura eutettica (quindi all'inizio della solidificazione). La microstruttura risultante differisce da una lega di alluminio standard, in quanto la struttura primaria di α-Al non è più dendritica, bensì assume una morfologia globulare.

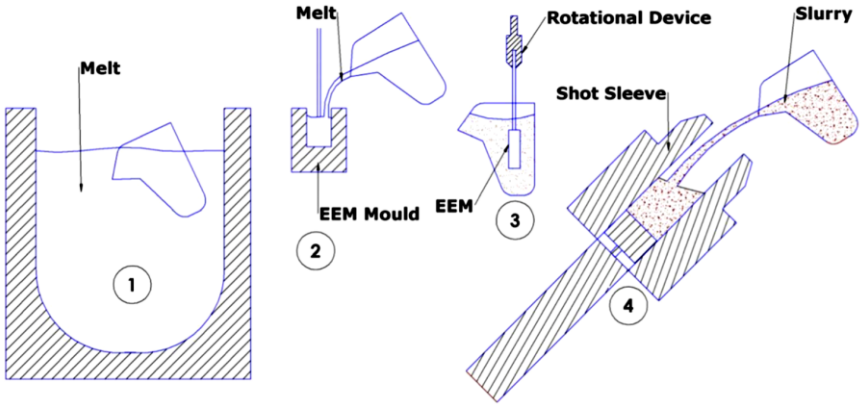

Figura 2: Processo Rheometal, esempio di possibile procedura di preparazione di una lega semi-solida

La massa fusa, dopo l'agitazione meccanica, ha una viscosità molto più elevata di un fuso d'alluminio standard, perché sarà composta da una frazione liquida (che solidificherà dentro lo stampo) e da una frazione solida della fase α -Al. Tale massa fusa (detta "slurry") può essere utilizzata in un macchinario da pressocolata e, vista la sua maggiore viscosità, riempirà lo stampo tramite un flusso laminare. La colata in semi-solido ha alcuni potenziali vantaggi: causa meno ritiri volumetrici e meno porosità da gas; permette di velocizzare i cicli produttivi e aumentare la vita dello stampo (avendo molto meno calore da asportare a fine stampaggio); è particolarmente apprezzato per ottimizzare la duttilità del materiale (per la microstruttura globulare).

Per sfruttare appieno i potenziali vantaggi, è necessaria un'accurata scelta e ottimizzazione dei parametri di processo. I principali parametri differiscono da un processo di pressocolata standard in quanto la viscosità del fuso è maggiore, per cui vengono richieste forze di iniezione maggiori. Le velocità di prima e seconda fase (v1, v2), la pressione di intensificazione, la velocità di agitazione e le temperature del processo devono essere scelti e controllati attentamente per raggiungere qualità dei getti e proprietà meccaniche elevate.

Il secondo obiettivo dell'industria riguarda il primo. La valutazione della qualità determina le proprietà meccaniche del getto e stabilisce se un pezzo (o un lotto di produzione) soddisfa gli standard richiesti. La valutazione della qualità deve essere rapida (per generare meno ritardi possibili nella produzione industriale) e attendibile.

È stato proposto un nuovo approccio nella valutazione della qualità, che si basa sul calcolo dell'accelerazione quadratica media del pistone durante la seconda fase di iniezione (detta root-mean-square acceleration). Questo parametro viene ottenuto a partire dall'integrale della funzione di accelerazione del pistone durante la seconda fase di iniezione (la più critica). Fisicamente rappresenta la forza media trasmessa al fuso durante la seconda fase della pressocolata. La letteratura suggerisce che per più elevate accelerazioni quadratiche medie si ottengono maggiori resistenze statiche nel materiale (maggiori tensioni di rottura e allungamento), e viceversa.

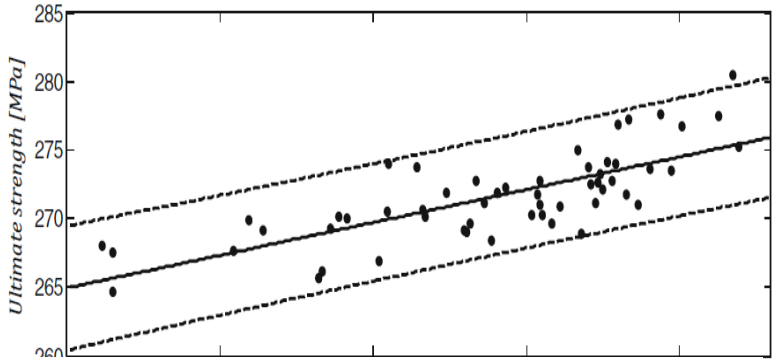

Figura 3: Grafico di correlazione tra tensione di rottura e acclerazione RMS del pistone.

Il principale vantaggio del calcolo dell'accelerazione RMS è che può essere calcolata tramite i parametri di processo della macchina di pressocolata, coinvolgendo le velocità di prima e seconda fase e la pressione di intensificazione. Per cui, diventa possibile correlare i parametri utilizzati durante la pressocolata con i valori di accelerazione ottenuti in ciascun getto.

Lo scopo di questo lavoro di tesi è di seguito riassunto. Il punto di partenza è il processo di pressocolata di una lega semi-solida di alluminio (in particolare la EN-AC 42000). Dai getti ottenuti si ricaveranno dei provini di trazione che serviranno a verificare le proprietà meccaniche in una serie di diverse impostazioni di processo, che varieranno nella pressione di intensificazione, nella seconda fase di iniezione, nella velocità di mescolamento della frazione solida e nel metodo di pulizia del bagno liquido a inizio processo. In ogni impostazione dei parametri verrà determinata l'accelerazione RMS, e questa verrà confrontata con le proprietà meccaniche ottenute dalle prove di trazione a temperatura ambiente.

Verrà quindi studiato il valore della correlazione tra le proprietà meccaniche e i parametri di processo, con l'obbiettivo di verificare se esiste una correlazione perfetta (1:1). Se questo si verifica, il potenziale vantaggio sarà la possibilità di prevedere le prestazioni meccaniche delle leghe da pressocolata senza la necessità di test fisici, migliorando quindi la velocità delle prove e la frequenza delle stesse, migliorando di conseguenza anche la qualità dei getti per il maggior numero di test effettuati.

Procedura sperimentale

La procedura sperimentale si è sviluppata a partire dalla scelta di un numero di impostazioni di processo. Si è deciso di valutare due diverse modalità di pulizia del fuso, la velocità di mescolamento della frazione solida (4 valori), la velocità di iniezione della seconda fase (3 valori) e la pressione di intensificazione (4 valori) da applicare a fine iniezione. Utilizzando un software di pianificazione degli esperimenti, sono state individuate 19 diverse impostazioni di processo da valutare, in cui in alcune si prevedono buone proprietà meccaniche (con elevati valori di accelerazione RMS, e in altre si prevedono scarse proprietà con basse accelerazioni RMS.

DESIGN OF EXPERIMENTS: Ogni impostazione composta da 4 variabili					
Metodo di pulizia	Holding			Transportation	
Velocità di mescolamento [rpm]	650	765	810	940	1100
Pressione di intensificazione [bar]	120	140	150	180	
Velocità di seconda fase [m/s]	1		2	2.5	

Figura 4: Scelta delle impostazioni di processo tramite software di programmazione degli esperimenti

Il processo è iniziato con la preparazione del fuso di alluminio, unendo il 70% di lingotti secondari (provenienti dal fornitore Stena Metall) e il 30% di pezzi di scarto. La lega da ottenere era la 42000, e la composizione chimica è stata verificata con uno spettrometro di massa prima di procedere con il processo di pressocolata.

La preparazione del fuso è stata eseguita con due differenti procedure di pulizia, che sono state studiate separatamente. Nella procedura "Holding" il fuso è stato prelevato dal forno di fusione, una siviera ha trasportato il fuso nel forno di attesa accanto alla macchina di pressocolata, dove qui è stato degassato e scorificato. La procedura "Transportation" differisce in quanto il fuso prelevato dalla forno di fusione viene degassato e scorificato direttamente nella siviera di trasporto, e successivamente viene versato nel forno di attesa.

La fase di degasaggio e scorificazione è la medesima nelle due procedure: il degasaggio si è effettuato mediante immissione di gas Argon per 20 minuti; ad esso è seguita la scorificazione del bagno tramite immissione di un composto di ARSAL 2125.

La preparazione del composto semi-solido è stata effettuata con il metodo "Rheometal", presso l'azienda Comptech AB (Skillingaryd, Svezia). Il metodo prevedeva di prelevare il fuso metallico dal forno di attesa, e destinare una parte del bagno per far solidificare un piccolo cilindro (denominato Entalpy Exchange Material- EEM). Dopo essere stato solidificato e raffreddato, l'EEM veniva ricongiunto e dissolto dalla parte di bagno precedentemente prelevata, tramite agitazione meccanica con la velocità di mescolamento prestabilita. In questa maniera si creava la frazione solida nel fuso semi-solido, che era pronto per il processo di pressocolata.

La pressocolata è stata svolta dapprima impostando la macchina con le impostazioni di processo prestabilite. Successivamente, per ogni impostazione di processo venivano creati 20 getti: i primi 10 venivano scartati per permettere l'equilibratura della temperatura e il controllo dei parametri di processo, mentre i successivi 10 sono stati utilizzati per gli esperimenti.

Il getto era composto da due piastre (una sinistra e una destra) su cui è stato possibile ricavare i provini di trazione.

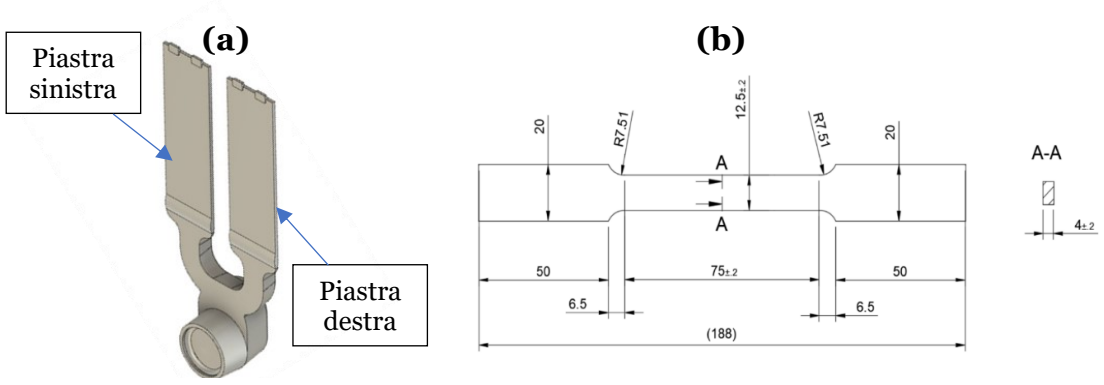

Figura 5: (a) esempio di getto ottenuto per le analisi sperimentali (b) provino utilizzato di dimensioni unificate

Dopo aver ricavato i provini, si è scelto di effettuare prove di trazione a temperatura ambiente, rispettando la normativa ISO 68-92/1. Le prove sono state condotte con una cella da 100 kN, misurando le deformazioni con un estensimetro a clip, con un precarico di 5 MPa, e una velocità di deformazione di 0,00025 s^{-1}.

Oltre alla correlazione meccanica, sono state condotte delle analisi microstrutturali per trovare una correlazione aggiuntiva tra proprietà meccaniche e microstruttura. Si sono svolte analisi a raggi x dei provini, un conteggio della frazione solida in varie impostazioni di processo, e un analisi delle superfici di frattura con l'intento di

individuare possibili difetti che possono aver influenzato negativamente le prestazioni meccaniche di alcuni campioni.

Analisi dei risultati

L'analisi dei risultati è stata sviluppata a partire dalla caratterizzazione meccanica delle impostazioni di processo utilizzate. Il modulo elastico e la resistenza allo snervamento sono rimasti pressoché costanti in tutte le condizioni. Le differenze tra le impostazioni di processo si sono riscontrate nei valori di tensione di rottura e allungamento a rottura, in cui le impostazioni a più elevate velocità di seconda fase di iniezione mostravano in generale proprietà migliori.

È stata notata una sostanziale differenza nei valori di tensione di rottura e allungamento a rottura tra i provini provenienti dalle piastre sinistra e destra. Si è notato che i provini destri hanno migliori proprietà meccaniche in quasi tutte le impostazioni di processo, con differenze più accentuate nelle impostazioni con le più alte velocità di seconda fase (2 e 2.5 m/s). I campioni sinistri e destri mantengono comunque tra loro costanti la tensione di snervamento e il modulo elastico. I risultati di correlazione con i parametri di processo sono stati quindi studiati separatamente tra provini destri e provini sinistri.

La prima indagine ha puntato a stabilire quale dei tre parametri di processo influenzasse maggiormente le proprietà meccaniche della lega. Dai grafici di dispersione tra allungamento a rottura e i parametri di processo, si è notato che la velocità di mescolamento non sembra avere una tendenza definita e ha coefficienti di correlazione molto bassi. Maggiori pressioni di intensificazione sembrano aumentare l'allungamento a rottura della lega, ma i coefficienti di correlazione restano di valori limitati. La velocità della seconda fase di iniezione sembra il parametro che più influenza le proprietà meccaniche della lega; per più alte velocità di iniezione, si è notato un aumento dell'allungamento a rottura e i coefficienti di correlazione sono i più elevati tra i parametri studiati in questa analisi.

La seconda indagine è valutare se ci fossero differenze tra i due metodi di pulizia utilizzati. È stato notato, in tre condizioni di processo equivalenti tra i due metodi di pulizia, che la differenza media nell'allungamento a rottura è di circa lo 0,5% a vantaggio del metodo "Holding". La differenza aspettata era limitata in quanto i tempi e i metodi di degasaggio e scorificazione rimangono gli stessi tra i due metodi.

La terza e più importante indagine è stata stabilire la correlazione tra l'accelerazione RMS e le proprietà meccaniche. Si sono costruiti grafici di dispersione tra l'accelerazione RMS e tre differenti proprietà meccaniche: l'allungamento a rottura, l'indice di hardening e l'energia a frattura. In ogni grafico i risultati sono stati differenziati tra provini destri e sinistri. Si è notata una differenza importante negli indici di correlazione tra provini destri e sinistri, che sono risultati maggiori nei provini destri e con valori massimi di 0.88 nel caso del metodo di pulizia "Holding".

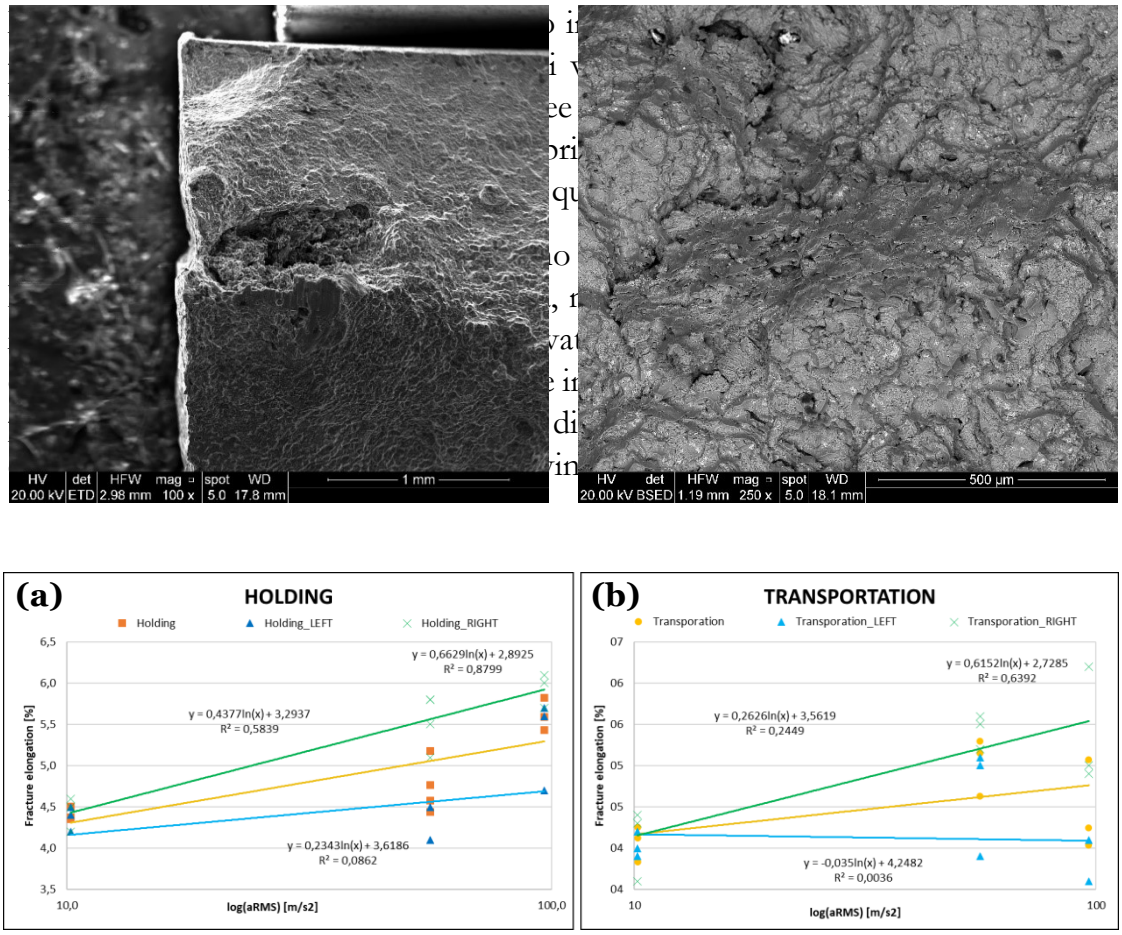

Figura 6: Grafici di correlazione tra accelerazione RMS e allungamento a rottura, nei due metodi di pulizia del bagno studiati (a) Holding (b) Transportation.

Le accelerazioni RMS sono state calcolate in due metodi distinti costruendo gli stessi grafici di correlazione con le proprietà meccaniche. I valori degli indici di correlazione sono risultati molto simili tra i due metodi di calcolo, nonostante i principi di base nel calcolo fossero diversi. Ciò ha dato un ulteriore conferma ai risultati ottenuti nella correlazione tra proprietà meccaniche e parametri di processo.

L'analisi microstrutturale è stata condotta per trovare correlazioni aggiuntive tra proprietà meccaniche e microstrutturali. Non sono state riscontrate evidenti differenze microstrutturali per differenti condizioni di processo: la frazione di solido ha poca variazione nelle condizioni di estremo della velocità di mescolamento. L'analisi delle superfici di frattura, condotta al microscopio elettronico a scansione, ha suggerito che parte delle differenze tra i campioni di placca sinistra e destra sono dovute a difetti all'interno dei getti: in quasi tutte le superfici di frattura dei campioni sinistri scelti per le analisi sono state trovate porosità, inclusioni e film di ossido. Questi difetti generano intensificazioni locali degli sforzi che portano a fratture anticipate, e quindi influenzano negativamente le proprietà meccaniche dei campioni provenienti dalle piastre sinistre.

(a) (b)

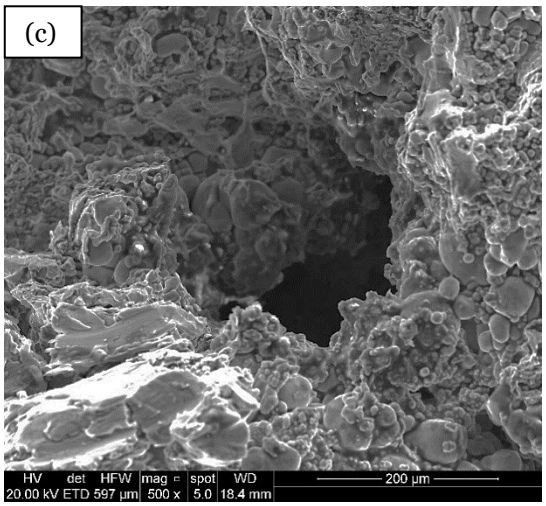

Figura 7: Esempi di difetti trovati nelle superfici di frattura (a) inclusione (b) pelle d'ossido (c) porosità.

Summary

This report describes the work conducted at the Department of Materials and Manufacturing of Jönköping University, as part of the Erasmus exchange programme attended from February 2022 to July 2022. This work was possible thanks to the collaboration between University of Padua and Jönköping University which provided the possibility of an exchange period during the Master program in Product Innovation Engineering; and thanks to the relationship with Comptech AB, which has made available its competences, experienced personnel, and facilities that made this thesis work possible.

The purpose of this research is investigating the correlation between static mechanical proprieties of a 42000 Semi-Solid aluminium alloy and the process parameters of High Pressure Die Casting. The importance of a 1:1 correlation stands on the possible way to predict the material performance and therefore the casting quality in a more fast and effective way compared to the conventional destructive tests which are usually done.

To achieve this purpose, the material preparation and the high pressure die casting process took place at Comptech AB. The castings were studied with two different procedures of cleaning the melt and with three variables changing in different parameter settings: the stirring speed used to prepare the semi-solid slurry, and the second phase speed and intensification pressure during the casting process. The number of different castings obtained was 19, each with different mechanical proprieties and different mix of parameter settings. From every parameter setting were casted 10 items, each containing 2 plates to use for investigations and to make the tensile test bars. After the tensile bar cutting and the tensile tests conducted at Jönköping University, the next step was correlating the mechanical proprieties with the mix of process parameter. The mix of parameters were synthesized in the root-mean-square acceleration of the motion of the injection plunger in the casting process. This is a novel parameter proposed in recent literature work, and it was computed with two proposed methods of calculation, to make a comparison between them.

The results suggested this trend: an increase in mechanical proprieties for higher values of RMS acceleration. The correlation got close to a 1:1 ratio, but not in all cases. From the tensile tests, it appears that the castings have two distinct qualities depending on the region where the tensile bars were taken. The samples were studied separately, and where the mechanical proprieties seem to be higher, the correlation with RMS acceleration seems stronger, and vice-versa. It also appeared that the correlation is influenced by the different cleaning method, which was noted higher in the "Holding" process route described in the experimental procedure section.

Keywords

Metallic materials; Aluminum Alloys; High Pressure Die Casting; Semi Solid Metal casting; Enthalpy exchange material; Second phase speed; Intensification pressure; Stirring speed; Root Mean Square acceleration; Fracture elongation; Hardening rate index; Fracture energy.

Contents

List of figures

List of tables

1 Introduction

1.1 Background

Aluminum is one of the few metals that can be shape cast by essentially all existing processes. It is one of the most versatile materials used to design, develop and product components, due to its high strength proprieties, its high availability, its low density (2,7 g/cm^3) and its low melting point which is 660°C (for pure aluminium) [1]. As the material is widely used, a lot of work has been conducted by the research community to keep improving the alloys and discovering new innovative applications for the material. The studies [2, 3] focused on the aluminium alloys aims to discover all the potential of the material but also to improve the production methods to achieve the best possible qualities in the products.

The aluminum alloys are divided in wrought alloys (typically dedicated for lamination and extrusion processes) and foundry alloys (for metal casting). Foundry processes for aluminum alloys can be divided into two main families: the first is mold-type filling, which include sand casting, core package casting, and lost foam casting; the second is usually referenced as molding technologies (or permanent die casting), and include gravity die casting, low pressure die casting and high pressure die casting [4].

Figure 1.1 show the production rate for several casting technologies. One of the most important processes is High Pressure Die Casting: it is suited for hi range of productions (between 10^3 and 10^6 casting/year) and for a big range of casting weight, between 0.1 and 100 kilograms [5].

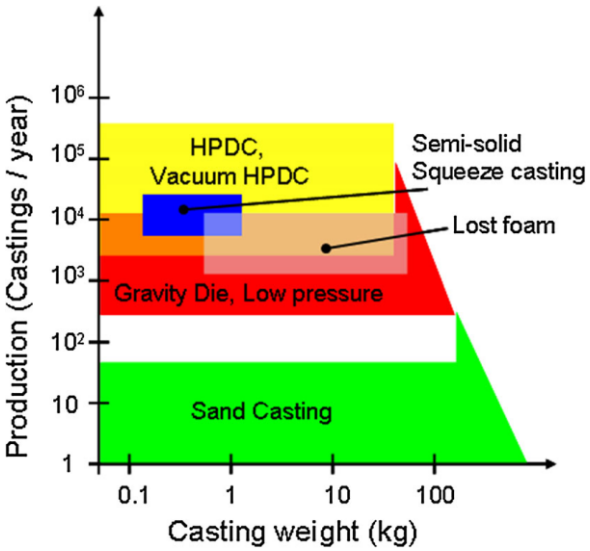

Figure 1.1: Production rate for the most common casting processes [5].

The HPDC process is a continuous production process based on consecutive manufacturing cycles. It has a strategic importance for casting high production rates, and it is applied in several industrial fields. Approximately, half of the world production of light metal castings is obtained by this technology [6]. However, this process generates defects by its nature, such as gas porosity, shrinkage porosity, cold shuts, and hot tearing, leading to high amounts of scraps, higher costs, higher lead times to customers [7].

To overcome this problem, three innovative processes have been developed: Semi-Solid Metal casting, (splitted into two variants, Rheocasting and Thixocasting), Vacuum casting and Squeeze casting, which are putted in the same area of the conventional HPDC process in the "production-casting weight" chart shown in Figure 1.1 [5].

The Semi-solid casting is considered a very interesting solution, because the main objective of the industry is to improve the quality of its products [8]. Semi-solid casting still has the advantage of high rate-productions like a standard HPDC process, and almost the same configuration of the injection system. However, semi-solid casting has the purpose to dramatically reduce (or in some case delete) defects in the casted parts and reduce the amount of scrap created [6, 9].

The semi-solid metal casting process begins with preparation of a semi-solid metal slurry, which has the chemical composition of a normal HPDC alloy, but it's created mixing a part of material that is already solid with molten metal of the same composition. To create a "stable" fluid, two stirrings can be done, so that the slurry formed has the proprieties of a fluid and it can still be casted, while at the same time contains a certain solid fraction, and the microstructure of the initial alloy is changed in morphology, from a dendritic to a globular and well distributed α-Al primary phase [3, 9] (Figure 1.2).

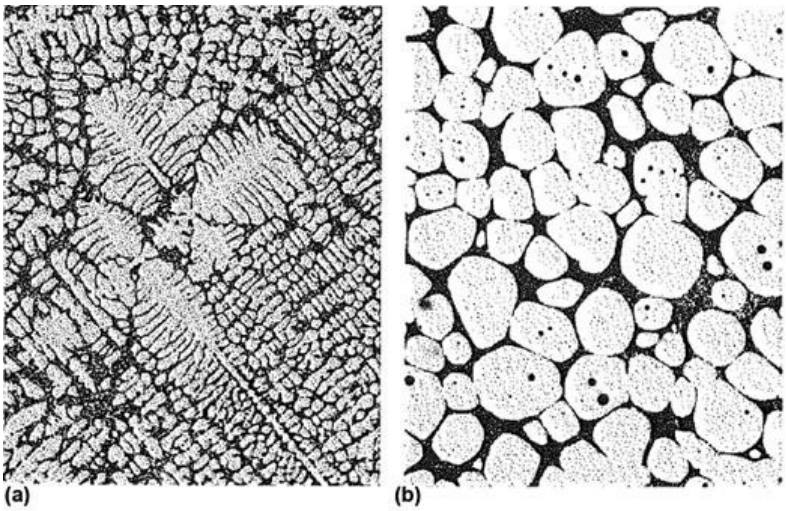

Figure 1.2: (a) Dendritic structure of a standard Al-Si system
(b) Globlular Al-Si after Semi-solid metal casting [3].

After the preparation, the semi-solid metal slurry is poured into the shot sleeve of the high-pressure machine and the process of casting take place in the same way a conventional HPDC process would do [9].

Several studies [10, 11, 12] suggested that an accurate process parameter choice and control is essential to take full advantage of the semi-solid metal slurries and therefore to maximise the alloy mechanical proprieties. This work investigates if exists a 1:1 correlation between the mechanical proprieties and the process parameters.

The effect of the parameter settings will be studied with a single analytic finding, the Root Mean Square acceleration of the plunger, which incorporates the characteristic speeds, times, and pressures of the High Pressure Die Casting process.

1.2 Purpose and research questions

The purpose to find correlations between mechanical proprieties and process parameter has the intent to discover new ways to evaluate the proprieties of aluminium alloys. Conventionally, the mechanical characterization of the material is conducted with physical tests, such as Tensile tests, Charpy tests, Hardness test, which are time consuming and involves great investments and costs [13, 14]. In recent years, there has been a tendency to move from physical testing to virtual simulations and analytic predictions, which are less expensive and faster, enabling to do a greater amount of test on the material, and ultimately affecting positively the quality of castings (more tests mean more reliable materials) [14].

The experimental work will be based on castings of semi solid aluminium plates. The casting process was done in collaboration with Comptech AB, which gave availability their facilities and their experience on slurry casting to make possible this thesis work. The type of casting process will be Rheocasting, developed from the collaboration between Comptech and academia.

The casting process will study several settings parameters which differs with the alloy cleaning process, the secondary stirring speed of the Semi-Solid metal slurry, the second phase speed of injection and the intensification pressure. For each setting, 10 dummies and 10 casted parts to examine will be created. Every casted part contains two plates, and each can be used to cut up to two tensile test bars that will serve to do tensile tests that gives the mechanical characterization of the alloy.

The mechanical characterization of the alloy will determine: the Young modulus, the Yield strength, the Tensile strength, and the Fracture elongation of the alloy in each cast setting. Moreover, two other parameters will be determined from the mechanical proprieties: the Hardening rate index and the Fracture energy (toughness) of the material.

The process parameter characterization will be studied in the intent of finding if there is one dominant parameter influencing the mechanical proprieties. There will be a comparison between the fracture elongation of each setting with the secondary stirring speed, the second phase injection speed, and the intensification pressure. Every comparison will be done considering different two cleaning method of the alloy to establish the effect of the cleaning method to the mechanical proprieties.

The Root Mean Square acceleration measures the force transmitted to the melt during the injection process, and therefore will be the parameter used to investigate the existence of correlations with the mechanical proprieties. The literature works [15, 16] suggested that better mechanical proprieties should be achieved for bigger values of RMS acceleration.

The parameter can be determined in several ways [15, 17], which involves the speeds and the times of the high pressure die casting process and the intensification pressure kept on the melt in the last phase of injection. In this study, two different methods of calculations found in literature [15,17] will be used, to find which is the one to be used in future works.

The RMS acceleration will be compared with the static mechanical proprieties extrapolated from the tensile tests, to verify the amount of correlation indexes.

1.3 Delimitations

Several process parameters will be studied: second stirring speed, intensification pressure and second phase speed of injection and two different cleaning method during the casting process. However, the temperatures in the process will not be studied as a changing parameter. Other two important parameter that could be evaluate are the first phase speed and the position of the switching point in the machine, however, in this work was considered more interesting to evaluate the second phase speed and the intensification pressure.

The type of alloy composition will not change, the EN AC-42000 will be considered. This means that chemical characterization is not necessary in this work. A mass-spectrometer will be used just to control if the chemical elements in the alloy respect the typical values of a foundry 42000 alloy.

The mechanical proprieties of the alloy will not be compared with another alloy or with threshold values.

1.4 Outline

The report is organized into eight chapters. The first chapter is the introduction to the work, highlighting the background and the purpose of the research. The second chapter describes all the theoretical concepts that have been necessary to organize what experiments were needed for the purpose. All the techniques, methods and implementation of the experimental work are described in the third chapter. The fourth chapter reports and discusses all the results of the measurements. Chapter five provides the conclusions, the observations, and the next directions to investigate in the future works. Chapters six, seven and eight are respectively: References, Search terms and Appendices.

2 Theoretical background

2.1 High Pressure Die Casting

High Pressure Die Casting is a manufacturing process that uses a permanent mold design, widely used for casting metal alloys. The popularity of the process stands on its short cycle time, which allows to product large quantities in high dimensional accuracy [3].

The process is realized by pouring molten metal in an enclosed shot sleeve, in which a plunger (moved by a piston connected to a hydraulic system) initially pressurizes the metal with a constant velocity movement, and then forces the molten metal into a mold with high pressure and velocity [4].

The High Pressure Die Casting process is commonly divided into two variants:

1) The hot chamber process in which the molten metal and the hydraulic actuator are in intimate contact. This configuration is common for lower-melting metals, such as zinc, tin, lead, and magnesium alloys [3]. This configuration can minimise exposure of the molten metal to turbulence, oxidising air, and heat loss during the transfer of hydraulic energy. However, the prolongated contact between molten metal and system components can lead to severe material problems in the production process and is not recommended for Aluminium Alloys [4].

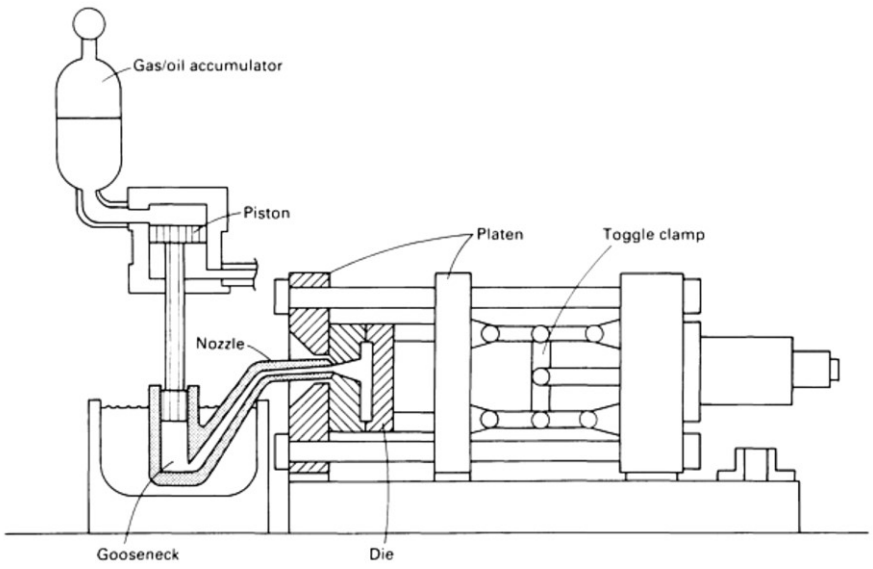

Figure 2.1: Hot Chamber Process configuration [2].

2) The cold chamber process in which the molten metal is poured in the shot sleeve by a transporting ladle. This system ensures that the molten metal and the hydraulic system are in contact for a few seconds only. This minimal exposure allows to cast higher temperatures alloys, such as aluminum and even some ferrous alloys and guarantees less thermal stress on the system components [4].

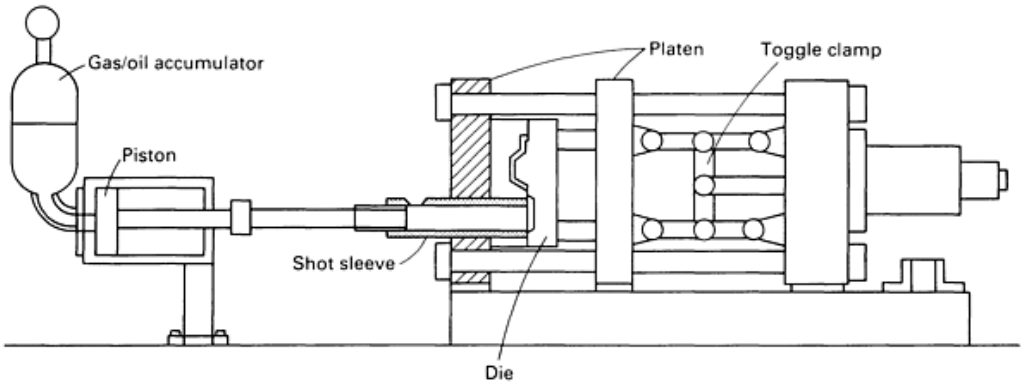

Figure 2.2: Cold Chamber Process configuration [2].

The cold chamber HPDC process is the most common configuration to work with aluminum alloys [4]. The process begins with metal ladling: the molten metal coming from a ladle is picked up and poured in the shot sleeve. After that, the injection of the metal into the mold cavity takes place and it's controlled by the movement of the plunger [11]. The filling, which is the topic part of the process, is summarized in three fundamental stages, which are slow shot stage, fast shot stage and upset pressure stage (also referred as intensification stage):

1) Slow shot stage: the hydraulic system moves a piston, which is connected to a plunger in contact with the molten metal and moves the metal into the die. The plunger moves with a precise and constant speed, and the molten metal is pushed until the shot sleeve cavity is filled [11]: the main things to avoid in this phase are air entrapments and turbulence of the molten metal [18].
2) Fast shot stage: the plunger is accelerated from the speed of the slow shot stage to a much higher speed in an interval of just few milliseconds. The cavity of the die is quickly filled and the pressure inside the die has raised from the first phase [11], to avoid premature solidification at the gate and incomplete casting caused by cold shuts [18]. The transition between the first and second phase is termed as the switching point [11].
3) Intensification stage: in this phase the plunger is still, but it's keeping force into the die, causing a big increase in pressure and the material reaches the intensification pressure Ip [11]. This stage is necessary to limit the formation of porosity due to solidification shrinkage porosity, gas evolution and the expansion of entrapped air [18].

When the intensification pressure is released, the casted part will solidify, then the mold will be opened, and the part will be ejected from it. The mold must cool down from the heat transferred by the molten metal in the process. When the mold reaches the correct working temperature, it is closed and the whole process can restart cyclically [11]. A typical cycle time for cold chamber HPDC process takes between 30 seconds and one minute and 30 seconds [19].

The three main phases of the process cycle are illustrated in Figure 2.3 in terms of process applied pressure and plunger travel. The most visible step in pressure takes place in the intensification phase, where a big increase in pressure is necessary to have a correct mold solidification and avoid shrinkage porosity defects [11].

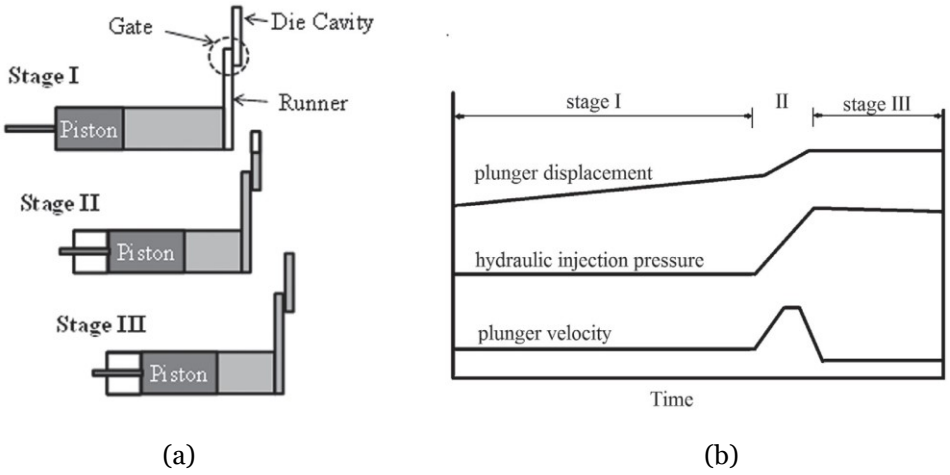

(a) (b)

Figure 2.3: (a) Illustration of the three stages of injection. (b) Diagram of displacement, velocity, pressure of the plunger in the three stages of injection [11].

There are several advantages offered by High Pressure Die Casting, which makes it one of the most common processes in the foundry industry. First, it is a fast process: the common production rate is 150 to 250 cycles per hour [19]. The process suits both product complexity and variety: high pressure die castings have a hi range of weights (between a few grams up to 30 kilograms) and a hi range of wall thickness (from 1 millimeter up to 15 millimeters), with a minimum hole size (obtained with inserts) of 3 millimeters [20]. The dimension accuracy obtained is higher than other processes, such as gravity casting, low pressure die casting and sand casting: this permits little or no machining after the casting process [19, 20].

Thanks to the developing technology, in recent years the HPDC process has been improved, generally reducing the cycle times, improving the quality of the castings, expanding the dimensions and the variety of products suited for the process. Despite the advantages and its importance in the industry, it has been considered a "defect generating process", since an average of 5–10 % scrap is typically manufactured [7].

Having a process that generates big amounts of components with defects, and, in worst case, big amounts of scrap is indeed against the primary goal of the companies: their request is higher quality of products to satisfy highly demanding customers and to challenge a very competitive market [21].

More scrap means wasted money, less productivity and bigger lead times from the product development to the consumer. The HPDC process is widely used for high-demand components, so the amount of scrap generated increases wasted costs much more than those generated by a less used process [7].

A research study conducted by Bonollo et al. [5] summarized all the typical problems related to a HPDC process, highlighting the frequency of occurrence, if the problem is predictable by simulation, and the monitoring parameter. The results are presented in Table 2.1.

Defect subclass	**Frequency of occurrence (%)**	**Predictable by simulation?**	**Monitoring parameter**
Shrinkage defects	20	Partially	Temperature, pressure
Gas related defects	15	No	Air pressure, humidity
Filling related defects	35	Yes	Air pressure, temperature
Undesired phases	5	No	Shot chambering sensors
Metal-die interaction defects	5	Partially	Temperature, ejection force
Out of tolerance	5	Advanced simulation	Geometry measures
Lack of material	5	Yes	Geometry measures
Excess of material	5	Advanced simulation	Geometry measures
Thermal contraction defects	5	Yes	Temperature

Table 2.1: Typical defects associate with a HPDC process [5].

2.2 Process parameters influence on casting quality

The HPDC process is controlled and defined by several process parameters, related to temperature, velocity, pressure, and time in certain conditions. An accurate control of this parameters is required to achieve an efficient production, and these values changes depending on the part to cast, and the type of alloy used [22].

The main process parameters to take in consideration in HPDC process are [16]:

1) The velocity of the plunger in slow shot stage, referred as v_{PI}.
2) The velocity of the plunger in fast shot stage, known as v_{PII}. The corresponding velocity of the melt at the gate is called gate velocity v_g. The gate velocity is influenced by the velocity of the plunger and by the geometry and size of the gate.
3) The intensification pressure Ip applied once the die cavity is full.
4) The temperature of the mold when the melt is pushed into the die cavity.

The main goal of the industry is to improve the quality of the high pressure die castings [5]. The research community [10,11,12,22,24] has conducted several works investigating the correlation between process parameters and the quality of the casting, which are now summarized in their main points.

The velocity in the slow shot phase v_{PI} plays a very important role in the injection process: the melt is put in the shot chamber by a ladle, and the plunger moves with a constant velocity to fill the chamber cavity. It is important that the cavity is filled with a smooth melt wave, not presenting any turbulence and not entraps any air, otherwise these problems cannot be recovered in the next phases, and they will badly affect the quality of the castings [22].

When the melt is poured into the shot chamber two problems can occur: air entrapments and premature solidification. If the velocity is too low, both problems can occur: the melt will not reach the shot sleeve ceiling and, as a result, some air will remain between the top of the wave and the ceiling. Also, premature solidification of the melt can happen, causing incomplete fillings or internal defects [23]. Too high velocity is equally negative for the casting quality: if the shot chamber is filled too quickly, the melt will roll over in a turbulent motion and this will cause air entrapments and bad quality casting [12].

The principal two parameters in a HPDC process [11,12] are the plunger speed in the fast shot phase and the intensification pressure I_p. The velocity v_{PII} and the design of the gate have a direct influence on the gate velocity of the melt v_g, and this has a big influence on the melt flow into the die and, consequently, with the quality of the cast. The intensification pressure is a fundamental parameter to avoid porosity and shrinkage defects. It is agreed that higher intensification pressure helps to avoid porosity content in the casting, and a value around 61 MPa significantly increase the casting quality and the tensile proprieties [11].

The experimental works done by the research community [12] are mostly pointing out that an increase in the injection speed during the fast shot phase helps to reduce the defects of porosity and premature solidifications. However, some works [24, 12] exhibit conclusions in contrast with each other.

Jian and Wu [24] investigated the effect of different values of gate velocity on the filling time of the cavity. They observed that an increase in gate velocity reduces filling time and consequently the porosity, but after a certain value they observed that the surface finish gets worse, and gas entrapments increases.

Karban [12] suggested that an optical range of velocity between 1.7 and 3.4 m/s can produce casting with less porosity and better mechanical proprieties, however he pointed that an optical velocity needs to be searched for every specific application inside this interval.

In contrast of the work of Karban, an experimental analysis conducted by Choi et al. [10] observed that velocities inferior to 3.5 m/s are not able to fill the entire cavity when the casting has thin wall design. They proposed that velocities higher than 3,5 m/s are required to achieve higher mechanical proprieties and quality in thin-walled castings.

A possible conclusion in the debate about velocity and intensification pressure values is given by Arnberg et al. [11]: higher gate velocity and intensification pressure are good to improve the tensile proprieties, but there are limitations imposed by the machine and the gate design must be taken in consideration. It's been also proposed that the plunger velocity in stage II needs to be 10 times bigger than the plunger velocity in stage I, to avoid turbulence in the first phase of the process.

As regards the mold temperature, there is an optimal value for every application, that permits to have good quality on the casting while at the same time having a good productivity [16].

If the die temperature is too high, the viscosity of the solid stale metal slurry is decreased, so this would permit better castability and less danger of cold shuts. But there are drawbacks: having a higher temperature means longer solidification times and longer cycle times, so less productivity. More heat to the die means more energy must be spent to heat up, and, critically, the mould is subject to higher thermal stress. So, these facts clearly lead to an increase of production costs [25].

A low temperature is equally inconvenient: defects related to cold shuts and pre-solidification are more likely to happen [25]. The melt will be more viscous at the time of injection, and higher forces will be required by the hydraulic system [16].

The final quality is controlled by many parameters in the process. Controlling only one of them is not sufficient to obtain a high-quality casting process: high quality and repeatability is instead achieved by controls over all the parameters of the process, but this is not always possible and may require high-experienced personal, time and high costs.

2.3 The Semi-Solid metal casting

The Semi-solid metal casting is an innovative process for casting metal components. The original leading experiment was performed by Spencer in the 1970s [26]: in studying the viscosity of a partially solidified Sn-15Pb alloy, he noticed that when a dendritic micro-structure is broken up, the partially solidified alloy has the fluidity of an oil and exhibit a particular behavior, later called thixotropic. In the semi-solid aluminum casting, the primary α-Al dendritic micro-structure, after an agitation process during the transition between liquid and solid, changes in morphology, becoming a globular micro-structure [27, 28].

A SSM process forms semisolid slurries, obtained by mixing non-dendritic solid particles in a liquid matrix [27]. Semi-solid metal slurries describe distinctive rheological proprieties: the steady state behavior is pseudoplastic (the steady state viscosity depends on the applied shear rate), while the transient state behavior is thixotropic (the time dependence of transient state viscosity at a given shear rate) [29].

There are three major semi-solid processing common to the industry: thixocasting, rheocasting and thixomolding [1]. A schematic representation is given in Figure 2.5.

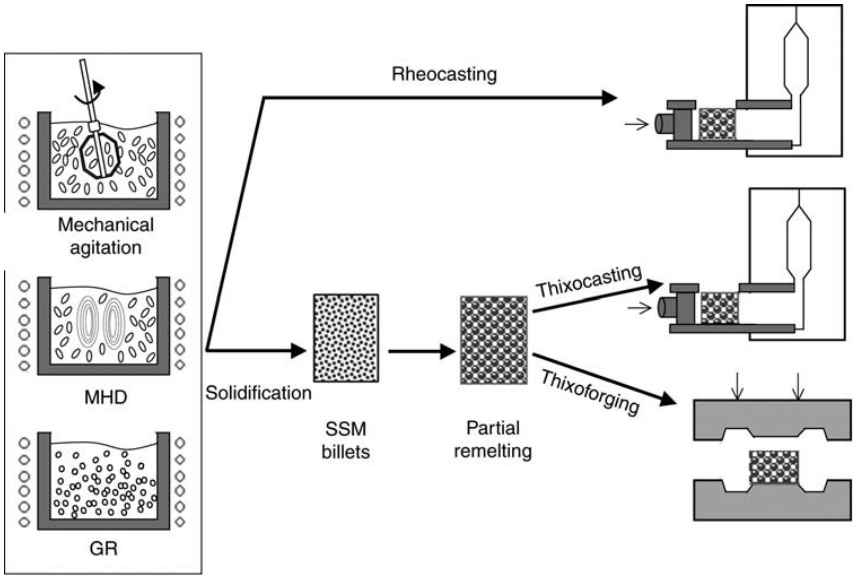

Figure 2.4: Summary of the semi-solid processes common in the industry [1].

Thixocasting was one of the first commercialized SSM process. It consists of two separate stages: first, the production of billet feedstock with a primary α-Al globular structure, obtained by applying shear force into a solidifying melt; second, reheating the solidified billets to the semisolid temperature range to form the slurry, followed by the die casting operation. Also, from the globular α-Al billet, it is possible to do a forging process after re-heating: the so-called process is Thixoforging [30].

Rheocasting processes forms a slurry starting from molten-state metal. The melt is subject to thermal treatment and management at the solidification stage, and these processes don't make a billet of material: the slurry is injected into the die cavity just after the formation of the material with thixotropic behavior [31].

Thixomolding methods (called also thixoforming) have similarities with the injection molding of polymers: solid chips or pellets (of conventionally solidified alloys) are fed into a heated injection system containing a reciprocating screw. The action of the screw and the heating generates a shear action and converts the metal pellet into a thixotropic slurry, with solid fractions less than 0.3 [1]. The slurry is fed into the shot accumulator by the rotation of the screw, and when the accumulation chamber is filled, the slurry is injected in the mold by a forward movement imposed by the screw [30].

The use of SSM based processes can be strategic to limit or even delete the defects in the High Pressure Die Casting, to get performance improvements on aluminum alloys [31]. The several benefits a SSM process can bring are now explained.

- Semi-solid formed components can be nearly free from shrinkage porosity. Because 50% of the material is already solid when pressing inside the die cavity, much less solidification shrinkage needs to be compensated for during further solidification of the casting [31]. Furthermore, a high intensification pressure is applied to the mold cavity after injection [12]. This further compensates solidification shrinkage. This leads to more complex components with large thickness variation in different [6].
- Semi-solid formed components can be nearly free from gas porosity. Having 50% of solid when pressing inside the die cavity means that the material has much more steady state viscosity. This leads to a laminar flux of material even at higher speeds and less air entrapments [31].
- Less macrosegregation and hot-tearing tendency. Higher viscosity of the material and an even distribution of solid particles inside the casting will dramatically decrease the intensity of natural convection inside the casting, thereby eliminating problems with macro segregation [31]. Also, in some studies is mentioned how there are less hot tearing problems [6, 30, 31].
- Good heat treatability: due to the low content of gas porosity a semi-solid formed component has less problems of blisters in the casting surface during heat treatments [31].
- Higher productivity and increased mold life. 50% of solid fraction formed before the slurry enters the die cavity means that only 50% of latent heat will be released during solidification. This will shorten cycle times improving productivity, decreasing thermal stress on the die while improving its lifetime, and ultimately resulting in cost saving [31].
- Less shrinkage and gas porosity and better heat treatments improves the strength and ductility in a material, while the casting proprieties are maintained [6].

Most of the alloys been used in the die-casting industry are secondary, coming from recycling processes or waste from other casting processes. The secondary alloys have usually lower performance than primary ones due to the presence of impurities, but they are a lot cheaper, and their production limits the CO_2 waste generation (to produce 1 kilogram of primary alloy, a corresponding amount of 4 kilogram of CO_2 is produced) [2].

The Al-Si-Cu-Mg alloys are one of the most common in high-pressure die casting applications: 352, 362, 364, 365, 367, and 368 are the most used alloy in the HPDC process [4], and their use has been proved suitable to solid-state metal casting.

On this type of alloys iron is usually added, a percentage of 0.6% may facilitate ejection from the die [4], however the iron content in most application is usually less than 0.4%, because higher concentrations reduce ductility [27]. Another important element typical in these alloys is magnesium. Its presence can minimize the problems related to oxidation [4]. Copper is also a fundamental element: its presence enhances the mechanical proprieties of the alloy, improving tensile strength and yield strength. The copper addition will result in a decrease in ductility and an increase in costs (copper is an expensive and rare element), so its percentage in weight is highly controlled [4].

EN-AC 42000 is one of the most popular aluminium foundry alloys [2,4,10]. The popularity of this alloy is due to its good mechanical proprieties, its good anti-corrosion proprieties (sea water and weather conditions). This alloy has a good castability and a low solidification shrinkage, which makes it suitable for a high pressure die casting process. The typical use of this alloy is medium-duty aircraft castings, engine components, and parts used in shipbuilding industry [10].

The typical chemical composition of EN AC-42100 is reported in Table 2.2.

Chemical element	**Wt. %**
Aluminum (Al)	balance
Silicon (Si)	6.5 ÷ 7.5
Magnesium (Mg)	0.25 ÷ 0.65
Copper (Cu)	0.15 max
Manganese (Mn)	0.35 max
Iron (Fe)	0.45 max
Titanium (Ti)	0.05 ÷ 0.20
Zinc (Zn)	0.15 max

Table 2.2: Nominal chemical composition of EN-42000 alloy [2]

2.4 Rheometal™ process

There are several technologies for dealing with solid-state metal processing. Specifically, for Rheocasting methods, there are three common technologies:

1) GISS (Gas Induced Superheated Slurry): the slurry is prepared into a ladle, where a graphite rod is inserted and blows nitrogen gas into the melt. This causes a local supercooling around the rod and the solid particles are created. As the liquid phase is still warmer than the induced cooling, the slurry is considered superheated, as the name suggested [32].
2) Rheometal™: formerly known as RSF (Rapid Slurry Forming). A solid element, called Enthalpy Exchange Material (EEM) is created, and cooled typically by forced convection. The EEM is joined with the liquid via mechanical stirring, and the shear action won't melt the solid entirely, instead a characteristic solid fraction will be created [31,33].
3) SEED (Swirling Enthalpy Equilibration Device): the shear action for making the slurry is created by an oscillating table that induce a swirl motion to the melt. The so created slurry is then put into the shot sleeve [11, 30].

The fundamental difference between the three methods is the solid fraction. The GISS method creates a slurry with 5% of solid fraction, which is then pushed up to 25-30% when injected into the mold. The Rheometal™ creates slurry with 30-45 % solid fraction. The SEED creates the biggest percentage of solid fraction: up to 50% [11].

The Rheometal™ process is an innovative method to prepare semi-solid slurries, which uses a consumable solid stirring device made from the same alloy of the casting, referred as Enthaply Exchange Material (EEM). The EEM is used for two purposes: contribute to the solid fraction of the slurry while at the same time act as a stirring device [31].

The process steps of the Rheometal process are described as follows and shown in Figure 2.6.

1) The alloy is prepared into a furnace. It is subject to a de-gassing process (usually done by nitrogen N_2) to reduce the oxides inside the microstructure. Also, one or more waste cleaning is done. After the preparation work, the casting process can begin: a pre-heated ladle picks an amount of alloy which needs to be processed to became slurry.
2) The ladle pours a quantity into a cylindrical mold to cast the EEM. At the same time, a steel rod is inserted into the solidifying EEM, making possible to use it as a stirring device for the rest of the alloy still into the ladle. The amount of alloy required to cast the EEM is 5-8 % of the total content of the ladle [30]. Next, the EEM is cooled via water spraying or air blowing.

3) The EEM is immerse into the melt and the motor (connected to the rod) induce a rotation motion to do a mechanical stirring. As a result, the EEM will mostly melt, giving contribution to the solid fraction of the slurry. The melt temperature is just above the liquidus temperature, and the shear stress created by the stirring breaks the dendritic α-Al into a globular microstructure. With a separate blade stirrer, a second stirring can be done to make a better and more refined primary phase distribution [33].
4) The now formed slurry is put into the shot chamber of the HPDC machine, and the injection process starts.

The ladle is then cleaned and re-heated to start a new cycle of slurry formation. Also, the steel rod is cleaned and re-used [30].

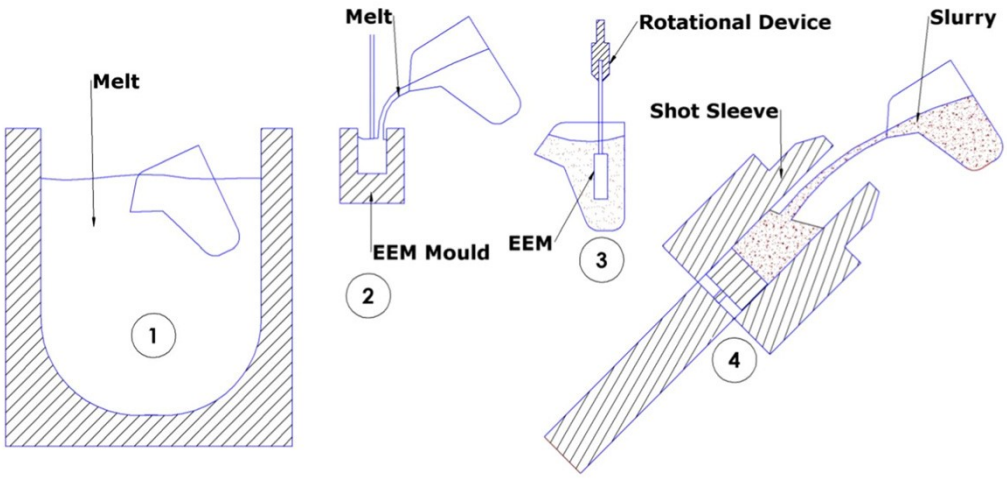

Figure 2.5: Steps for slurry preparation. (1) ladle picking; (2) EEM casting; (3) stirring; (4) shot chamber loading [30].

The Rheometal™ process have two main advantages: first, it is considered a fast slurry-making process for the level of solid fraction that is possible to obtain. The process takes between 5 to 40 seconds [30], with an average time often less than 30 seconds [6]. The second main advantage is that the process is highly flexible, it has shown that the process is able to produce components with wall thickness up to 40 mm high walls, and down to 0.35 mm [30], extending the limits of the standard HPDC process.

Similarly, to a standard HPDC process, there are many process parameters that must be controlled, such as the stirring speed and time of the EEM stirring.

Studies have been conducted [28,34,35] to search an optimal value for the stirring speed. An increase in stirring speed will certainly result in a higher shear rate on the slurry [30]. What is been investigated more deeply, is the effects in the casting quality: some studies [28] reported that shear rate influences the microstructure: increasing stirring speed makes rounder α-Al primary phases and can reduce flow

resistance and hence viscosity as an effect. This effect would produce a smooth molten metal wave when the plunger fills the shot sleeve cavity, in the first stage of HPDC.

Another research work [34] experienced that stirring velocity and time of stirring are connected: higher rotation speed leads to shorter slurry formation time, but they also pointed out that higher stirring speed promote a grain refinement effect. A rotation speed to average grain size chart from the work is reported in Figure 2.7.

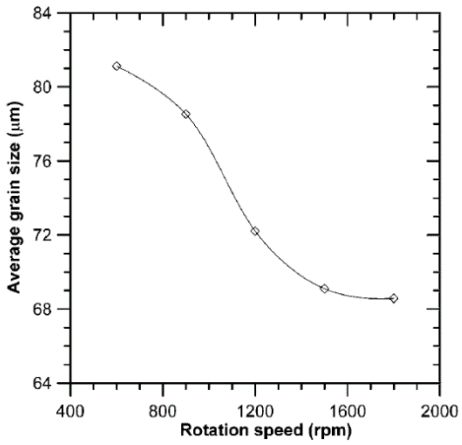

Figure 2.6: For higher rotation speed, the average grain size drops [23].

A work by Gupta et al. [35] agreed on the fact that higher stirring speed reduce average grain refinement, and explained that as the shear force increases, the particles will adopt a spherical morphology.

2.5 The root-mean-square acceleration

Finding a correlation between process parameters and the mechanical proprieties can reduce the complexity of parameter optimization.

A solution to this has been proposed in a work by Fiorese, Bonollo and Richiedei [15, 16]. They propose a new approach: combine several process parameters into a one parameter related to the plunger motion during the phase between the switching point and the beginning of the intensification pressure stage. The parameter is called root-mean-square acceleration (aRMS) of the plunger during the "fast shot phase" of the HPDC process. This parameter gives an indication of the casting condition: the higher the RMS acceleration is, the higher speeds were used during the injection process [16].

The RMS acceleration was presented [15, 16] as follows:

(2.1)

$$a_{RMS} = \sqrt{\frac{\int_{t_{SW}}^{T} \ddot{x}(t)^2 dt}{T_2}}$$

Where:

- x(t) denotes the plunger displacement, hence $\ddot{x}(t)$ its acceleration.
- T_2 is the duration of the second stage between the switching point (t_{SW}) and the complete filling of the die cavity (T).

Mathematically, the RMS acceleration is the integral of the acceleration function of the plunger in the second phase of injection. Phisically, it's considered a measure of the average force transmitted to the melt from the motion of the injection plunger during the second phase of injection [15]

For higher RMS acceleration, the alloy should have better mechanical proprieties because there should be less porosities and better soundness of the castings [16]. The effect of higher proprieties achieved with higher RMS should, however, be considered within an upper limit of second phase speed: after a certain value the melt becomes too turbulent, and air could be entrapped during filling, causing porosities inside the cast [36].

The work conducted by Fiorese [15] compared the yield strength and the tensile strength with RMS acceleration. The analysis has been conducted with different values of first and second phase speeds, and different positions of switching point, while keeping a constant value of intensification pressure. The result is shown in the correlation chart in Figure 2.7, where the RMS acceleration is represented in a logarithmic scale. The fitting lines in the dispersion charts correlated aRMS with yield strength and ultimate strength, the R-square values (correlation indexes) obtained were of 0.65 and 0.58 respectively.

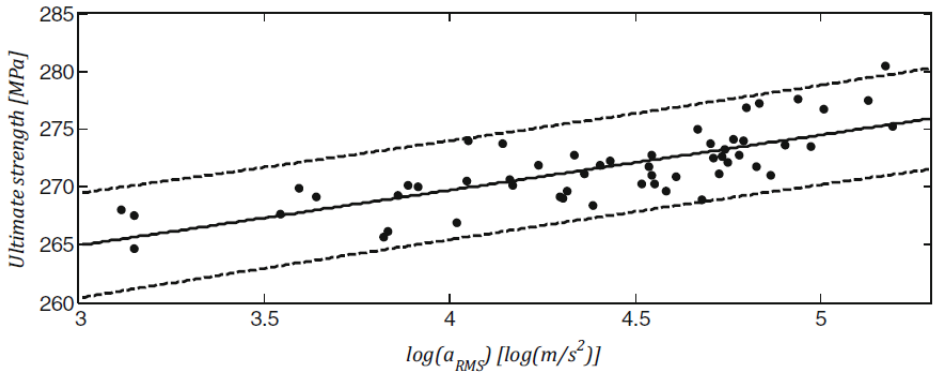

Figure 2.7: Correlation between aRMS acceleration and ultimate strength found by the research of Fiorese et al [15].

Fiorese, Bonollo and Richiedei proposed a mathematical formulation to determine aRMS [16]. They started from the definition presented by the Equation 2.1 and they solved the integral to obtain the solution presented in Equation 2.3.

It is necessary to have the duration of the second phase of injection: it is determined by Equation 2.2 from the first phase speed v1, the second phase speed v2, the duration T of the second phase of injection, the plunger travel h, and the position of the switching point x_{sw}. The entire duration of the injection T is determined by summing the duration of the first phase speed T1 (which can be calculated from the speed v1 and the position of the switching point) with the duration T2. The RMS acceleration is then calculated with Equation 2.3, which includes the durations and the speeds involved in the first two phases of the injection process and some constants, obtained to solve the initial integral in Equation 2.1 [16].

(2.2)

$$v_2 \cong \frac{3750 * (h - x_{sw})}{2000 * (\lambda_2 T)} - \frac{875 * v_1}{2000} \quad => \quad T_2 = 1{,}875 * \frac{(h - x_{sw})}{[v_2 + 0{,}4375 * v_1]}$$

(2.3)

$$a_{RMS} \cong \sqrt{\frac{512 * {v_2}^2}{105 * (\lambda_2 T)^2} - \frac{120 * v_1 * (h - x_{sw})}{7 * (\lambda_2 T)^3} + \left(\frac{14}{15} + \frac{192}{35}\right) * \frac{{v_1}^2}{(\lambda_2 T)^2}}$$

In literature another method to determine RMS acceleration has been developed: the research work conducted by Jarfors et al [17] started from the definition of RMS acceleration proposed by Fiorese [15] and solved the integral in a different way. The method assumes a balance between a driving pressure (P4) and a counter acting pressure (P5). The resulting force transmitted to the melt (F) depends on the mass "m" which is the sum of the plunger mass and the melt mass. The balance in pressures is showed by Equation 2.4 and graphically in Figure 2.8. The acceleration which can be obtained from the balance in pressures is inserted into the expression proposed by Fiorese (Equation 2.5).

(2.4)

$$F = P_3 A_3 - P_4 A_4 = m * \left(\frac{dv}{dt}\right)$$

(2.5)

$$a_{RMS} = \frac{1}{T} * \int_0^T \sqrt{\left(\frac{dv}{dt}\right)^2}\, dt = \frac{1}{T} * \int_0^T \sqrt{\left(\frac{P_3 A_3 - P_4 A_4}{m}\right)^2}\, dt$$

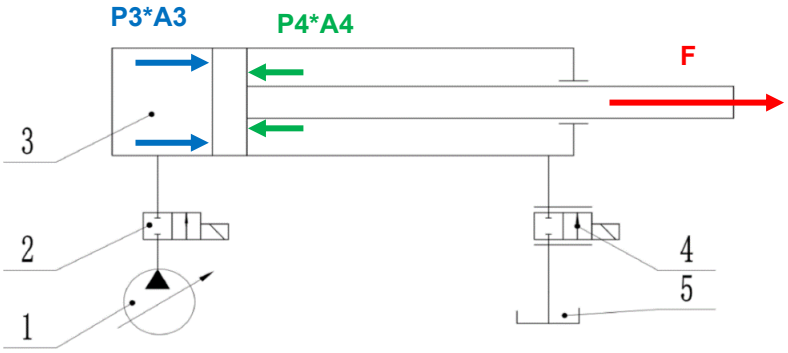

Figure 2.8: Schematic image of the plunger motion system, showing the pressures involved during motion [17]. Represented in the image are: 1-pump, 2-conical on-off valve, 3-hydraulic cylinder, 4-conical proportional/servo valve and 5-oil tank

The solution of the integral gives the formulation show in Equation 2.6 [17]. The mathematical expression contains the first and second phase speeds, the intensification pressure applied in the third phase of injection, the sum of the mass of the plunger and the mass of the melt (m) and two constants K1 and K2 which depends on the machine used in the casting process.

(2.6)

$$a_{RMS,J} = -2(v1 - v2) * K1 * \frac{P^{\frac{3}{2}}}{m} * esp\left(-2 * K1 * \frac{P^{\frac{3}{2}}}{m} * t\right) + \frac{K2}{2 * K1 * P^{\frac{1}{2}}}$$

3 Method and implementation

3.1 Design of Experiment (DOE)

Design-Expert™ software was used for determining the set of parameters to use for every cast. The number of variables used for testing was four: the secondary stirring speed, the second phase pressure (intensification pressure), the second phase speed (plunger velocity in fast shot stage), and the type of cleaning method.

For the secondary stirring values between 650 and 1100 rpm were chosen, considering the possible speeds that an electric motor (which stirs the rod connected to the EEM) can cope. For the velocity of the plunger in the fast shot stage, a range between 1 and 2.5 m/s was used, considering the capability of the HPDC machine. As regards the intensification pressure, the chosen range of values was between 120 and 180 bar. The cleaning process was the last variable, and it was differentiated between cleaning in the holding furnace and cleaning in the transportation ladle.

The software made a mix of conditions and gave in output 19 different parameter settings.

3.2 Material preparation before casting

3.2.1 Alloy preparation

The alloy was prepared with 70% of secondary ingots of AlSi7Mg (EN AC 42000) provided by Stena Metall Group and of 30 % reused scrap material.

3.2.2 Chemical composition of the alloy

The chemical composition was determined with the following procedure. From the shaft furnace where the melt was prepared, one cylinder of alloy was casted, using a round steel mould. After the sample solidified, 5 millimeter was cutted away from the upper surface of the sample, to evaluate the result in a more representative position and to have a flat surface to examine.

To evaluate the chemical composition a mass spectrometer was used. Three measurements were made, and the final value was calculated as the arithmetic average between the three. The Table 3.1 show the composition obtained, which respects the nominal composition of the 42000 alloy for the research purpose.

Alloy composition obtained: AlSi7Mg (EN AC 42000) [wt. %]											
Al	**Si**	**Fe**	**Cu**	**Mn**	**Mg**	**Zn**	**Ni**	**Cr**	**Pb**	**Sn**	**Ti**
bal.	6.85	0.42	0.05	0.23	0.22	0.05	≈ 0	0.02	≈ 0	≈ 0	0.09

Table 3.1: Alloy composition determined with a mass spectrometer.

3.3 Casting process

The casting procedure was divided into three steps: melt preparation (I), slurry making process (II), and casting process (III). The entire procedure is represented in Figure 3.1.

Figure 3.1: Process flow chart.

3.3.1 Melt preparation

The melt preparation was done with a pre-heated shaft furnace, which had a capacity of 2 tons of material. The furnace was set at a temperature of 900 °C, so the complete melting of the alloy was reached after 4 hours. The bath temperature was constantly controlled, kept stable in a range between 750 and 760 °C.

After alloy preparation, the next step was cleaning the alloy melt. There were two different routes for the cleaning method, used for alloy characterization:

1) Cleaning process into the holding furnace. The material from the shaft furnace was putted into a transportation ladle which transferred the material into the holding furnace. In here, the de-gassing and cleaning process was done.
2) Cleaning process into the transportation furnace. The material from the shaft furnace was putted into a transportation ladle and here the de-gassing and cleaning step took place. After cleaning, the melt was inserted into the holding furnace, ready to start the slurry making process.

The cleaning procedure was the same between the two methods. It included a de-gassing process and a waste removal step. The cleaning is essential to get rid of oxides and to limit the presence of impurities into the cast that may influence the mechanical proprieties. For the de-gassing step, Argon gas was injected into the melt for 20 minutes: the oxygen into the melt is attracted by Argon and forms a chemical compound that floats above the melt surface. After the argon-pouring stage, to drag away efficiently the oxides deposited above the surface, particles of ARSAL 2125 salt were sprinkled above the melt. The salt attaches to the oxides, and after approximately one minute a steel tool was used to do a manual stirring of the melt. The waste composed by all the oxides was consequently dragged away, to finish the cleaning process of the melt. The alloy melt was now ready for the next step of the casting process.

3.3.2 Slurry making process

The preparation of the slurry was next, the used method was the Rheometal™ process. The machine was disposed with this equipment:

- The holding furnace with the melt alloy.
- An articulating arm grabbing a transportation ladle. Into the ladle, the preparation of the slurry was made.
- A die to cast the EEM material.
- A rotating device with six steel rods, one rod served one EEM at a time.
- An articulating arm connected to an electric motor, with two functions: grabbing the steel rod and doing the mechanical stirring for the EEM.
- Two blades to clean the steel rods from the excess EEM.

The slurry making started with a ladle that grabbed an amount of alloy. To grab the melt, the ladle was inserted into the liquid with a certain angle, to prevent the collection of air into the melt. The ladle stayed into the melt for 5-10 seconds for temperature equilibration.

The ladle poured a certain quantity into a mold, to gravity-cast the EEM together with one steel rod. The solidification of the EEM took around 30 seconds, after that the mold opened and the EEM was spray-cooled, effectively doing a quenching. Cooling took a time between 15 and 30 seconds. After cooling, the sprue and gating system of the casted EEM were trimmed off. Both these parts will be reused as scrap metal.

At this point, the cooled EEM re-joined the melt into the transporting ladle. The rod inserted into the melt was putted into a rotating motion by the motor. During the spinning, the transportation ladle was moving sideways to make a more even stirring process. After around 10 to 15 seconds, the EEM was dissolved by the melt, the steel rod was extracted and cleaned by trimming from the residues of EEM still attached. At this point, the slurry was formed and was ready to be die-casted.

3.3.3 Casting process

The final step was high pressure die casting: the transportation ladle poured the slurry into the shot chamber, and the injection machine was casting the component with the accorded parameter setting. For every parameter setting the changed variables were the stirring speed of the EEM, the second phase velocity of the HPDC process, the intensification pressure, and the type of cleaning method.

The parameter settings used in casting process are described in Table 3.2 (holding) and Table 3.3 (transportation).

Cast codification	**Plunger travel [mm]**	**Stirring speed [rpm]**	**Second phase speed [m/s]**	**Intensification pressure [bar]**
HAX	430	765	2.5	160
HAY	435	765	2	120
HAZ	445	765	1	150
HAU	435	765	2	130
HBX	430	650	2.5	145
HBY	445	650	1	120
HBZ	435	650	2	184
HCX	445	1100	1	150
HCY	435	1100	2	120
HCZ	430	1100	2.5	180

Table 3.2: Parameter settings used for castings, holding cleaning method.

Cast codification	Plunger travel [mm]	Stirring speed [rpm]	Second phase speed [m/s]	Intensification pressure [bar]
TAX	435	810	2	180
TAY	445	810	1	180
TBX	430	940	2.5	150
TCX	445	1100	1	120
TCY	435	1100	2	180
TDX	435	650	2	150
TDY	430	650	2.5	180
TDZ	430	650	2.5	120
TDU	445	650	1	150

Table 3.3: Parameter settings used for castings, transportation cleaning method.

The parameter setting was inserted into the HPDC machine computer, and then the casting could start. The first 10 shots produced were considered as dummies, because the mold needed temperature equilibration and the parameters of the machine needed adjustments, to respect the velocity and the pressure imposed.

After the first 10 shots not being considered, the next 10 shots were kept. Every cast contained two plates, which were the parts used in the experimental analysis. The two plates were distinguished between left and right plates: the left plate was near the pouring ladle of the high pressure die cast machine, while the right plate was the one near the articulating arm which was extracting the cast from the machine. The casted part and his 2D drawing are shown in Figure 3.2.

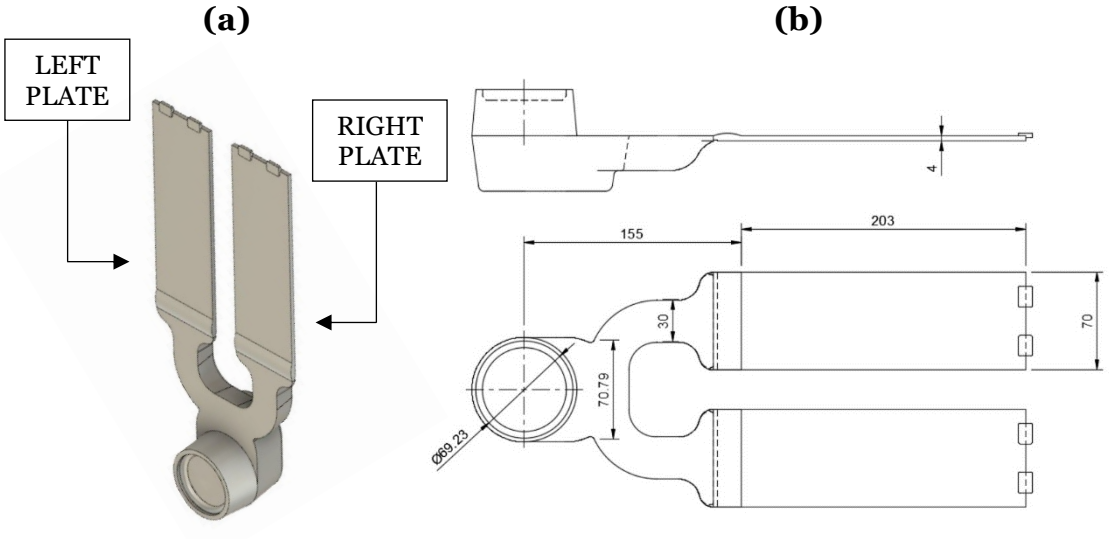

Figure 3.2: (a) CAD model of the casted part, the left and right plates has been distinguished; (b) 2D drawing of the part with measurements.

3.4 Tensile bar making

The tensile bar making was the first step after the casting process.

The casted parts, described in the previous paragraph, were composed by the two plates to analyze and by all the feeding system, with the sprue, the runner, the gate, and the feedstock.

A blade saw was used to cut away all the excess parts from the plate.

To make the tensile test bars from the plates, a milling CNC machine was used, shown in Figure 3.3. With the help on an operator, the machine was programmed with a part program able to cut four tensile bars from two plates at the same time.

The operator inserted two plates into the machine and clamped them on the base. Then, the milling process was started, while a water jet was sprayed on the plates for cooling.

Figure 3.3: Milling machine used to make tensile bars from the plates

After the cutting, the tensile bars were extracted. Any eventual residues of excess material were trimmed away with a steel file, and the tensile bars were labeled with the same code of their plate. To make the tensile bars, five of the ten casting shots were used from each parameter setting: a total of 20 bars for each setting was obtained.

The dimensions of the tensile test specimen were following the SS-EN ISO 6892-1 normative. A 2D drawing of the tensile bar is displayed in Figure 3.4.

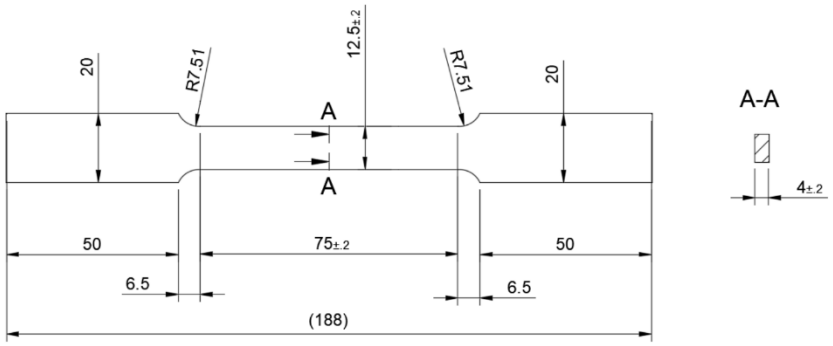

Figure 3.4: 2D drawing of the specimen used for the tensile tests.

3.5 Tensile tests

Tensile tests are used to get the static characterization of materials. It is a destructive-type mechanical test, which involves the application of a tensile load to specimens that comes from the material to be studied. The procedures to use to conduct the tests and the dimensions of the specimens are defined according to specific regulations, in this case ASTM-E8 (SS-EN ISO 6892-1) standard has been used, regarding tension testing of metallic materials.

The tensile tests were carried out with the ZwickRoell™ z100 machine, capable of applying up to 100 kN of force. Figure 3.5 shows the machine used for the tests.

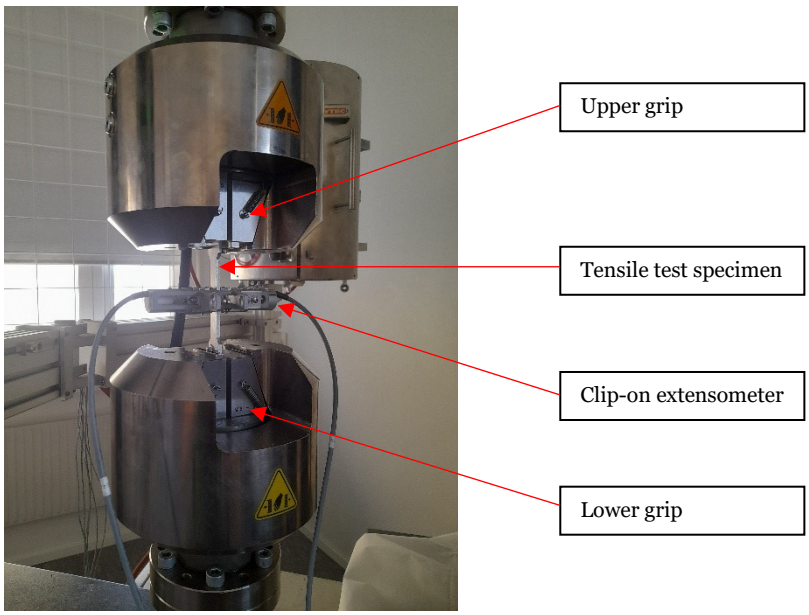

Figure 3.5: ZwickRoell™ machine used for the tensile tests.

For the tests, the following equipment were used:

- One clip-on extensometer for real-time measurement of specimen deformation. The extensometer had a stroke of 20 mm.
- A computer to start and stop the test and acquire the data of the stress-strain graph to detect the mechanical proprieties.
- One vernier scale to verify the dimensions of the specimens before every test.

The tests were conducted at room temperature, with a strain rate of 0.00025 s^{-1}. From every tensile bar was measured the specimen width and the specimen thickness, with the vernier scale. The two measures were inserted into the software of the tensile test machine, to correctly determine the output proprieties.

The procedure of the test is described as follows.

The tensile bar was inserted into the first grip of the machine. Before closing the upper grip, it was given the machine the command to apply no force during the closing. After the upper grip was closed, the test started. A 5 MPa pre-load was applied, and the clip-on extensometer was inserted. The test load was started to be applied, and the extensometer was kept on the specimen for the entire elastic deformation. When the yield strength of the specimen was reached, the extensometer was removed to avoid the risk of damaging due to the fracture of the specimen. The removal of the extensometer from the specimen caused a brief variation in the strain, which can be seen from one of the standard force - strain chart in Figure 3.6. However, this variation had no effect on the tensile proprieties of the bar, so the tests were considered representative. When the specimen was broken, the tests stopped, and the two halves of the specimen were removed from the grips. The tensile test software automatically calculated the mechanical proprieties of each tensile bar.

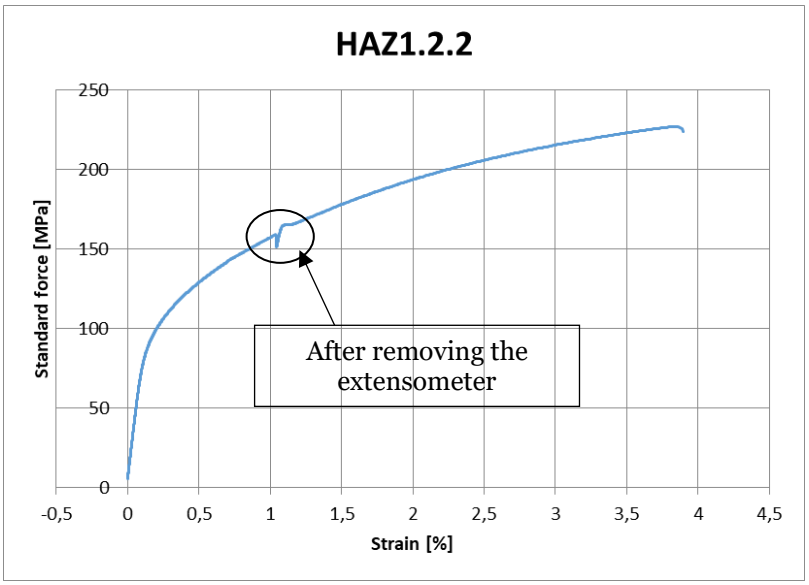

Figure 3.6: Standard force – strain chart calculated from the tensile tests.

3.6 Metallographic analysis

A metallographic analysis was carried out to observe the microstructure of the alloy in different process conditions and verify the presence of defects.

3.6.1 Sample preparations

The samples to analyze were chosen in the settings in which there were great differences in the tensile proprieties and picking up two conditions for each cleaning method, (one with highest and one with lowest stirring speed values. For each sample, one tensile bar for left and one for the right plate were studied.

Specifically, the chosen samples were:

a) For holding cleaning method:
   - HCZ, casts number 1,2,3 (1100 rpm; 180 bar; 2.5 m/s)
   - HBZ, cast number 2,3,4 (650 rpm; 184 bar; 2 m/s)

b) For transportation cleaning method:
   - TDY, cast number 1,2,3 (650 rpm; 180 bar; 2.5 m/s)
   - TBX, cast number 1,2,3 (940 rpm; 150 bar; 2.5 m/s)

The preparation procedure for the analysis is now explained, in reference to the illustration in Figure 3.7. Using a miter saw, a cross section of the sample was obtained, picked up below 10 mm the yielding area of the specimen.

With a hot-englobing machine, two cross section to analyze were incubated in a round sample made of phenolic resin. The machine englobes the samples at 185°C with a pressure of 210 bar for 6 minutes, and 5 minutes of cooling.

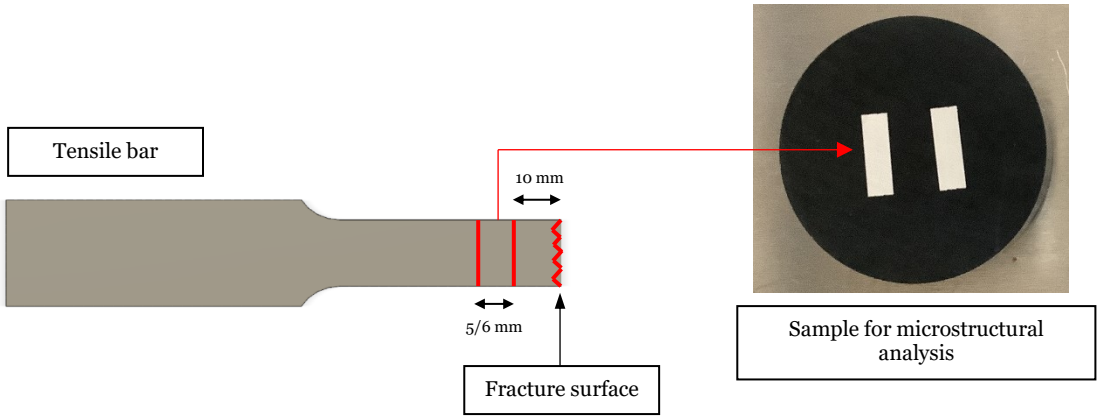

Figure 3.7: Tensile bar sample with indications where the metallographic analysis were conducted.

The next step was roughing and polishing the samples, with the aim of obtain a mirror finished surface to inspect.

For the roughing, Silicon Carbide abrasive pads were used with finer and finer grain size: P180, P600, P1200 and P2400. The polishing was done in two stages, first with a 6 μm diamond paste and then with a buffing wheel soaked in colloidal silicon.

Using an optical microscope, images of the microstructure were taken, in Figure 3.8 is presented an example of the alloy microstructure. The images were taken after polishing the specimen to a mirror finish, at a magnification of 100x, 250x, 500x. The images were taken in the center of the samples, near the surface and in the mid zone between the center and the surface of the samples.

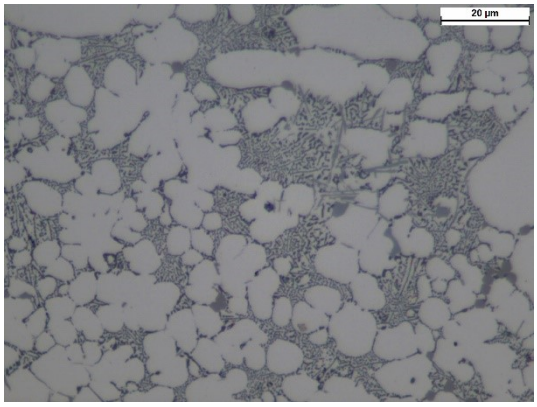

Figure 3.8: Example of microstructure of the alloy taken in the centre of the tensile test specimen.

3.6.2 Solid fraction counting

To enhance the contrast between the α-Al matrix and the eutectic phase, the samples were chemical etched with a Keller solution, prepared with 95 ml of distilled water, 2.5 ml of Nitric acid, 1.5 ml of Hydrochloric acid, 1 ml of Hydrofluoric acid.

Each sample was immersed into the solution for 35 seconds, and then rinsed in running water to remove the excess solution. Figure 3.9 shows one example of a sample after the etching.

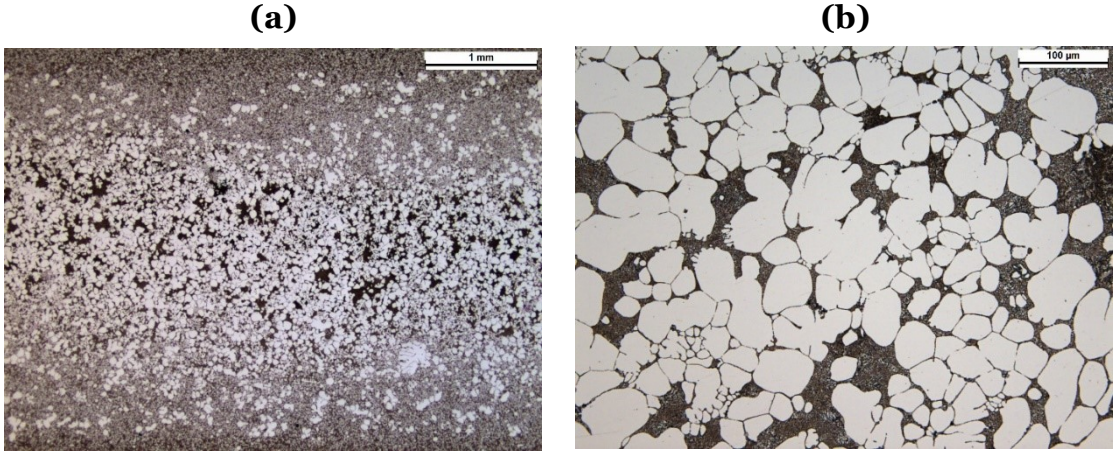

Figure 3.9: Microstructure of the alloy after Keller chemical ecthing (a) panoramic view at 12.5x magnification and (b) 250x magnification.

The solid fraction counting was conducted using the Leica LAS software. At a 50x magnification, 8 images of the microstructure were taken along the thickness of the sample (the thickness is 4 mm, so each image calculate the average solid fraction every 0.5 mm).

The software converted the image in binary. The area to analyze was 248400 μm2, on it a threshold value was inserted to determine the areas occupied by the a-Al matrix which the software must consider. In this case, the gamma color to consider had a tonality between 139 and 142, a saturation between 0 and 31, and an intensity between 170 and 255. The software elaborates the image as in Figure 3.10, and compares the area occupied by the solid fraction with the total area of the image, giving the percentage of solid fraction.

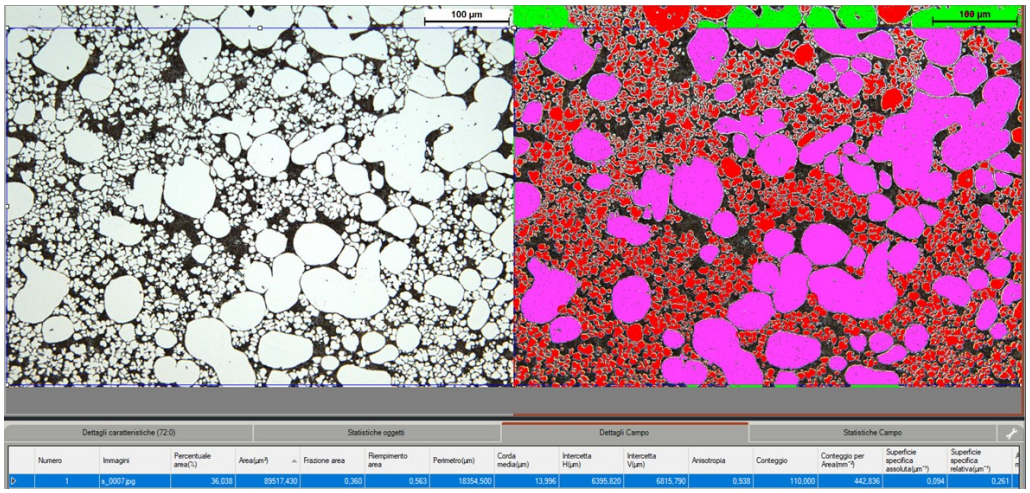

Figure 3.10: Example of investigated micrography in which solid fraction counting was conducted.

3.6.3 SEM inspections on fracture surfaces

Further inspections on the fracture surfaces were conducted in a Scanning Electron Microscope (SEM). The machine used was provided by FEI, and the model was the Quanta FEG (Field Emission Gun) 250, presented in Figure 3.11.

The SEM analysis was conducted for two purposes:

1) Further analyze the microstructure of the alloy.
2) Inspect the fracture surfaces of the specimens with suspected defects.

The machine at disposal had two signals: SE (Secondary Electrons) useful to get information on the roughness and the topography of the surfaces, and BSE (Back Scattered Electrons) to inspect chemical variations inside the microstructure. To determine the chemical composition, the machine used an EDS signal (Energy Dispersive X-Ray Spectroscopy).

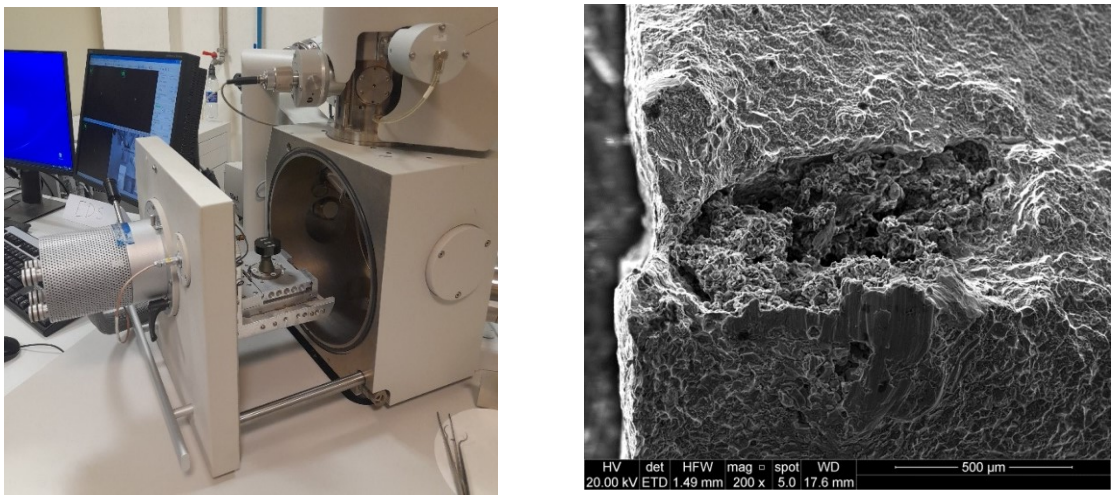

Figure 3.11: (a) SEM machine displacement. (b) defect captured with Secondary Electron (SE) beam.

The sample was etched in alcohol for 1 minute and then rinsed in running water. This permitted to have a clean surface to analyze, without any alteration in the measures with EDS signal to recognize the chemical elements in the defects noted in the fracture surfaces. The SE and BSE beams were setted with a 20 kV voltage, and to get the images the brightness and the contrast were adjusted to get the maximum information and clarity on the alloy microstructure morphology and chemical composition.

3.6.4 X-Ray image taking

The x-ray analysis consists in spreading an x-ray beam in the tensile test specimens. The beam highlight porosities and imperfections inside the cast that can't be seen from the outside, and it was possible to take pictures of the specimens under x-ray beam to assess presence of defects inside the casts.

The dimensions of the machine, displayed in Figure 3.12, permitted to take up to four specimens with a single photo, so it was possible to include all the samples from a single cast, differentiating between left and right plate specimens.

The specimens were held to a metal support with bi-adhesive tape. The metal support had a square hole in which the specimens were exposed to take to image. The support was held to a vice, always at the same distance from the camera (260 mm).

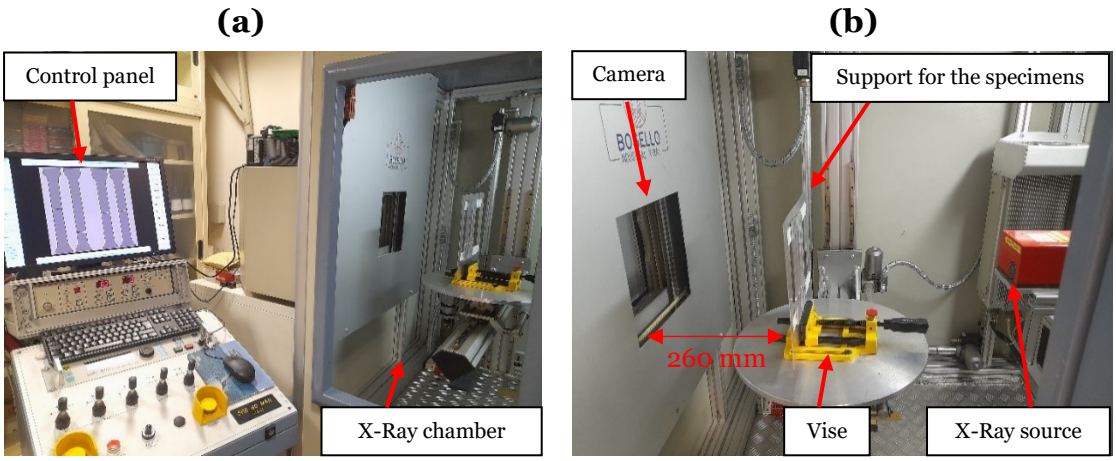

Figure 3.12: (a) X-Ray chamber with control panel to take the images (b) support system for the specimens to analyze.

The x-ray source was set with 80 kV voltage and 100 μA current. The camera was used with an exposure time of 500 ms, with an ELDO dynamic filter, doing an average between three filters. The level of ELDO dynamic filter used was 2.

4 Results and discussion

4.1 Mechanical characterization

4.1.1 Tensile test results

Each of the 19 total shot setting has been tested, taking between 16 and 20 tensile tests for every setting. The total number of tensile tests was 180 for holding and 160 for transportation. The proprieties found in each tensile test were:

- The Young Modulus **E**, measured in GPa.
- The Yield Strength **YS**, measured in MPa.
- The Tensile Strength **TS**, measured in MPa.
- The Fracture Elongation **El%**, measured in percentage value.

As regards the holding cleaning method, it's been observed that the young modulus values are stable, with an average of 75 GPa with 1 GPa deviation. The yield strength is also stable in the values, settling at an average of 115 MPa with a standard deviation of 1 MPa.

The difference between the settings is represented by the different values of tensile strength and fracture elongation. The samples with the biggest tensile strength are HAU with 246 MPa, HAX and HBX, both with 244 MPa. The lowest tensile strength values are HBZ with 231 MPa and HAZ with 235 MPa. HAX, HBX and HCZ samples, all been casted with the highest second phase speed, have the best values of fracture elongation (respectively 5.6 %, 5.8 %, 5.4 %). HAZ, HBY, HCX, casted with 1 m/s, have the lowest values of elongation: respectively 4.5 %, 4.4 % and 4.4 %. The results for the parameter setting with holding cleaning method are shown in Table 4.1.

Holding	vII [m/s]	E [GPa]	YS [MPa]	TS [MPa]	El_F [%]
HAX	2.5	75	116	244	5,6
HAY	2	75	117	243	4,8
HAZ	1	75	116	235	4,5
HAU	2	75	117	246	5,2
HBX	2.5	76	114	244	5,8
HBY	1	75	114	236	4,4
HBZ	2	75	116	231	4,4
HCX	1	76	115	236	4,4
HCY	2	74	114	236	4,6
HCZ	2.5	74	115	239	5,4
	average	**75 ± 1**	**115 ± 1**	**231 ÷ 246**	**4.4 ÷ 5.8**

Table 4.1: Tensile test results for holding cleaning method.

For transportation cleaning method, it's also been observed stable values of the young modulus, the average between the samples is 75 GPa. The same could be said for yield strength, the average value settles at 116 MPa with 2 MPa of standard deviation.

There is more variation in tensile strength and fracture elongation through the settings. For the tensile strength, the settings with the highest value are TDX with 245 MPa and TCY with 244 MPa, while TDY, TDU and TDZ have the lowest values, respectively with 228, 230 and 231 MPa.

The biggest values in terms of fracture elongation are in TAX with 5.6 %, TDX with 5.2 %, and TCY with 5.3 %. The samples with the lowest values of elongation are TCX and TDU (both injected with 1 m/s speed and respectively with 4.1 % and 3.8 % fracture elongation).

The results for the parameter setting with transportation cleaning method are shown in Table 4.2. The complete details on the tensile tests are included in the appendix, in Table 8.1 and 8.2.

Transportation	vII [m/s]	E [GPa]	YS [MPa]	TS [MPa]	El_F [%]
TAX	2	75	116	238	5,6
TAY	1	76	113	229	4,8
TBX	2.5	75	118	240	5,1
TCX	1	75	117	238	4,1
TCY	2	75	116	244	5,3
TDU	1	76	117	230	3,8
TDX	2	75	118	245	5,2
TDY	2.5	75	116	228	4,0
TDZ	2.5	75	114	231	4,2
	average	**75 ± 0**	**116 ± 2**	**229 ÷ 245**	**3.8 ÷ 5.6**

Table 4.2: Tensile test proprieties for transportation cleaning method.

4.1.2 Hardening rate index and fracture energy

Using the yield strength, the tensile strength, and the fracture elongation from the tensile tests, two other mechanical proprieties were determined: the **Hardening rate index** measured in MPa, and the **Fracture energy** measured in MJ/m^3.

The fracture energy is a measure of the amount of energy necessary to be applied to the material to reach the fracture, so it's a measure of the toughness of the material. The hardening rate index is a measure of the material ductility. The two proprieties have been so calculated for each setting:

Hardening rate index [MPa]: $\frac{\Delta\sigma}{\Delta\varepsilon} = \frac{(\sigma_{TS}-\sigma_{YS})}{el_f-(0,2)\%}$

Fracture energy [MJ/m³]: $\psi = \frac{(\sigma_{TS}+\sigma_{YS})}{2} * el_f$

The samples with low values of fracture elongation shows high values of hardening rate index but also a lower value of fracture energy.

In holding cleaning method, the hardening rate index values are between 23 MPa from HBX setting, and 29 MPa from HBY and HCX settings. As regards fracture energy, the values are from 761 MJ/m³ from HBY, and the highest values are above 1000 MJ/m³, for HAX and HBX settings.

For transportation cleaning, the hardening rate index values are between 25 MPa from TBX and TCY samples, and goes up to 31 MPa from TDU, TCX settings. As regards fracture energy, the lowest values are from TAX, TCX and TDZ (respectively 728, 733 and 731 MJ/m³) and the highest values are TCY and TDX with 955 and 935 MJ/m³.

The results of the values of hardening rate index and fracture energy for holding and transportation cleaning method are included in Table 4.3.

(a)

Holding	El_F%	**Δσ/Δε [MPa]**	**Ψ [MJ/m³]**
HAX	5,6	24	1007
HAY	4,8	28	858
HAZ	4,5	28	790
HAU	5,2	26	939
HBX	5,8	23	1043
HBY	4,4	29	761
HBZ	4,4	27	770
HCX	4,4	29	770
HCY	4,6	28	800
HCZ	5,4	24	960

(b)

Transp.	El_F%	**Δσ/Δε [MPa]**	**Ψ [MJ/m³]**
TAX	5,6	27	823
TAY	4,8	29	728
TBX	5,1	25	909
TCX	4,1	31	733
TCY	5,3	25	955
TDU	3,8	31	665
TDX	5,2	26	935
TDY	4,0	29	695
TDZ	4,2	29	731

Table 4.3: Hardening rate index and fracture energy for (a) Holding; (b) Transportation.

4.1.3 Difference in proprieties between cast plates

During the tensile tests, it was noted difference in mechanical proprieties between the specimens coming from the left plates and from the right plate of the cast. The differences were on tensile strength and fracture elongation, while the young modulus and the yield strength were stable.

For the parameter settings of holding, the tensile strength and the fracture elongation are higher in the right plates, in most settings. For the tensile strength values, it can be seen big differences in values in setting HBZ (219 MPa in left plate, 244 MPa in right plate); HCZ (234 MPa in left plate, 244 MPa in right plate); HAY (237 MPa in left plate, 250 MPa in right plate). As regards elongation, we also have high variation in HBZ (3.0 % in left plate, 5.8 % in right plate); HCZ (4.7 % in left plate, 6.1 % in right plate); HAY (4.1 % in left plate, 5.5 % in right plate). The only setting to have the left plates with higher proprieties is HCX (240 MPa and 4.5 % in left and 232 MPa and 4.2 % in the right). The found differences for holding cleaning method are in Table 4.4.

Holding	vII [m/s]	TS [MPa]			El_F [%]		
		ALL	LEFT	RIGHT	ALL	LEFT	RIGHT
HAX	2.5	244	244	244	5,6	5,6	5,7
HAY	2	243	237	250	4,8	4,1	5,5
HAZ	1	235	235	235	4,5	4,4	4,6
HAU	2	246	241	251	5,2	4,5	5,8
HBX	2.5	244	243	246	5,8	5,7	6,0
HBY	1	236	234	238	4,4	4,2	4,5
HBZ	2	231	219	244	4,4	3,0	5,8
HCX	1	236	240	232	4,4	4,5	4,2
HCY	2	236	231	241	4,6	4,1	5,1
HCZ	2.5	239	234	244	5,4	4,7	6,1

Table 4.4: Differences in the values of tensile strenght and fracture elongation through the settings (Holding cleaning).

As regards the parameter settings of transportation, there are also higher proprieties in the right plates. For the tensile strength values, it can be seen big differences in values in setting TBX (233 MPa in left plate, 250 MPa in right plate); TDY (221 MPa in left plate, 237 MPa in right plate); TDZ (224 MPa in left plate, 237 MPa in right plate). As regards elongation, we also have high variation in TBX (4.1 % in left plate, 6.1 % in right plate); TDY (3.3 % in left plate, 5.0 % in right plate); TDZ (3.6 % in left plate, 4.9 % in right plate). These three explained settings have all been injected with 2.5 m/s second phase speed. The only setting which has higher proprieties in the samples taken from the left plates is TDU: 233 MPa and 4.0 % in

left plates and 226 MPa and 3.6 % in right. Table 4.5 report the found differences in transportation cleaning for elongation and tensile strength.

Transp.	vII [m/s]	TS [MPa]			El_F [%]		
		ALL	LEFT	RIGHT	ALL	LEFT	RIGHT
TAX	2	238	235	243	4,6	3,9	5,6
TAY	1	229	228	231	4,3	4,2	4,4
TBX	2.5	240	233	250	5,1	4,1	6,2
TCX	1	238	236	241	4,1	3,9	4,3
TCY	2	244	243	246	5,3	5,0	5,5
TDU	1	230	233	226	3,8	4,0	3,6
TDX	2	245	243	247	5,2	5,1	5,2
TDY	2.5	228	221	237	4,0	3,3	5,0
TDZ	2.5	231	224	237	4,2	3,6	4,9

Table 4.5: Differences in the values of tensile strenght and fracture elongation through the settings (Transportation cleaning).

The differences on elongation and tensile strength proprieties from left to right plates, generated differences also on the values of hardening rate index and fracture energy. The results are reported in the appendix (Table 8.3 and 8.4).

4.1.4 aRMS estimations

The Root Mean Square acceleration was the parameter used to find the correlation between the process parameter and the mechanical proprieties of the alloy found in the tensile tests. This parameter is fundamental for this work because it can be determined with the process parameters used during the casting process.

There can be several ways to calculate the RMS acceleration. In this work, two estimation methods were used for both cleaning procedures, considering:

a) The method proposed by Fiorese, Bonollo, and Richiedei [15]; this involved the first phase speed v1, the second phase speed v_2 specific for each setting, the position of the switching point of the plunger from the total stroke length of the plunger, and the specific plunger travel of each setting.

b) The method proposed by the work of Jarfors, Du, Zhou, Zheng, and Yu [17]; this involved the first phase speed v1, the second phase speed v_2 and the intensification pressure specifics for each setting, the position of the switching point of the plunger from the total stroke length of the plunger, the specific plunger travel of each setting and the total mass of plunger and aluminium melt.

The following parameters were kept constants for all the settings:

- The first phase speed: $v_1 = 0{,}35$ m/s
- The position of the switching point of the plunger: $x_{sw} = 360$ mm
- The total mass of plunger and aluminium melt: m = 17,95 Kg

Table 4.6 resumes the values of RMS acceleration for holding cleaning method. The method of Fiorese, Bonollo and Richiedei impose to calculate the acceleration without considering the intensification pressure of the third phase of injection. Therefore, the value of acceleration depends on the second phase speed values, and three values have been determined for the three different speeds: 96.5 m/s² for settings HAX, HBX, HCZ; 56.1 m/s² for settings HAY, HAU, HBZ, HCY; 10.2 for settings HAZ, HBY, HCX. The method of Jarfors also involves the intensification pressure as a variable, so there is more variation in the results. The two methods, especially in the settings with 1 and 2 m/s gave very similar results. There are more differences in the results in the samples with 2.5 m/s second phase speed: HAX have an acceleration of 106 m/s² with Jarfors method compared to 96.5 m/s² with the method of Fiorese; HBX have an acceleration of 111.4 m/s² with Jarfors method compared to 96.5 m/s² with the method of Fiorese;

Holding	Plunger travel [mm]	Second phase velocity [m/s]	IP [bar]	**aRMS Fiorese [m/s²]**	**aRMS Jarfors [m/s²]**
HAX	430	2,5	160	**96,5**	**106,0**
HAY	435	2	120	**56,1**	**61,2**
HAZ	445	1	150	**10,2**	**10,9**
HAU	435	2	130	**56,1**	**58,8**
HBX	430	2,5	145	**96,5**	**111,4**
HBY	445	1	120	**10,2**	**12,2**
HBZ	435	2	184	**56,1**	**49,4**
HCX	445	1	150	**10,2**	**10,9**
HCY	435	2	120	**56,1**	**61,2**
HCZ	430	2,5	180	**96,5**	**100,0**

Table 4.6: RMS acceleration for holding cleaning, including the results for the two methods of estimation.

For transportation cleaning, the values of RMS acceleration are shown in Table 4.7. With the method of Fiorese, Bonollo and Richiedei the same three values have been obtained for the three different speeds: 96.5 m/s² for settings TBX, TDY, TDZ; 56.1 m/s² for settings TAX, TCY, TDX; 10.2 for settings TAY, TDU, TCX. The results between the two methods are very similar especially for the settings with 1 and 2 m/s. The settings with the most variation between the two methods were: TBX which have an acceleration of 109.5 m/s² with Jarfors method compared to 96.5 m/s² with the method of Fiorese; TDZ have an acceleration of 122.4 m/s² with Jarfors method compared to 96.5 m/s² with the method of Fiorese.

Transp.	Plunger travel [mm]	Second phase velocity [m/s]	IP [bar]	**aRMS Fiorese [m/s²]**	**aRMS Jarfors [m/s²]**
TAX	435	2	180	**56,1**	**50,0**
TAY	445	1	180	**10,2**	**10,0**
TBX	430	2,5	150	**96,5**	**109,5**
TCX	445	1	120	**10,2**	**12,2**
TCY	435	2	180	**56,1**	**50,0**
TDU	445	1	150	**10,2**	**11,0**
TDX	435	2	150	**56,1**	**54,7**
TDY	430	2,5	180	**96,5**	**100,0**
TDZ	430	2.5	120	**96,5**	**122,4**

Table 4.7: RMS acceleration for transportation cleaning, including the results for the two methods of estimation.

4.2 Influence of process parameter on fracture elongation

In this section, the variables of the casting process are analyzed in terms of influence in the average fracture elongation obtained in each setting. This analysis is performed to see the optimal conditions in which the casting process should run to have the highest proprieties. The analysis distinguishes the different fracture elongation of the specimens coming from left and right plates, because, as it's been described in the previous paragraph, the difference cannot be neglected. A section of this paragraph will also investigate the differences on the two cleaning methods, to evaluate if one method should be preferred over the other in the future works.

4.2.1 Influence of stirring speed

The trend of the fracture elongation for different stirring speed is displayed in Figure 4.1 for Holding and Figure 4.2 for Transportation.

In holding settings, it has been observed that the right plates have a decreasing trend for higher values of stirring speed, however the slope of this trend is limited to 0.0007 with a correlation index of just 0.0389. The left plates (which show a gap in elongation with the right plates) have a constant trend line for higher stirring speeds, with a correlation index close to zero.

For transportation settings, both right and left plates have an increasing linear trend for higher values of stirring speed. The trend line for right plates has a slope of 0.0011 with a correlation index of 0.067, while the left plates have a trend line with a slope of 0.0009 with a correlation index of 0.087.

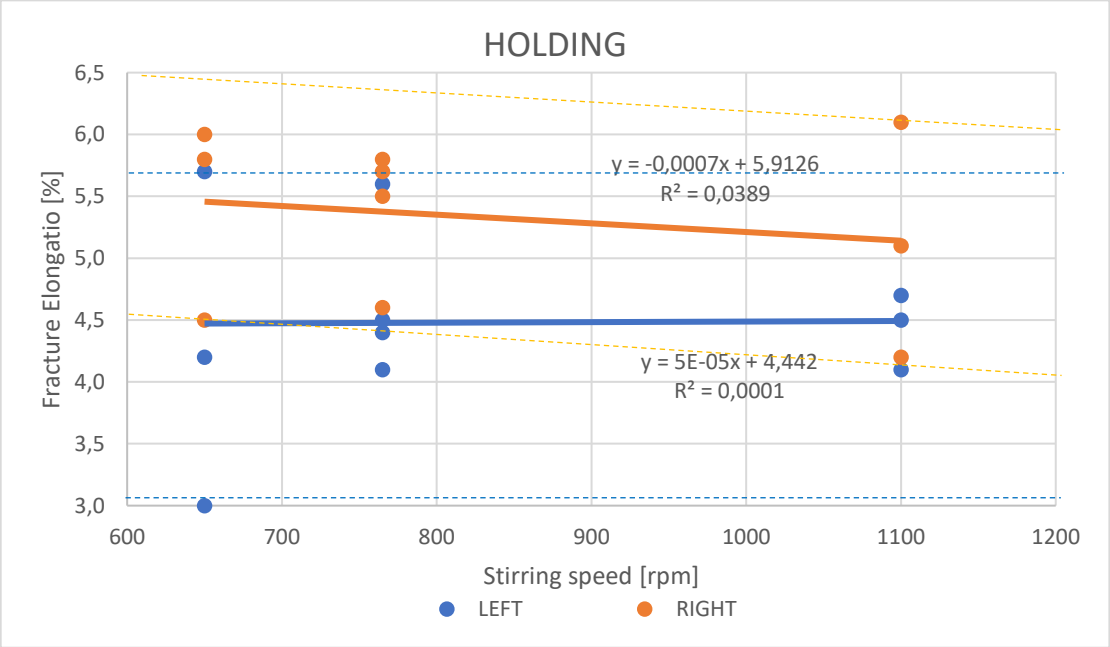

Figure 4.1: Trend of fracture elongation for different strirring speeds, in holding settings.

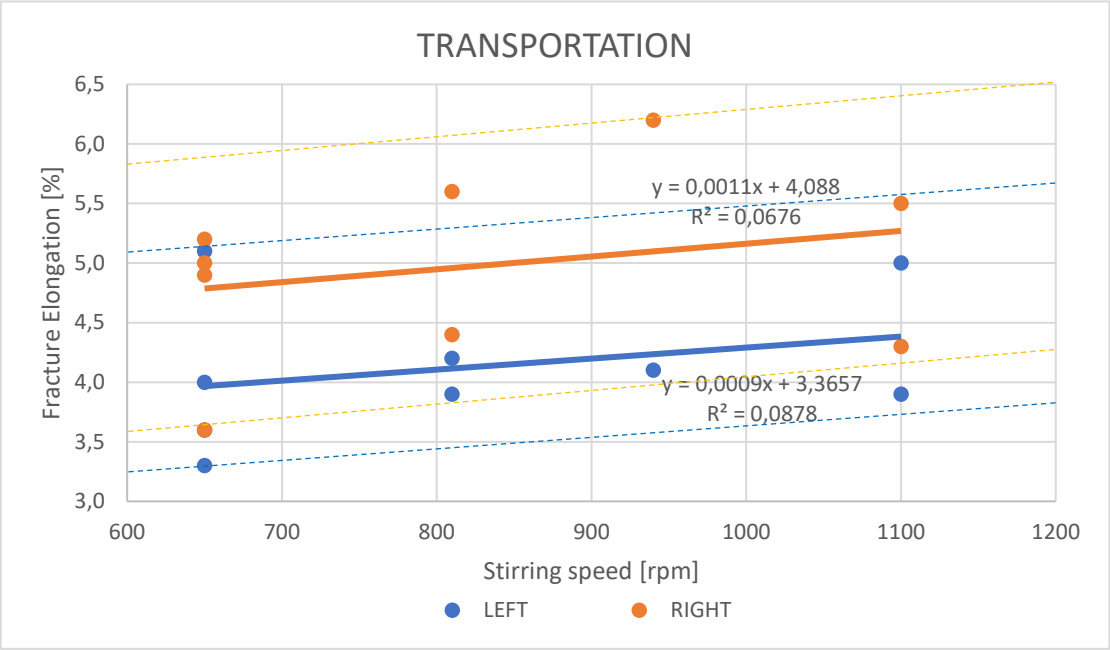

Figure 4.2: Trend of fracture elongation for different strirring speeds, in transportation settings.

4.2.2 Influence of intensification pressure

Figure 4.3 (Holding) and Figure 4.4 (Transportation) present the trend of the fracture elongation versus the changing intensification pressure used in the casting process.

In holding settings, it has been observed an increasing trend for higher values of intensification pressure in both left and right plate specimens. Specifically, the right plates showed an increase trend with a slope of 0.011, with a correlation index of 0.15. The left plates showed a slope of 0.016 in the trend line with a correlation index of 0.29. Between left and right specimens there is a gap in elongation of about 0.5 % in advantage for the right plates.

Transportation settings showed a very similar trend with holding settings. Both right and left plates have low but increasing linear trend for higher values of stirring speed: right specimens have a trend line with a slope of 0.0082; left specimens have a trend line with a slope of 0.0039. The correlation indexes are lower than holding settings: the trend line for right plates has a R square value of 0.068, while for the left plates the value is 0.0027. The gap between left and right plates is between 0.5 and 1 % of elongation, in favor of the right plates.

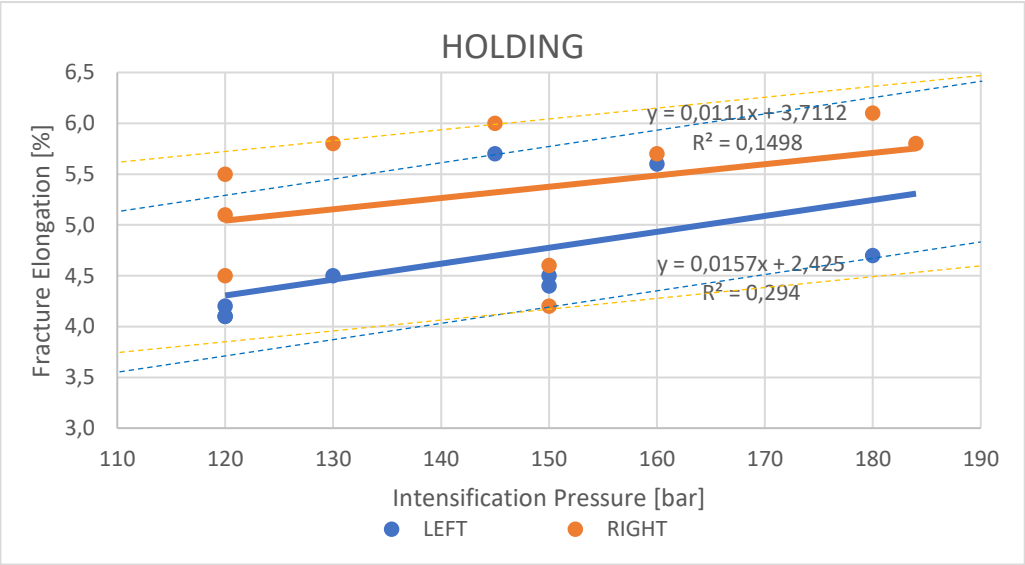

Figure 4.4: Trend of fracture elongation for different values of intensification pressure, in holding settings.

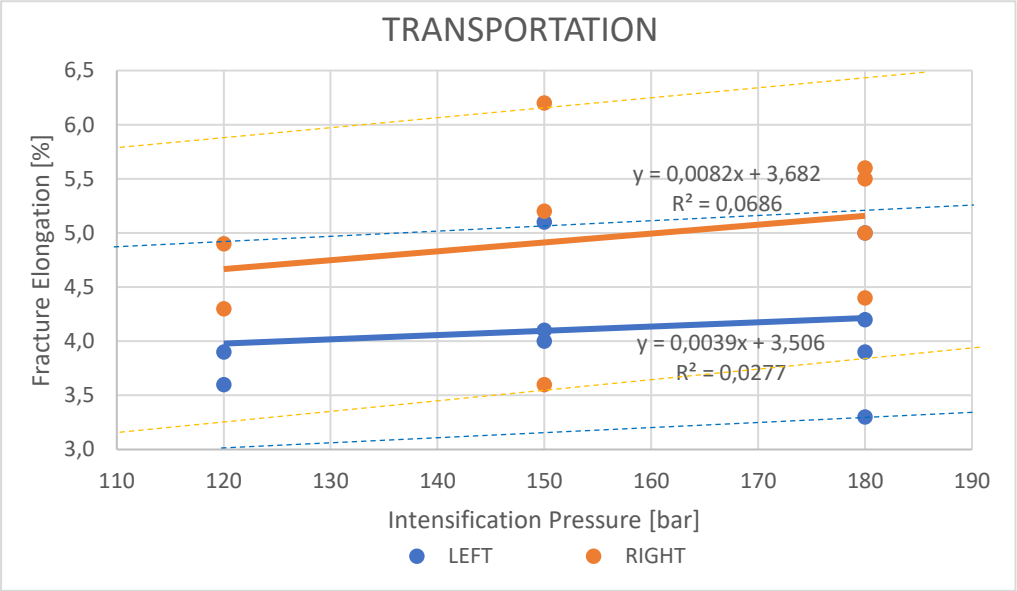

Figure 4.3: Trend of fracture elongation for different values of intensification pressure, in transportation settings.

4.2.3 Influence of second phase speed

The last variable of the casting process been compared with the fracture elongation in the settings was the second phase speed. The trend charts are displayed in Figure 4.5 (Holding) and Figure 4.6 (Transportation).

For holding settings, a stable grow in elongation for higher second phase speed has been noted. The right specimens have trend line with a slope of 1.02 with a correlation index of 0.87.

The left specimens have more variation and therefore the correlation index is limited to be 0.14, the fitting line show an increasing trend with a slope of 0.46.

The settings for transportation have a different trending from right to left plate specimens. The samples from right plates have an increasing trend line for higher speeds, with a slope of 0.91 and a correlation index of 0.6. The samples from the left plates have very similar elongation at 1 m/s speed compared to the right plates; however, the samples with 2.5 m/s speeds performed worse than the samples injected with 2 m/s, therefore the trend line is decreasing for higher second phase speeds, with a negative slope of 0.12 and a R square value of 0.017.

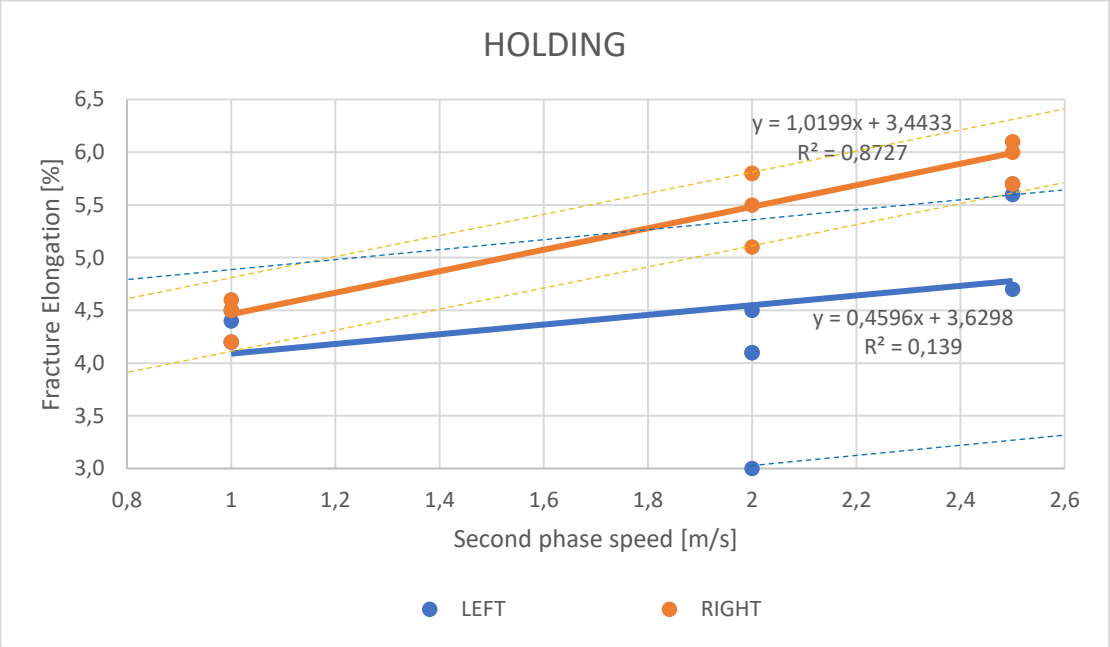

Figure 4.6: Trend of fracture elongation in changing second phase speed, in holding settings.

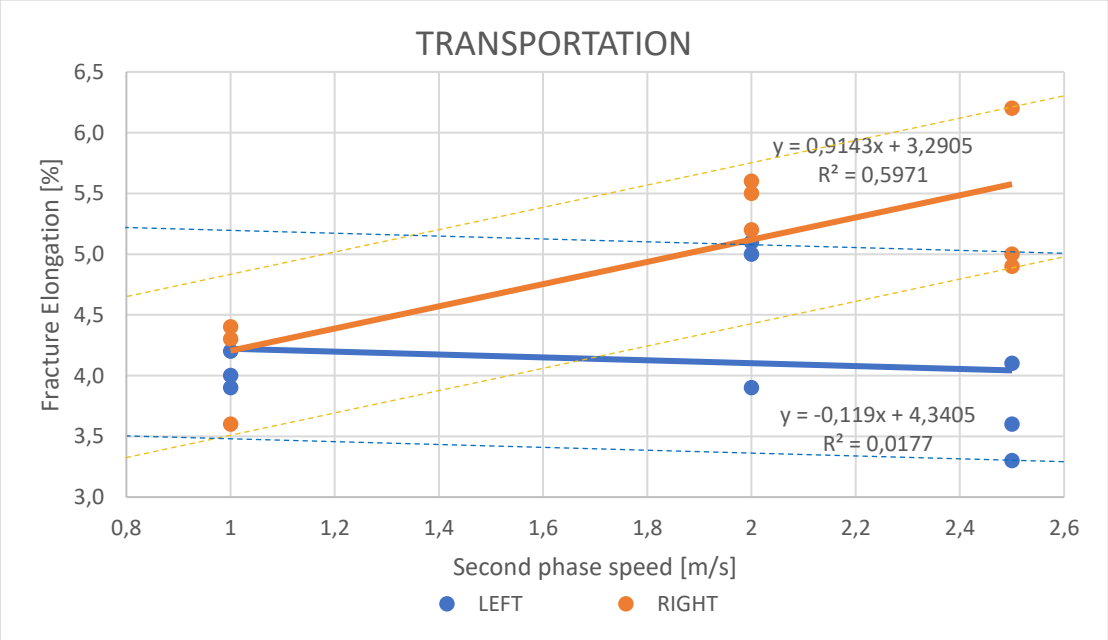

Figure 4.5: Trend of fracture elongation in changing second phase speed, in transportation settings.

4.2.4 Comparison between the two cleaning methods

To compare if one cleaning method gives the alloy better mechanical proprieties, for each cleaning method three conditions have been selected: one with lowest values of second phase speed, stirring speed and intensification pressure; one with the highest second phase speed, stirring speed and intensification pressure; and one last with mid-range values between the two extreme conditions. The existing differences in left and right plates mechanical proprieties have also been considered, so two separate charts were built.

The parameter setting chosen to do the analysis are presented in Table 4.8.

Cleaning method	Stirring speed [rpm]	vII [m/s]	Ip [bar]	**El_F left plate [%]**	**El_F right plate [%]**
Holding	650	1	120	**4,2**	**4,5**
	765	2	130	**4,5**	**5,8**
	1100	2.5	180	**4,7**	**6,1**
Transportation	650	1	150	**4,0**	**3,6**
	810	2	180	**3,9**	**5,6**
	940	2.5	120	**4,1**	**6,2**

Table 4.8: Parameter settings chosen to evaluate the effect of the two cleaning methods on mechanical proprieties.

The fracture elongation trends in three different process conditions are presented in Figure 4.7 (only samples from left plates) and in Figure 4.8 (only samples from right plates). As regards the trend in left plate specimens, the elongation changes from 4.2 % in the lowest setting conditions to 4.7 in the highest setting condition (for Holding method). In transportation cleaning, the values of elongation are very little influenced: the values are 4.0 %, 3.9 % and 4.1 % going from the lowest to the highest setting conditions. There is a gap between the two cleaning methods in favor of holding, however the difference in elongation never exceeds 0.5 %.

For samples coming from right side of the cast, the difference in process parameter settings is more evident. In holding, from the lowest to the highest settings, the elongation grows from 4.5 % to 6.1 %. In transportation the trend is the same, from the lowest to the highest settings the elongation grows from 3.6 % to 6.2 %. The difference between holding and transportation is evident in the lowest parameter settings (around 1% difference in elongation) but in the other two conditions the gap in fracture elongation closes.

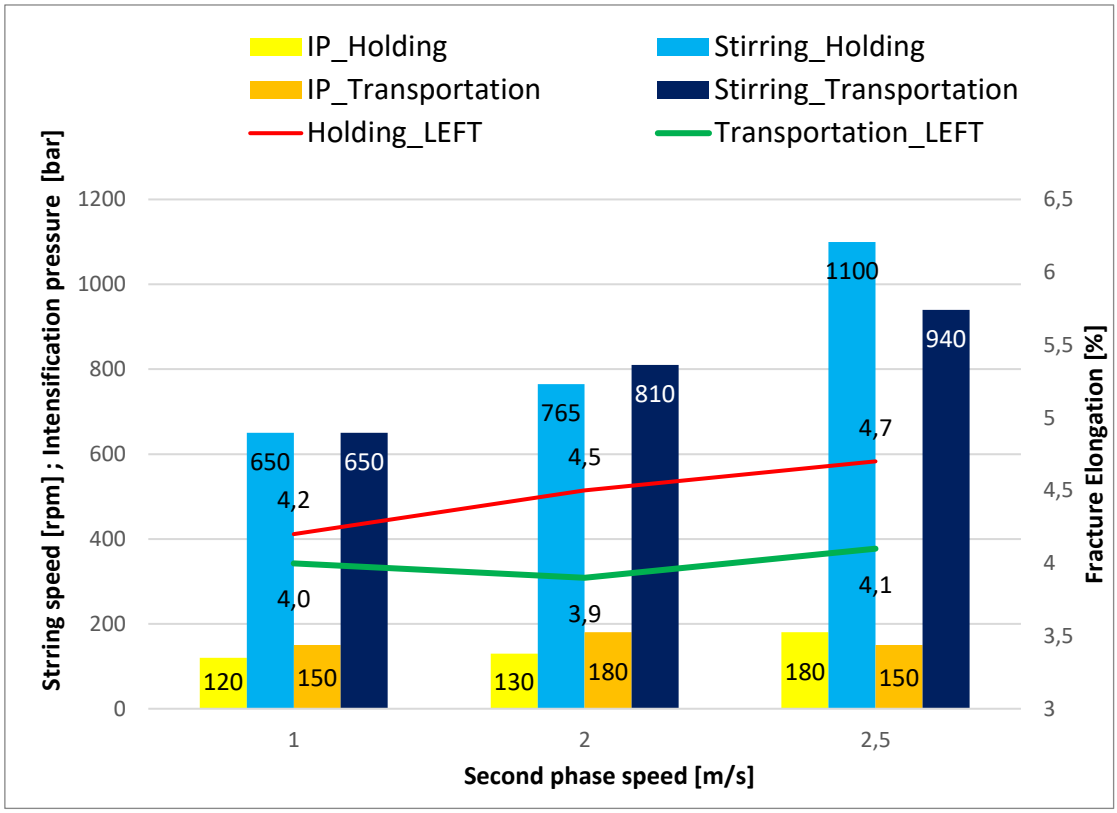

Figure 4.8: Comparisons between the two different cleaning methods, considering specimens coming from the left plates of the cast.

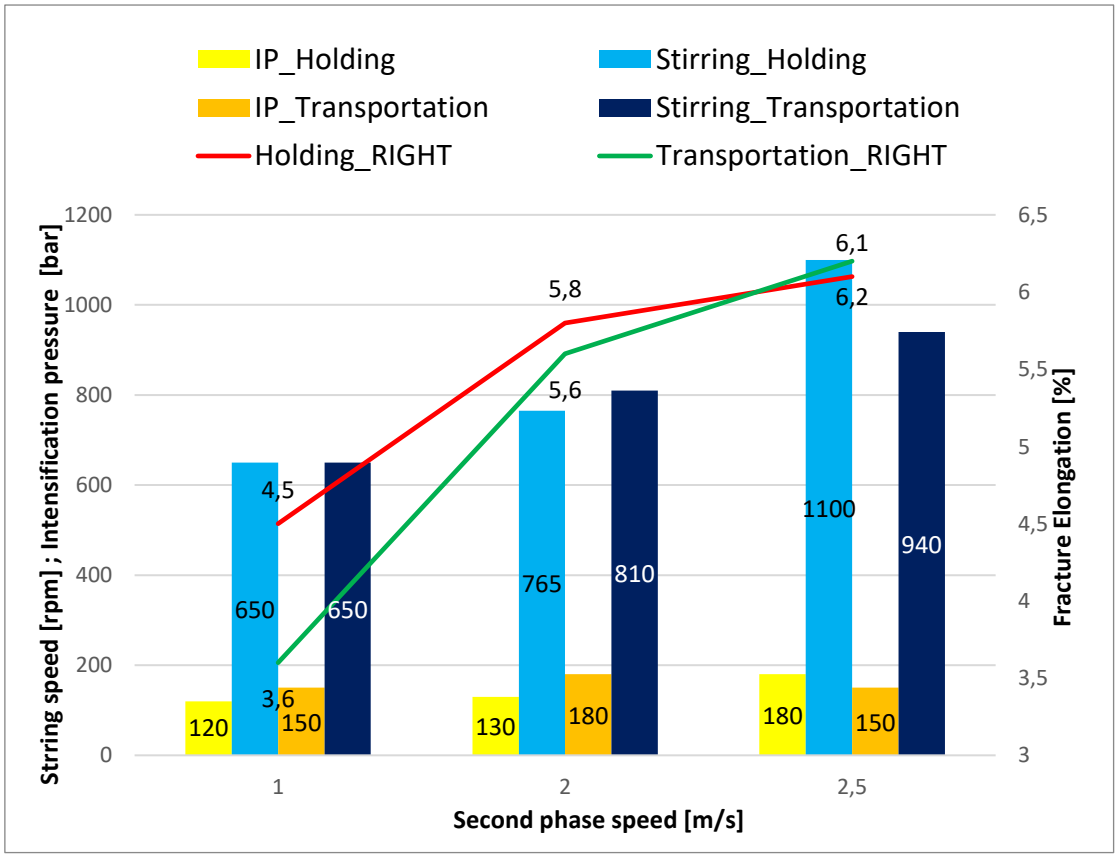

Figure 4.7: Comparisons between the two different cleaning methods, considering specimens coming from the right plates of the cast.

4.3 Correlation finding

This section compares the mechanical proprieties of the alloy with the root-mean-square acceleration, calculated with two different methods. For each setting, the mechanical proprieties used to make the comparisons were: the fracture elongation from the tensile tests; the hardening rate index and the fracture energy obtained by the calculations. The aim of this section is to assess the existence of 1:1 correlation between tensile proprieties and process parameter.

The charts used in the analysis are dispersion type, which includes the values of all the settings, distinguishing between holding and transportation cleaning method of the melt. The RMS values, in the x-axis, are studied in a logarithmic scale. Two types of charts have been used for each condition, one with the aRMS estimation from Fiorese and Bonollo, and one with the method of Jarfors. Furthermore, in each chart the specimens were distinguished in three different sets of data: one including all the specimens taken from a setting, and the other two considering separately samples from left and right plate. This distinction was necessary from the differences in mechanical proprieties assessed during the tensile tests. Each point in the chart represents the performance of a settings compared to his root-mean-square acceleration.

The datas used to construct the charts are included on tables in the appendix.

4.3.1 Correlation between fracture elongation and RMS acceleration

The fracture elongation is the mechanical propriety that quantifies the ductility of a material. The more ductile is a material, the more it can be deformed without braking.

In Figure 4.9 and Figure 4.10 are shown the charts that compares the fracture elongation and the RMS acceleration, for holding cleaning samples. In all three sets of data, the fracture elongation grows with the increasing values of RMS acceleration. From the chart, it was noted that the data set built with an average of all specimens have a trend line with a R square value of 0.58 (Fiorese) and 0.63 (Jarfors). If the results from left and right plates are studied separately, the amount of correlation changes dramatically: according to Fiorese method, the right plates have a trend line with a correlation of 0.88, which drops to 0.08 in the left plates. The results with the method of Jarfors are very similar, as the right plates have a correlation index of 0.86 while the left have 0.12.

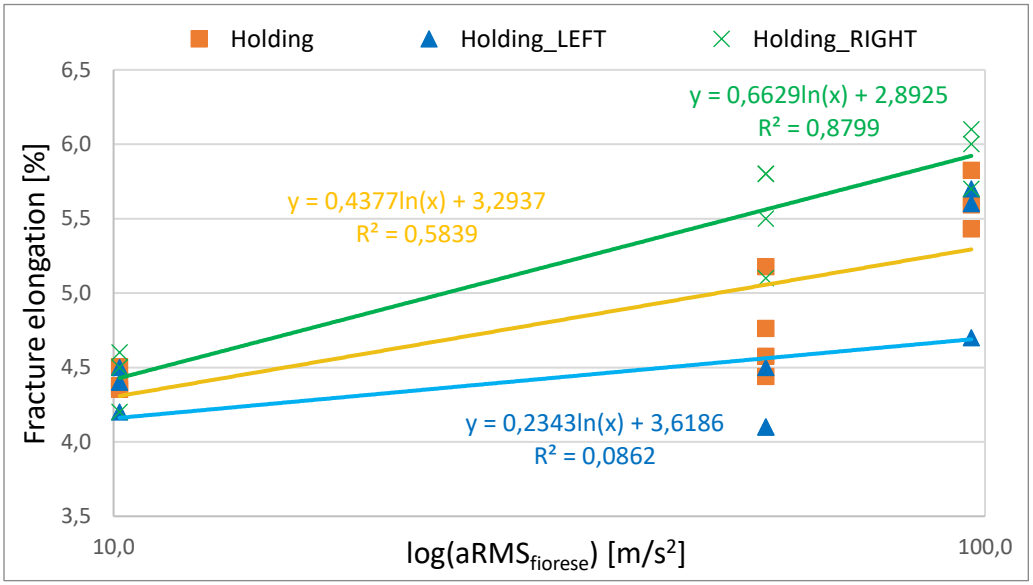

Figure 4.9: Correlation between fracture elongation and aRMS (calculated as suggested by Fiorese), for Holding cleaning samples.

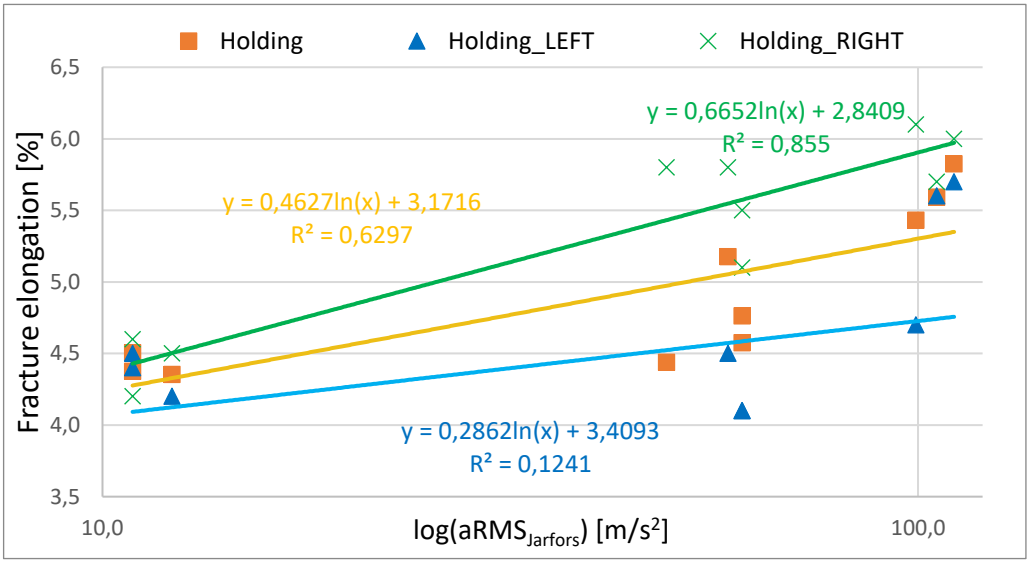

Figure 4.10: Correlation between fracture elongation and aRMS (calculated as suggested by Jarfors), for Holding cleaning samples.

For transportation cleaning samples, Figure 4.11 and Figure 4.12 display the dependance of the fracture elongation with RMS acceleration. Differently to what seen with samples of Holding cleaning method, there is a different trend between left and right samples. In right plate samples the fracture elongation grows with the increasing values of RMS acceleration, the trend lines have a R square value of 0.64 (Fiorese) and 0.58 (Jarfors). In left plate samples the trend lines are decreasing with the growth of RMS acceleration, with a correlation index close to zero in both estimation methods of RMS acceleration. The average between all the samples for transportation have a trend line with low correlation index, only 0.24 (Fiorese) and 0,19 (Jarfors), which are lower than what has been obtained with holding cleaning method.

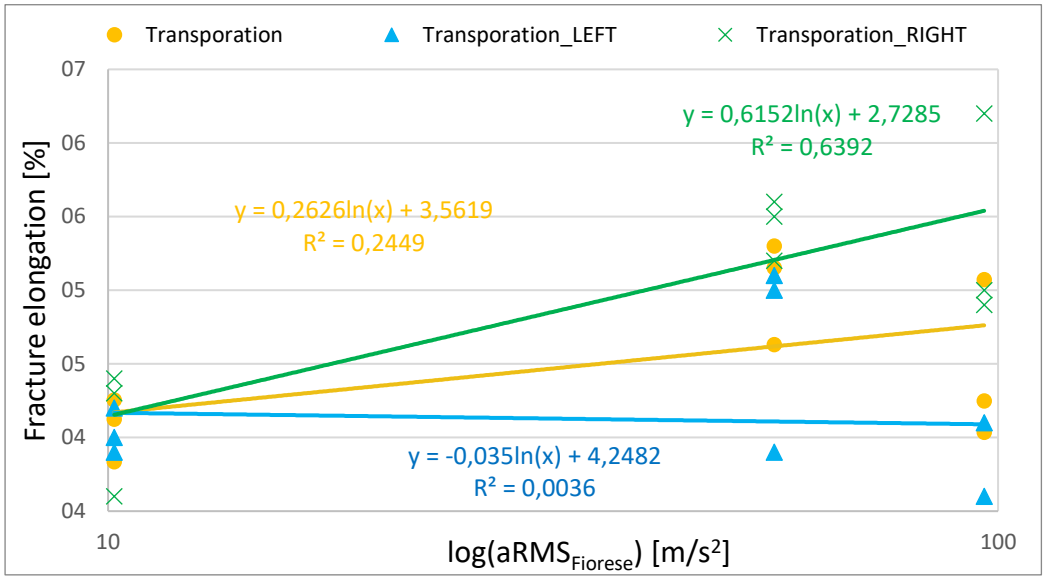

Figure 4.11: Correlation between fracture elongation and aRMS (calculated as suggested by Fiorese), for transportation cleaning samples.

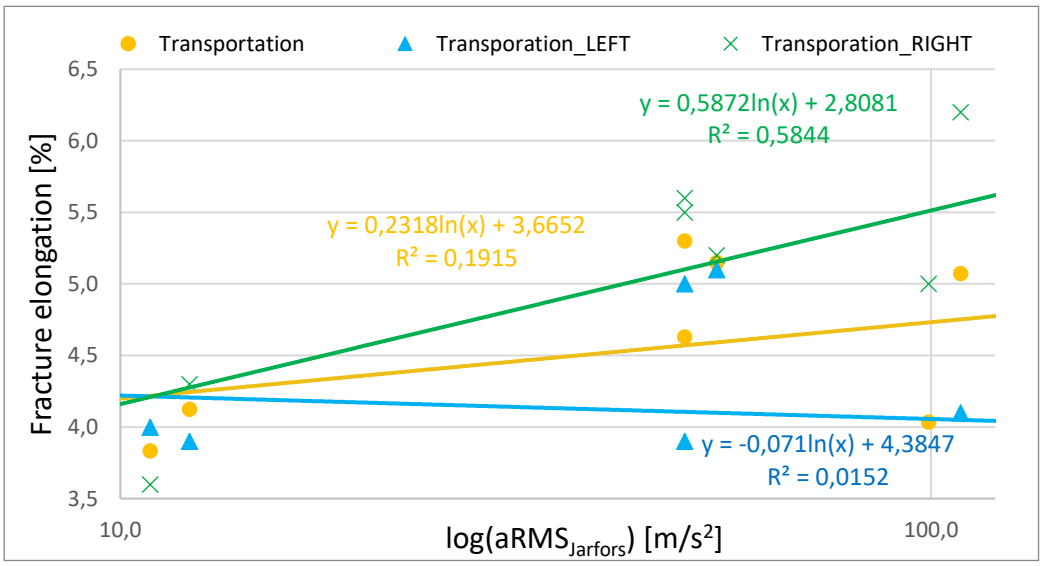

Figure 4.12: Correlation between fracture elongation and aRMS (calculated as suggested by Jarfors), for transportation cleaning samples.

4.3.2 Correlation between hardening rate index and RMS acceleration

As the fracture elongation growth, the hardening rate index in the alloy decreases (the two proprieties are inversely proportional). Therefore, what the dispersion chart should display, is a decrease in hardening rate index as the RMS acceleration growth.

The comparison between hardening rate index and RMS acceleration is shown in Figure 4.13 and Figure 4.14, for holding cleaning samples. For all three sets of data, the hardening rate index decreases for higher RMS acceleration.

The correlation index of the trend line average of all holding specimens are 0.64 (Fiorese) and 0.66 (Jarfors). The results from left and right plates are very different also in this investigation: with Fiorese method, the right plates have a trend line with a correlation of 0.86, which drops to 0.07 in the left plates. The results with the method of Jarfors are very similar, as the right plates have a correlation index of 0.83 while the left have 0.11.

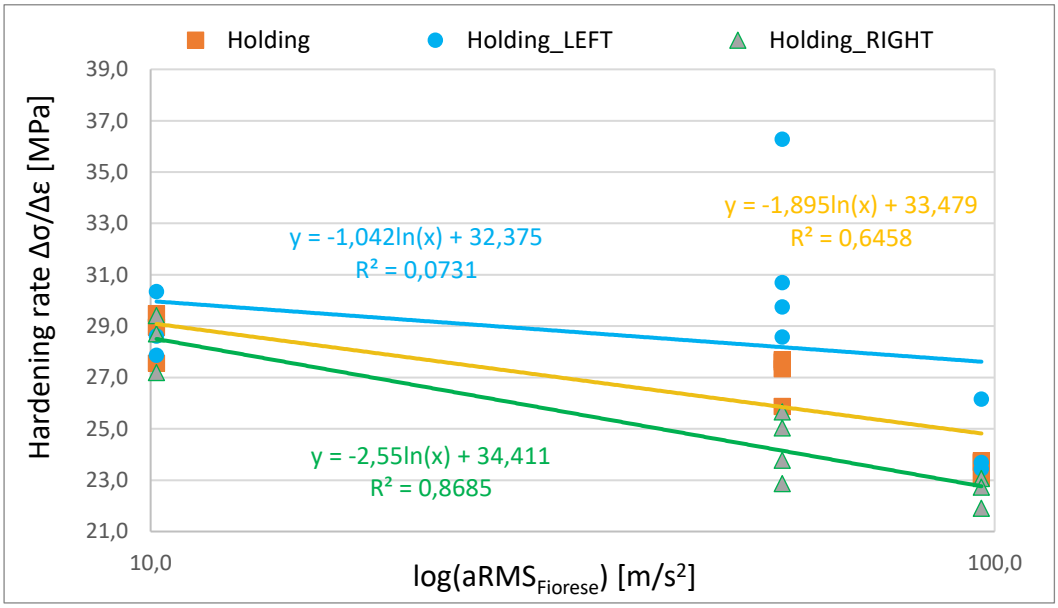

Figure 4.13: Correlation between hardening rate index and aRMS (calculated as suggested by Fiorese), for Holding cleaning samples.

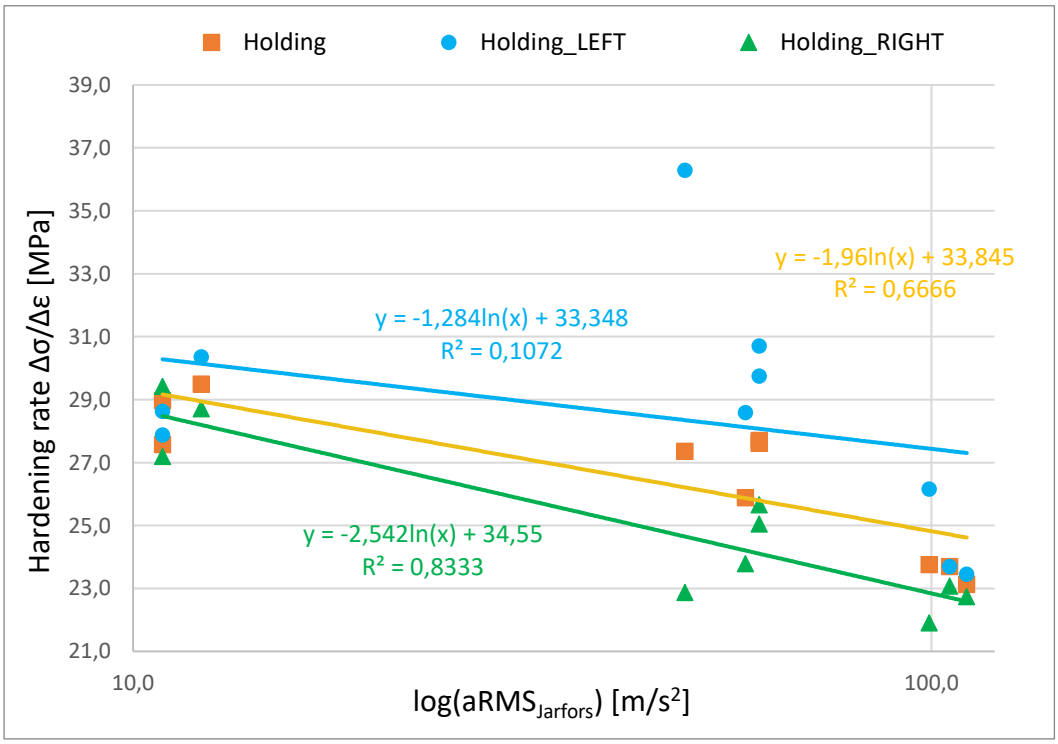

Figure 4.14: Correlation between hardening rate index and aRMS (calculated as suggested by Jarfors), for Holding cleaning samples.

Figure 4.15 and Figure 4.16 presents what has been obtained for transportation cleaning. In this case, the hardening rate index decreases for higher RMS acceleration in all the samples from the right plates, while the left plates show the opposite trend. The R squares values in the right plates are: 0.71 with Fiorese method and 0.65 with the method proposed by Jarfors. The correlation index obtained in the left plate specimens are close to zero, indicating a very poor correlation in this case. The average between all the specimens gave a correlation index of 0.36 (Fiorese) and 0.29 (Jarfors). The correlation indexes obtained in transportation samples are lower than the ones of holding cleaning, in all three sets of data and for both aRMS estimation methods.

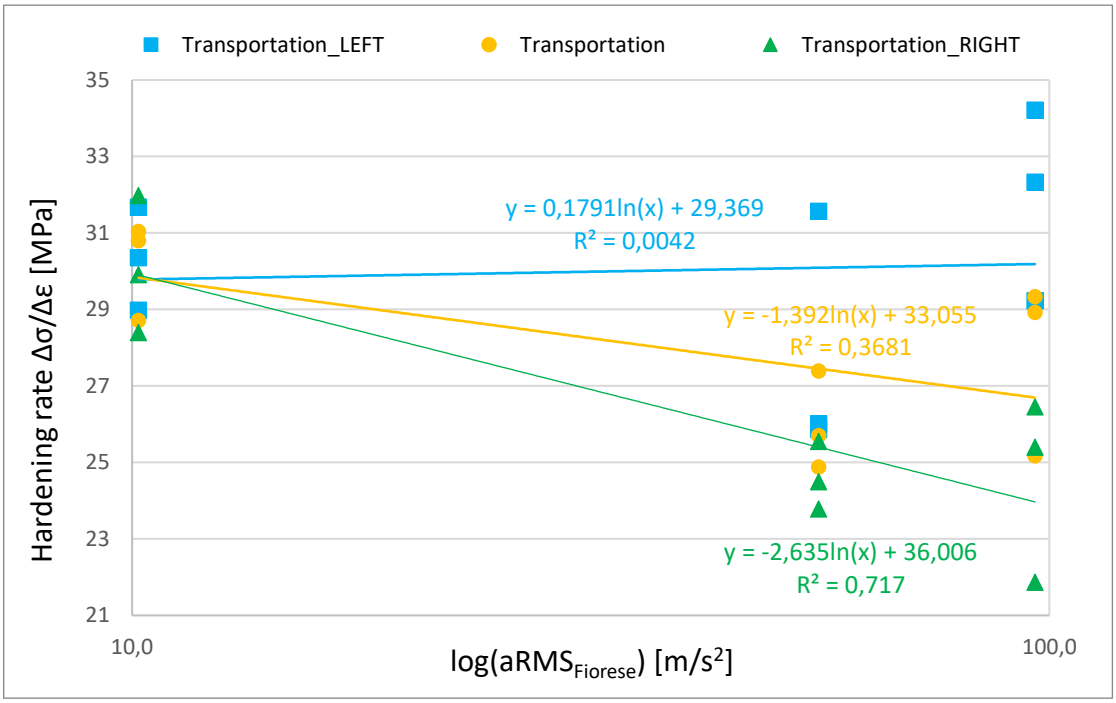

Figure 4.15: Correlation between hardening rate index and aRMS (calculated as suggested by Fiorese), for transportation cleaning samples.

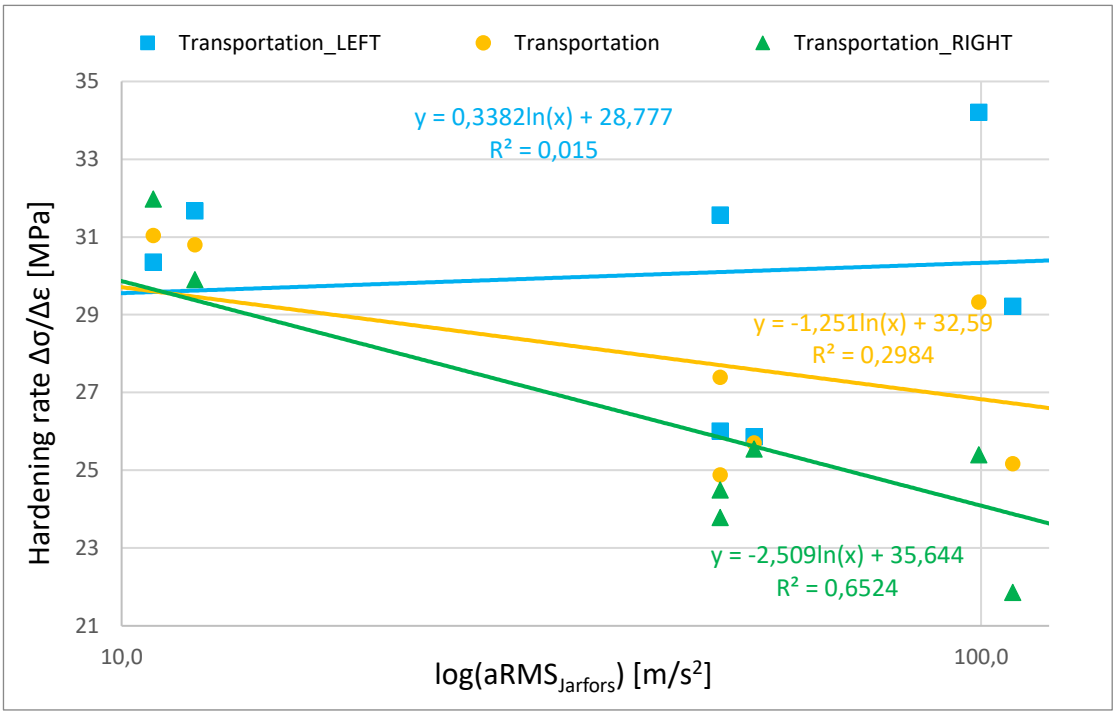

Figure 4.16: Correlation between hardening rate index and aRMS (calculated as suggested by Jarfors), for transportation cleaning samples.

4.3.3 Correlation between fracture energy and RMS acceleration

The fracture energy of a material gives the indication of the amount of energy necessary to apply to brake it. It is a mechanical propriety that involves both the tensile strength and the fracture elongation of the material, so it becomes an interesting mechanical propriety to try to correlate with the RMS acceleration.

For holding cleaning the two correlation charts for both RMS estimation method are in Figure 4.17 and Figure 4.18. As the RMS acceleration increases, the fracture energy growth in all three sets of the dispersion chart. Like the previous correlation charts, it has been noted different correlation results from right to left plate specimens. According to Fiorese method, the right plates have a trend line with a correlation of 0.87, which drops to 0.09 in the left plates. With Jarfors method there are similar results, as the right plates have a correlation index of 0.85 and the left plates have just 0.12. The average between all specimens has a trend line with a R square value of 0.57 (Fiorese) and 0.62 (Jarfors).

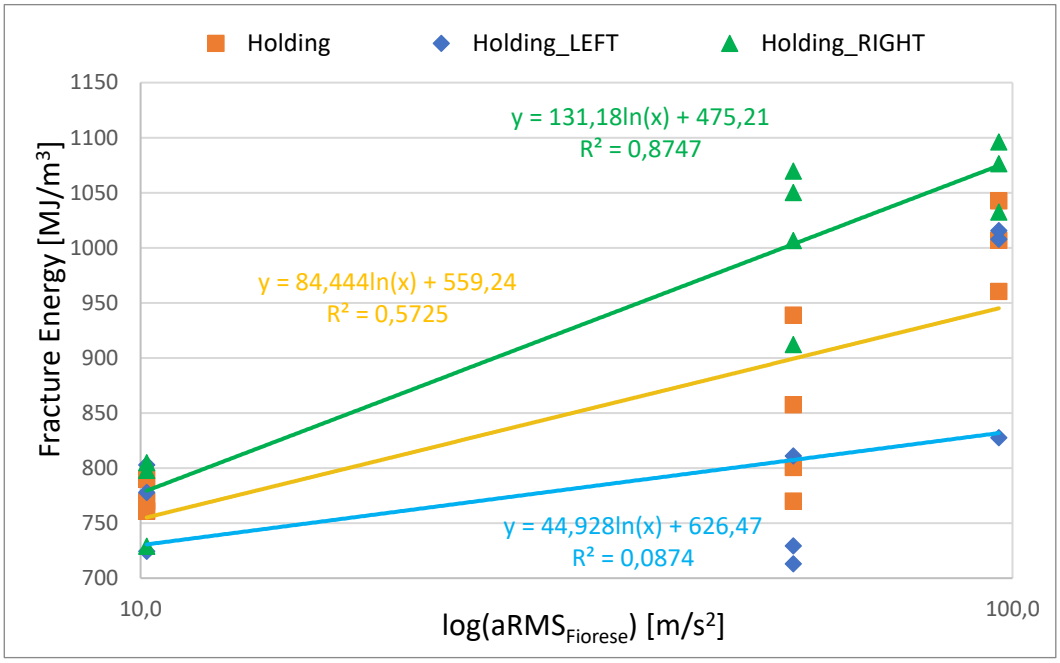

Figure 4.17: Correlation between fracture energy and aRMS (calculated as suggested by Fiorese), for Holding cleaning samples.

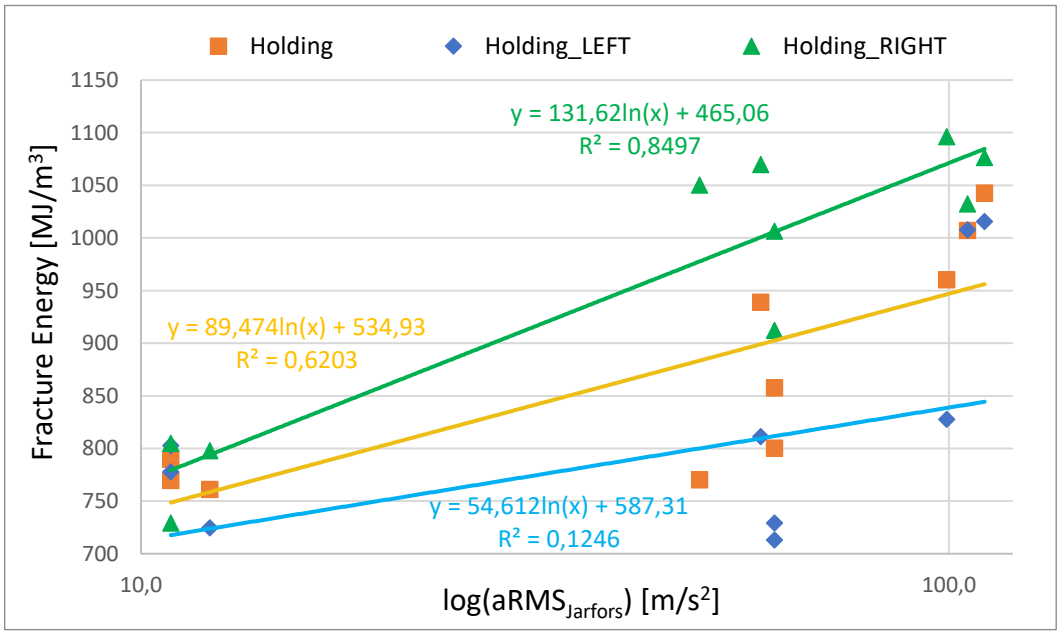

Figure 4.18: Correlation between fracture energy and aRMS (calculated as suggested by Jarfors), for Holding cleaning samples.

As regards transportation cleaning, the two correlation charts for both RMS estimation method are in Figure 4.19 and Figure 4.20. The trend showed in the previous correlation charts is repeated: in the right plate specimens more RMS acceleration means more fracture energy, while the left plate specimens showed a decrease in fracture energy as the RMS acceleration grow. The correlation indexes for right plates are 0.60 (Fiorese estimation) and 0.55 (Jarfors estimation).

For left plate specimens the trend lines have a correlation of 0.003 (Fiorese estimation) and 0.013 (Jarfors estimation), much lower to what obtained in the left plates. In comparison to holding cleaning method, the correlation indexes in transportation samples are lower in all three sets of data and for both aRMS estimation methods.

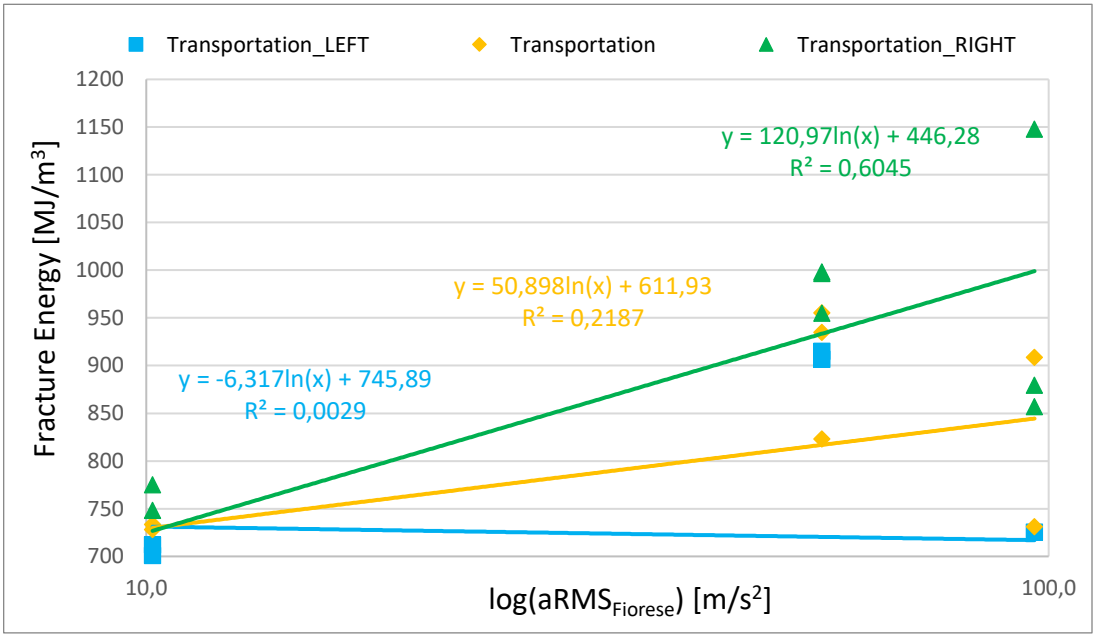

Figure 4.19: Correlation between fracture energy and aRMS (calculated as suggested by Fiorese), for transportation cleaning samples.

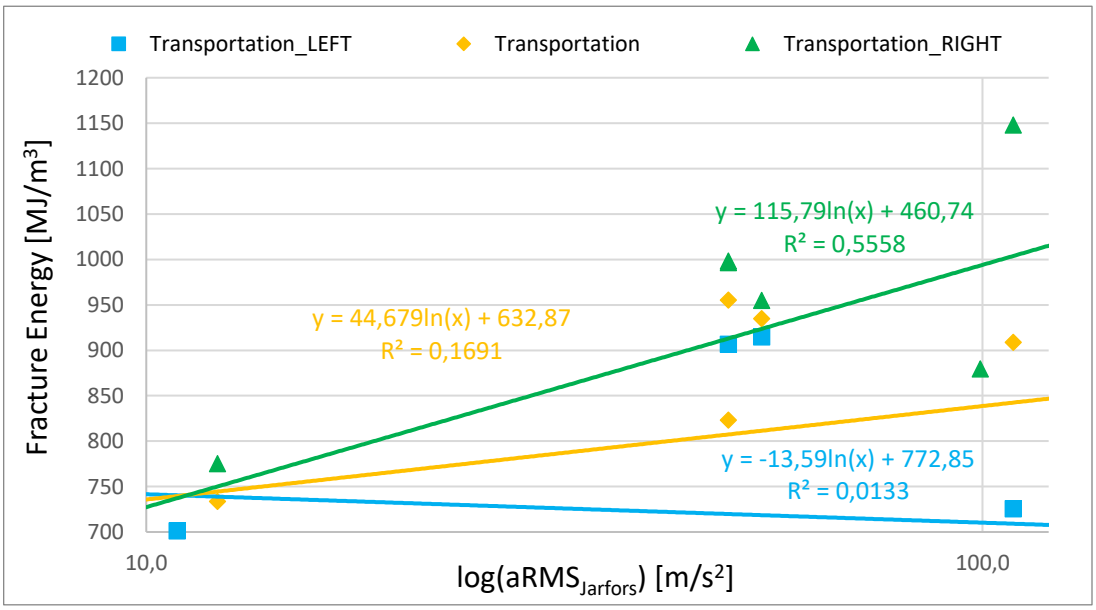

Figure 4.20: Correlation between hardening rate index and aRMS (calculated as suggested by Jarfors), for transportation cleaning samples.

4.4 Microstructural characterization

4.4.1 Alloy microstructure

One sample of the alloy microstructure is displayed in Figure 4.21. At low magnification it was possible to capture panoramic images of the microstructure (Figure 4.21 a), where it was possible to identify three zones in the samples where the microstructure can be characterized.

In the centre of the samples (Figure 4.21 b) the microstructure is composed by round white primary alpha aluminium, surrounded by the eutectic silicon structure. The alpha aluminum phases in this zone were created during the slurry making process, before entering the mould

In the zone "at quarter", between the centre and the border of the sample (Figure 4.21 c), the white alpha aluminium phases can be distinguished in one part created during the slurry making process (the bigger phases) and in a much smaller part created during the solidification inside the high pressure die casting mould.

Near the sample border (Figure 4.21 d) the microstructure is entirely composed by the alpha aluminum solidified after the injection of the slurry inside the mould, and by the eutectic silicon structure.

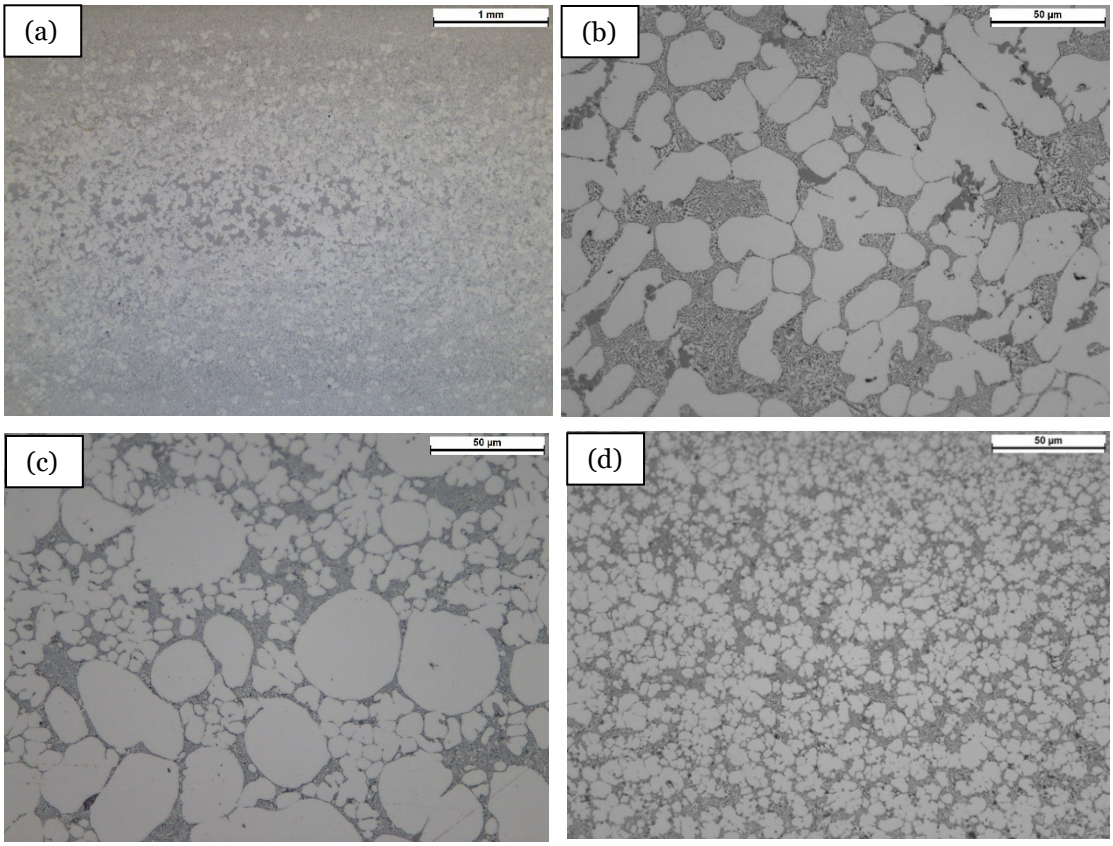

Figure 4.21: (a) Panoramic image of the alloy microstructure. Different microstructure (b) at centre (c) at quarter (d) near the border of the sample.

To have a more complete view of the alloy microstructure, a SEM inspection on the three different regions has been carried out with back-scattered electrons. In Figure 4.22 are displayed four micrographs of the alloy (a) in the zone near the border of the sample, (b) in a quarter of the sample, (c) and (d) in the centre of the sample.

From the SEM micrographs has been noted the presence of white particles between the eutectic structure and the primary alpha aluminium. These particles have different morphologies in the different zones of the samples. Near the sample border (Figure 4.22a) they appear fine and rounded; in the zone at quarter of the sample (Figure 4.22b) they tend assume a ramified morphology; while at the centre of the sample (Figure 4.22c) the particles assume a compacted and coarser morphology. Figure 4.22d show a detail of the microstructure in the centre of the sample, which shows that the eutectic structure is composed by silicon needles between the globular primary alpha aluminium.

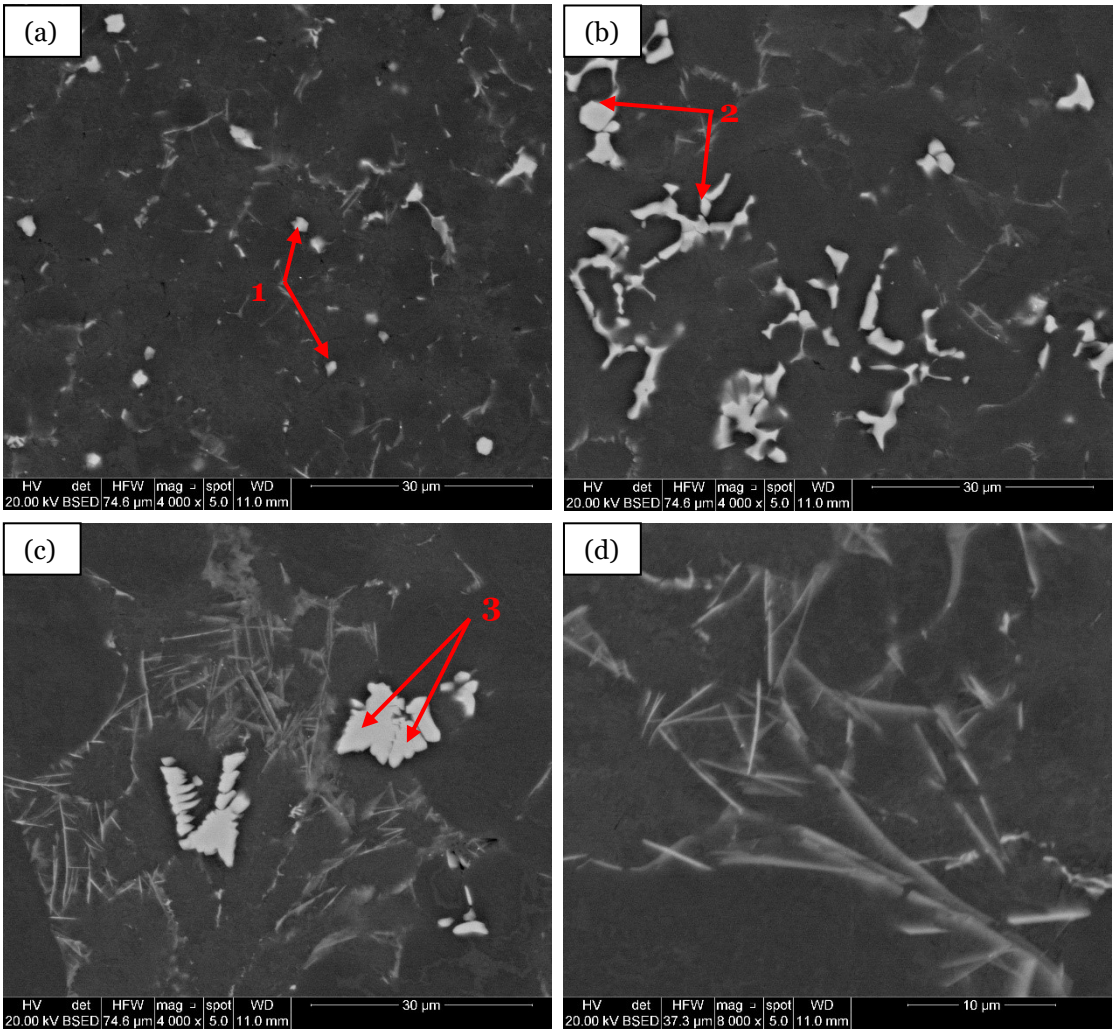

Figure 4.22: SEM micrographs of the alloy, showing white particles in the microstructure (a) near the border, (b) at quarter, (c) at centre of the sample. In picture (d) the eutectic microstructure in the centre of the sample is composed by acicular Si particles between the primary phase.

The white particles have been analysed to determine their chemical composition with an EDS spectrum. The results of the chemical analysis are presented in Table 4.9.

In all three morphologies has been noted a relevant percentage in weight of iron (Fe), respectively 9.35 for the rounded phases; 10.65 for the ramified phases; and 14.55 for the compacted phases. In the phases there is also a relevant quantity of manganese (Mn) which is 5.92 for the rounded phases; 6.56 for the ramified phases; and 8.65 for the compacted phases. The ratio between iron and manganese was noted to be similar in all the three morphologies, as it is 1.58 for the rounded phases; 1.62 for the ramified phases; and 1.68 for the compacted phases.

[%wt]	**Mg**	**Al**	**Si**	**V**	**Cr**	**Mn**	**Fe**	***Fe/Mn***
Rounded phases (1)	0,15	73,43	10,55	0,13	0,46	5,92	9,35	*1,58*
Ramified phases (2)	0,13	74,12	7,96	0,13	0,46	6,56	10,65	*1,62*
Compacted phases (3)	0,12	65,93	10,02	0,15	0,59	8,65	14,55	*1,68*

Table 4.9: EDS chemical composition of the white particles noted on the alloy microstructure.

4.4.2 Average solid fraction in different stirring speed settings

The solid fraction counting wants to assess in a quantitative way the differences in microstructure through the different process parameter settings. The counting was done in samples with a low and a high value of stirring speed, in both holding and transportation cleaning. For each speed, the average solid fraction was calculated on three specimens coming from different casts, to have a more representative counting.

Table 4.10 sum up the results obtained. For holding cleaning method, the average solid fraction value is 36.0 with a standard deviation of 4.0 in the samples with 650 rpm stirring speed. In the samples with 1100 rpm stirring speed, the solid fraction value is similar, with 34.8 and a standard deviation of 1.5. The mechanical proprieties in the samples that were analyzed stays similar for different stirring speeds: tensile strengths are respectively 245 and 242 MPa and elongations are respectively 5.5 and 5.6 %.

For transportation cleaning method, the average solid fraction value is 38.0 with a standard deviation of 1.3 in the samples with 650 rpm stirring speed. In the higher stirring speed samples (940 rpm) the solid fraction value is 33.0 and a standard deviation of 2.6. The mechanical proprieties in the analyzed samples are respectively 245 and 242 MPa for tensile strength and respectively 5.5 and 5.6 % for elongation.

Holding				Transportation			
Stirring speed [rpm]	TS [MPa]	El [%]	**fs [%]**	*Stirring speed [rpm]*	TS [MPa]	El [%]	**fs [%]**
650	245±4	5,5±0,5	**36,0±4,0**	*650*	238±8	4,9±1,2	**38,0±1,3**
1100	242±6	5,6±0,8	**34,8±1,5**	*940*	249±1	6,0±1,0	**33,0±2,6**

Table 4.10: Average solid fraction calculated in the samples.

In Figure 4.23 are represented the trend in the samples of the solid fraction values for (a) holding samples and (b) transportation samples.

For both cleaning methods the trends are similar. In the changing value of stirring speeds, the most difference in the values are in the center of the samples (between 1 and 3 mm thickness), where the 650 rpm samples trend line have bigger solid fraction values over the 940 and 1100 rpm trend lines.

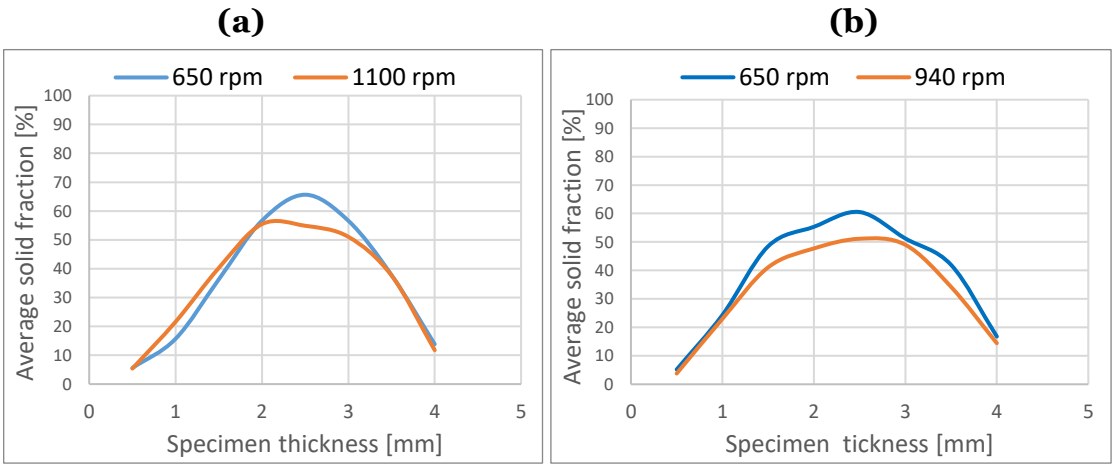

Figure 4.23: Average solid fraction in the sample thickness. (a) Holding cleaning (b) Transportation cleaning.

In Figure 4.24 the average solid fraction and the respective fracture elongation for different stirring speed samples is presented. From lower to higher stirring speed, the solid fraction values present a slight decrease for both holding and transportation. The fracture elongation values are 5.5 % at 650 rpm and 5.6 % at 1100 rpm for holding cleaning; whereas for transportation the values start at 4.9 % at 650 rpm and reaches 6.0 % at 940 rpm.

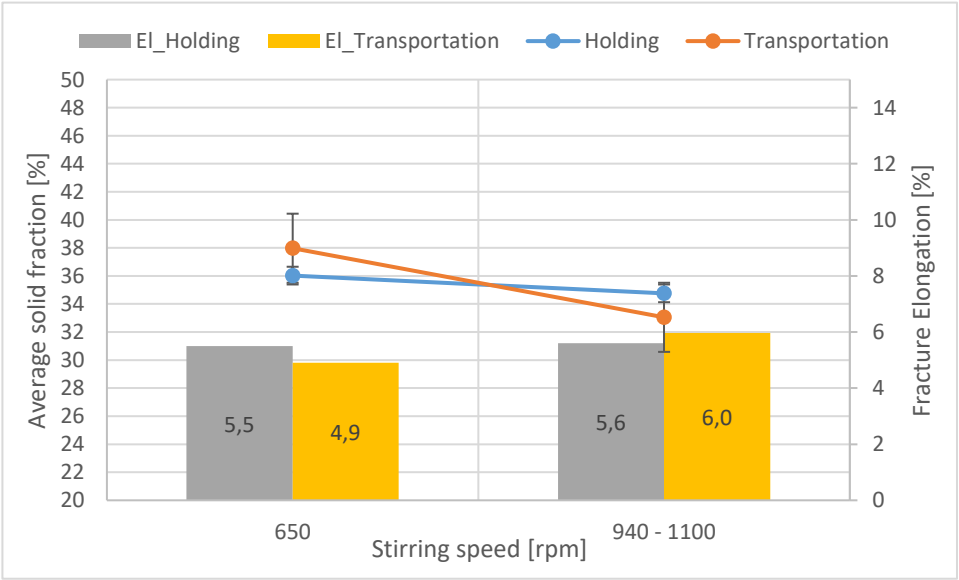

Figure 4.24: Average solid fraction and fracture elongation through the different values of stirring speeds.

4.4.3 Fracture surfaces

The analysis on the fracture surfaces were conducted comparing left and right samples from the same cast, with evident differences in the tensile strength value, and with possible presence of defects in the surface.

An EDS spectroscopic analysis was conducted to have a chemical characterization of the defects spotted in the surfaces. The emission of X-rays generated by an electron beam trough the sample creates peak of energy captured by the revelator.

The first sample analyzed comes from TBX cast number 4. In Figure 4.25 (a) it is presented the left plate sample, which appears to have an inclusion near the top-left corner, and a porosity in the right side. This sample had a tensile strength of 226 MPa, which is very different from 248 MPa obtained in the right plate samples, in Figure 4.25 (b), which had no visible defects in his fracture surface.

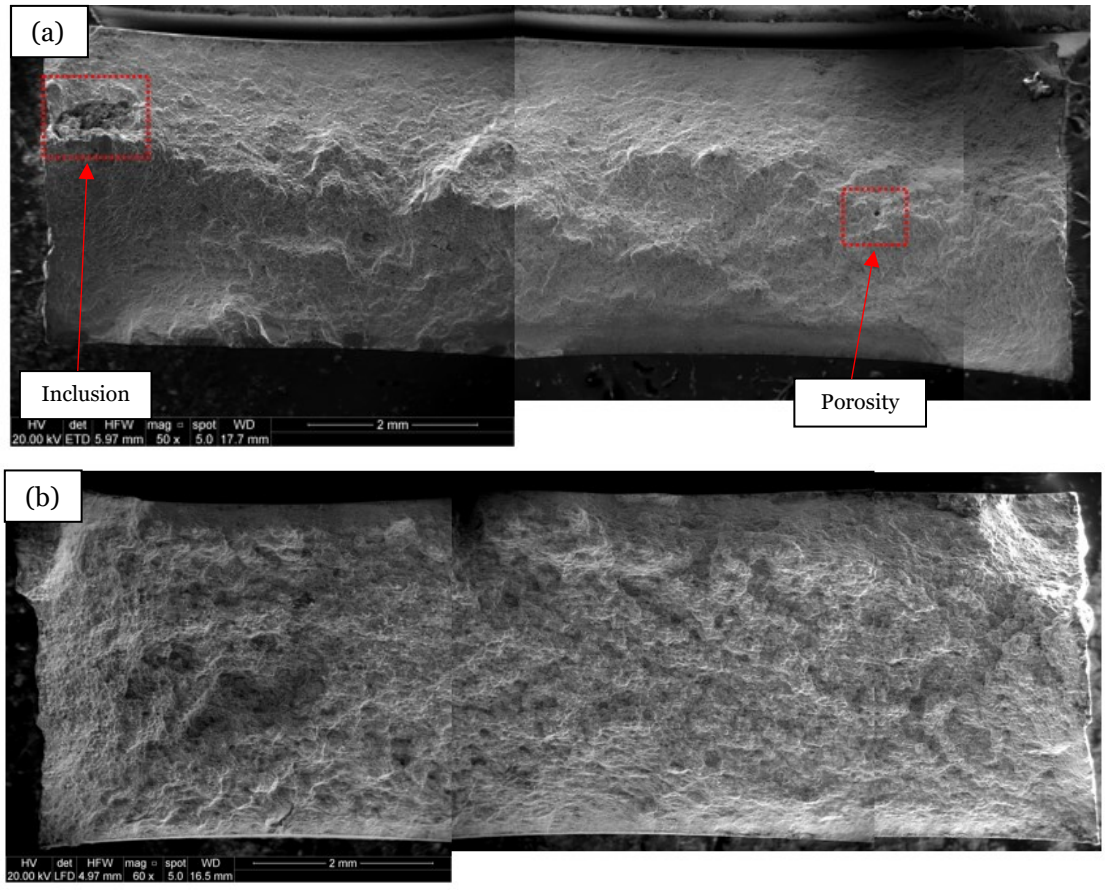

Figure 4.25: (a) TBX4 left plate sample with an inclusion and a porosity (b) right plate sample with no visible defects

In figure 4.26 (a) the view of the defect in detail is shown, and in Figure 4.26 (b) is presented the image captured with BSE with the two specific point chosen to analyze.

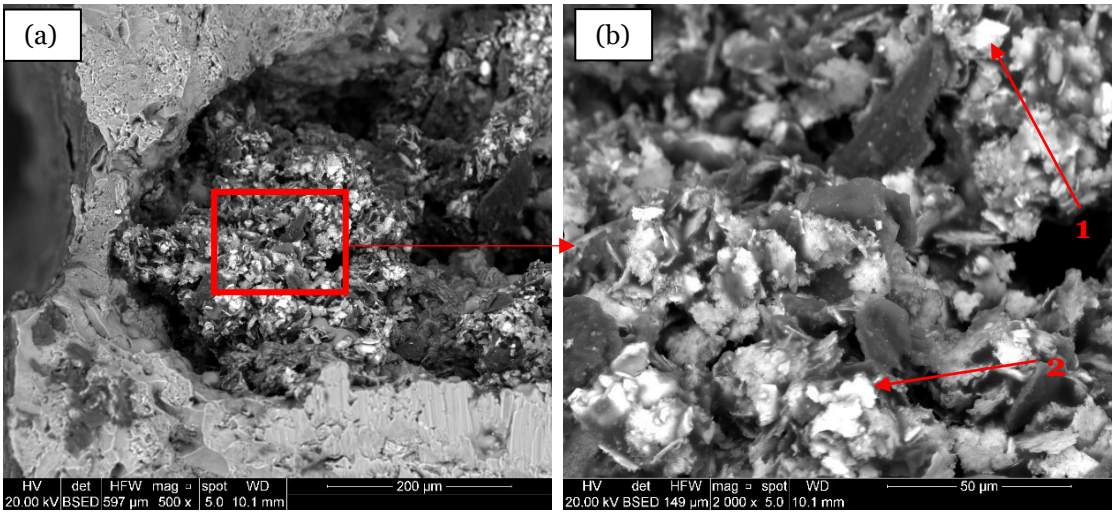

Figure 4.26: BSE images of the defect noted in TBX cast number 4. (a) panoramic view of the defect, (b) defect at higher magnification, with two indicated point of EDS chemical analysis.

The EDS spectroscopy produced spectrums which represents the peaks generated by the chemical elements inside the defects. Point "1" of the analysis is shown in Figure 4.27 (a) and suggested an amount of Copper (Cu) of 81.27 % in weight. Point "2" of the analysis is in Figure 4.26 (b) and indicates a relevant presence of Sulfur (S) and Molybdenum (Mo): respectively 28.92 % and 27.60 % over the total weight.

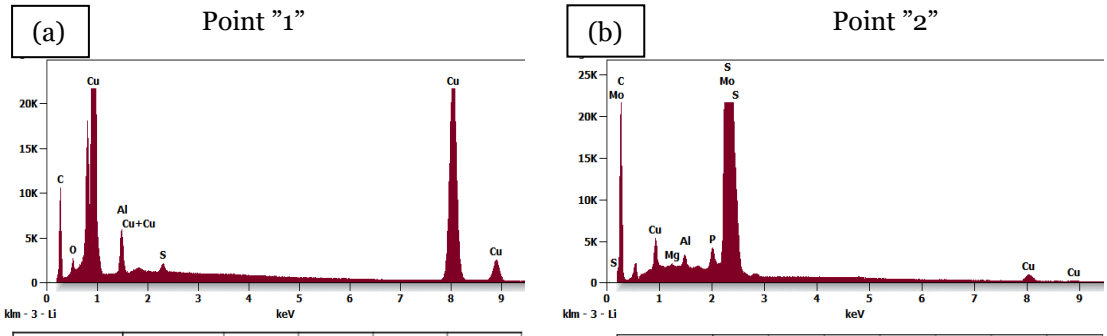

% wt	C	O	Al	S	Cu
Point "1"	13.48	1.24	3.57	0.50	81.21

% wt	C	Mg	Al	P	S	Cu	Mo
Point "2"	40.36	0.06	0.36	0.34	28.92	2.36	27.60

Figure 4.27: Spectrum generated by (a) point "1" and (b) point "2" with the correnspondingtable indicating the weight percentage of element.

The second sample analyzed comes from TBX cast number 5. The left plate sample is shown in Figure 4.28 (a) and has three black holes which were identified as gas porosities, and another defect, suspected to be a oxide bifilm. The left sample had presence of defects and a tensile strength of 228 MPa, while the right plate sample, in Figure 4.28 (b), shown no evident defects in the fracture surface and reached a higher tensile strength value of 252 MPa.

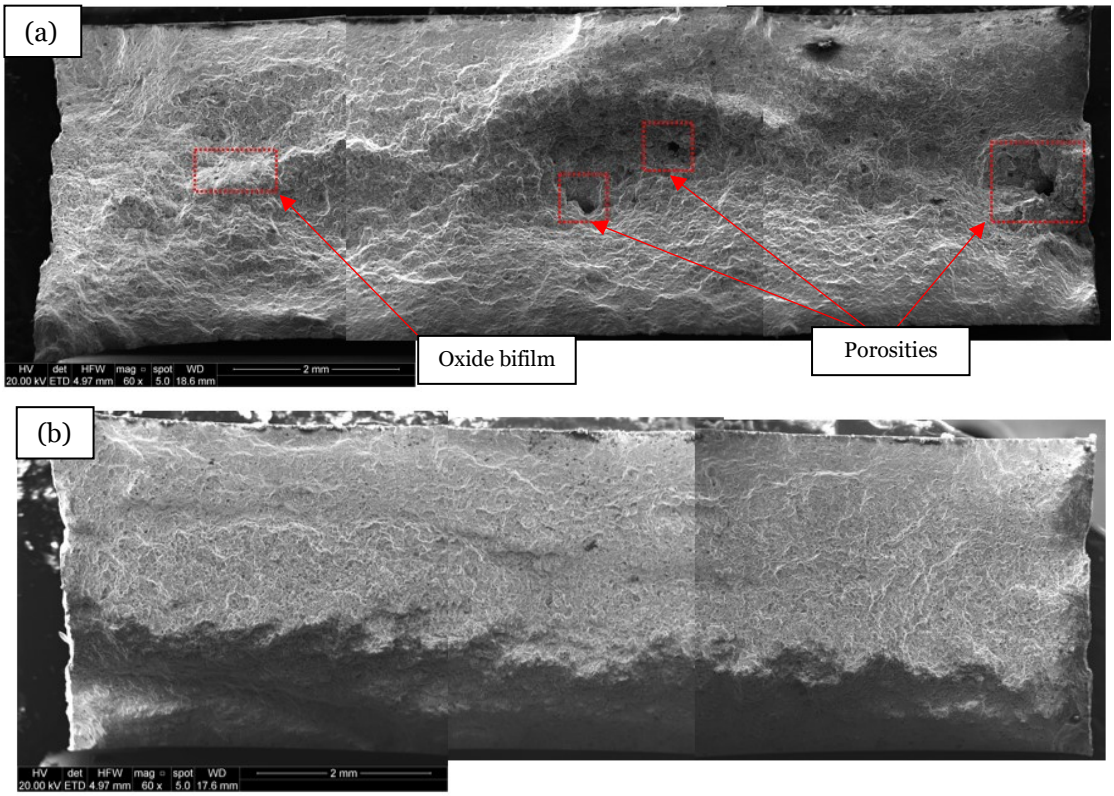

Figure 4.28: TBX5 (a) left plate sample with porosities, (b) right plate sample with no visible defects

Figure 4.29 give two detailed images of the porosities found in the left plate sample in Figure 4.28 (a).

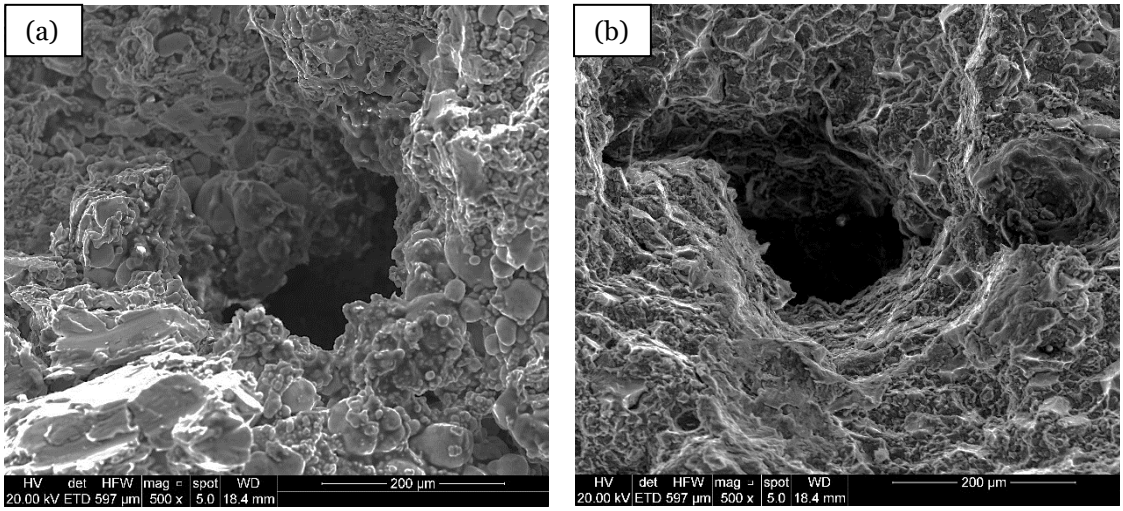

Figure 4.29: Two examples of porosities captured with secondary electrons from TBX cast number 5, left plate sample specimen.

The defect on the fracture surface in Figure 4.28 (a) was analyzed with back scattered electrons and with a chemical EDS analysis. The BSE image on where the analysis was conducted is in Figure 4.30 (a), and Figure 4.30 (b) shows the spectrum generated by the analysis.

This indicates a peak in oxygen content, with an oxygen percentage of 5.40 %, suggesting that the defect is an oxide bifilm.

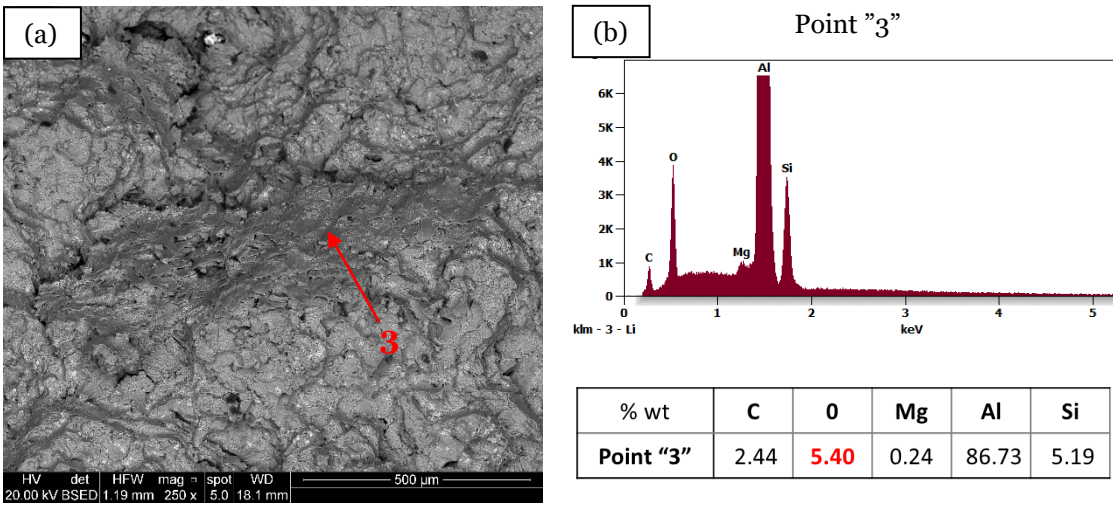

% wt	C	0	Mg	Al	Si
Point "3"	2.44	5.40	0.24	86.73	5.19

Figure 4.30: (a) BSE image of the defect in left plate sample, (b) EDS spectrum indicating a peak of oxigen content in weight.

The third sample analyzed comes from TAX cast number 1. The left plate sample is shown in Figure 4.31 (a) has two oxide bifilm in the surface and a tensile strength value of 232 MPa. The right plate sample, in Figure 4.31 (b), shown a porosity and an oxide bifilm which covers almost all the thickness, and a smaller tensile strength value than the left sample, of 208 MPa.

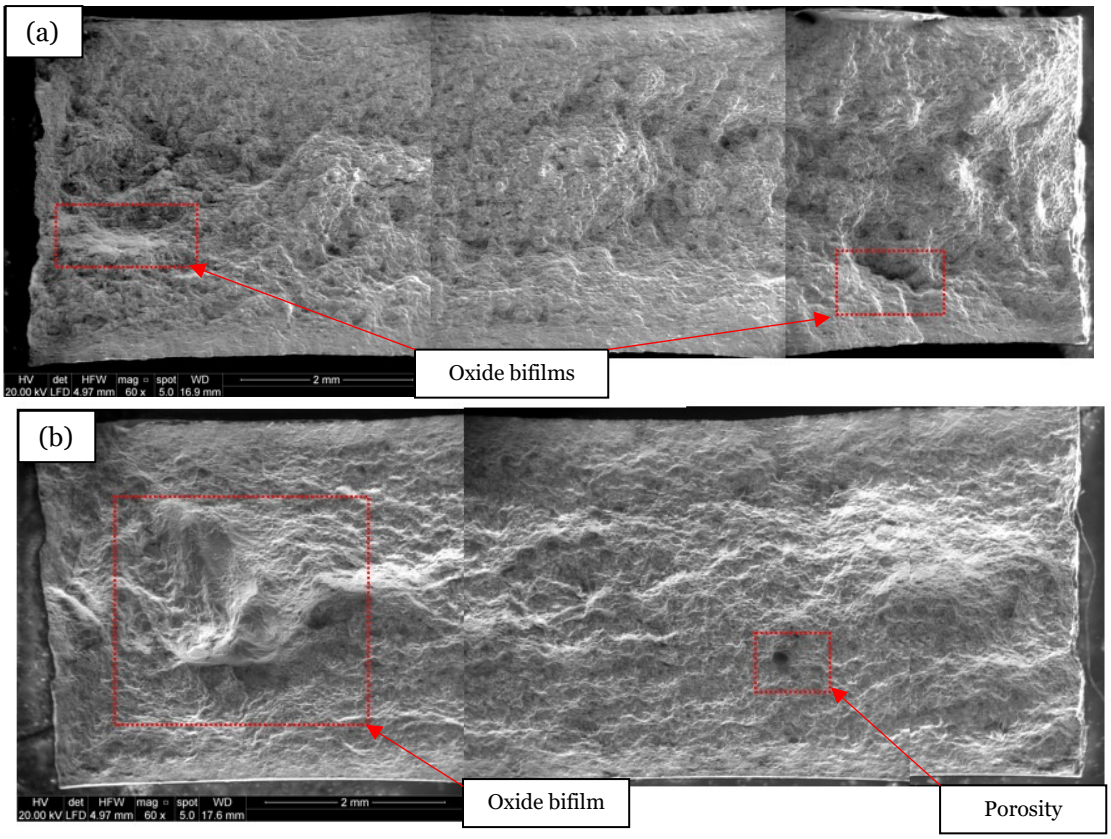

Figure 4.31: TAX (a) left plate sample (b) right plate sample, both with visual defects on the fracture surface.

The defect in right plate sample was studied in detail with the back scattered electrons, and an EDS analysis was conducted to see evidence of oxygen content (Figure 4.32). The spectrum in Figure 4.32 (c) had a peak in oxygen content, with an oxygen percentage of 3.41 %, confirming that the defect is an oxide bifilm.

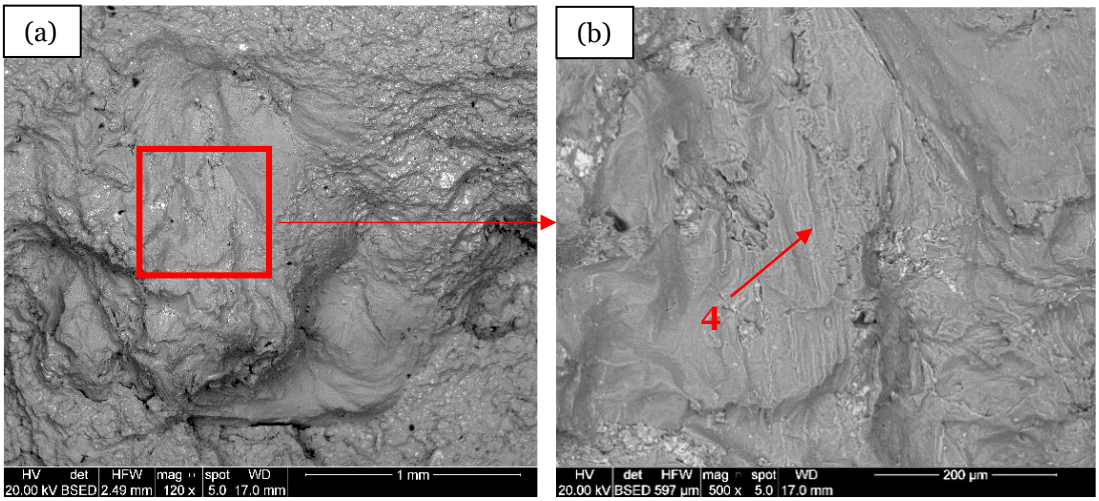

Point "4"

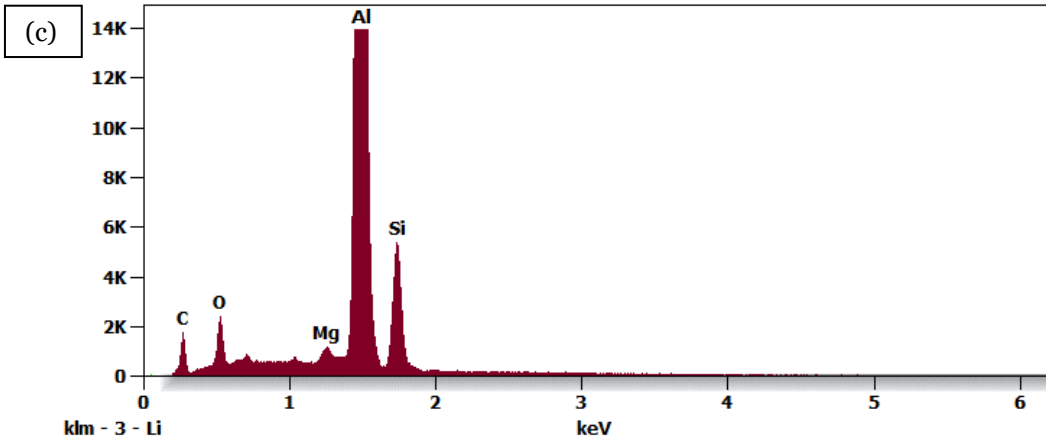

% wt	C	0	Mg	Al	Si
Point "4"	6.12	**3.41**	0.42	80.15	9.90

Figure 4.32: BSE images (a) at lower and (b) at higher magnification of the oxide bifilm. (c) EDS spectrum of the chemical analysis

4.4.4 X Ray image analysis

The X-Ray image analysis was used to verify the presence of porosities inside the cast that could have induced early fractures during the tensile tests, and therefore influenced the mechanical proprieties. The images taken for the analysis show all the four specimens from a cast, and the X-Ray beam highlights porosities or impurities, which appears as small white points inside the specimens.

A total of 32 casts were analysed with the x-ray beam, each containing all the four specimens of the cast. In the 128 total specimens, only 8 of them contained porosities. In this paragraph, are included the images of the four most representative castings which appeard to have defects inside.

The first image includes the specimens from HAY casting number 2, in Figure 4.33. The only specimen which appears to have porosities is the 2.1.2, but it was noted that the porosities were in the higher portion of the specimens, far from the surface fracture. This seems to have not influenced the mechanical proprieties of this sample, as the tensile strength is 234 MPa, versus 240 MPa obtained in the sample 2.1.1 coming from the same plate.

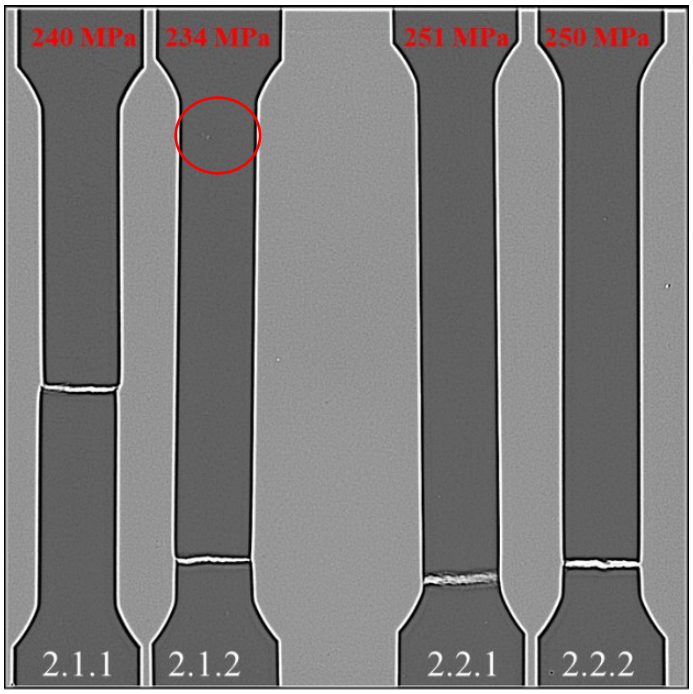

Figure 4.33: HAY2 casting (765 rpm, 120 bar, 2 m/s), with porosities found inside the specimen 2.1.2.

The second image show the specimens from HCZ casting number 4, in Figure 4.34. There are two specimens which appears to have porosities: 4.1.1 and 4.2.1. In the first specimen the porosities are near the fracture surface and seems to have negatively influenced the tensile strength, which is 211 MPa. The 4.2.1 specimen have porosities far from the fracture surface, which seems to not have influenced the mechanical proprieties, compared with the sample coming from the same plate.

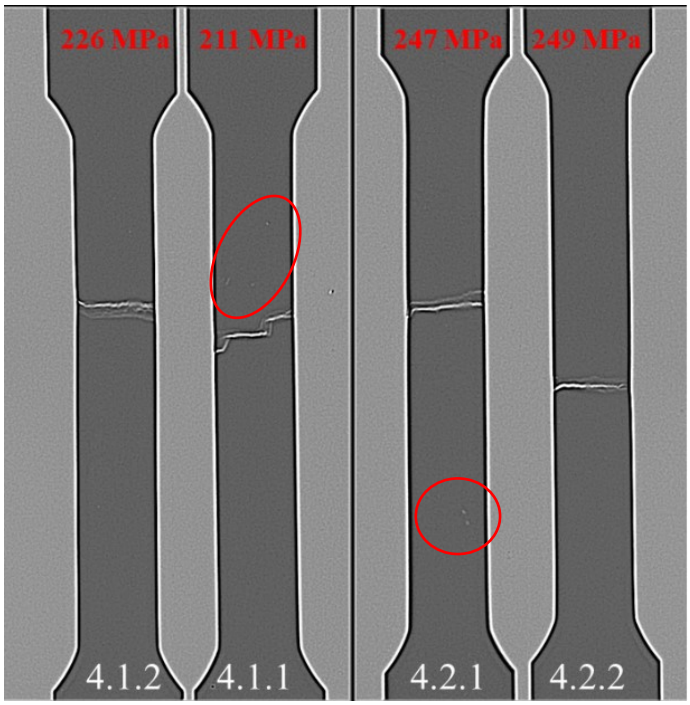

Figure 4.34: HCZ4 casting (1100 rpm, 180 bar, 2.5 m/s), with porosities in specimens 4.1.1 and 4.2.1.

The next image shows the specimens from TBX casting number 4, in Figure 4.35. Specimen 4.1.1 has some porosities near the fracture surface, but they seem not the principal cause of the difference in tensile strength from left to right plate, as the sample coming from the same plate (4.1.2) seems to not contain porosities.

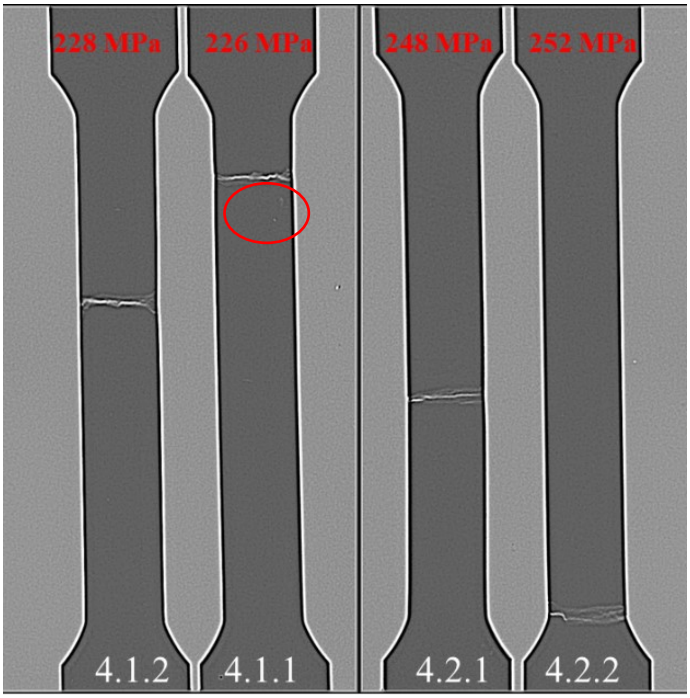

Figure 4.35: TBX4 casting (940 rpm, 150 bar, 2.5 m/s), with porosities in specimen 4.1.1.

The last image includes the specimens from TAX casting number 3, in Figure 4.36. Specimen 3.1.1 has some porosities far the fracture surface, in the upper part of the specimens. Its tensile strength was 228 MPa, and compared with sample 3.1.2, which has a tensile strength of 221 MPa, they seem to not have an influence on the mechanical proprieties of this sample.

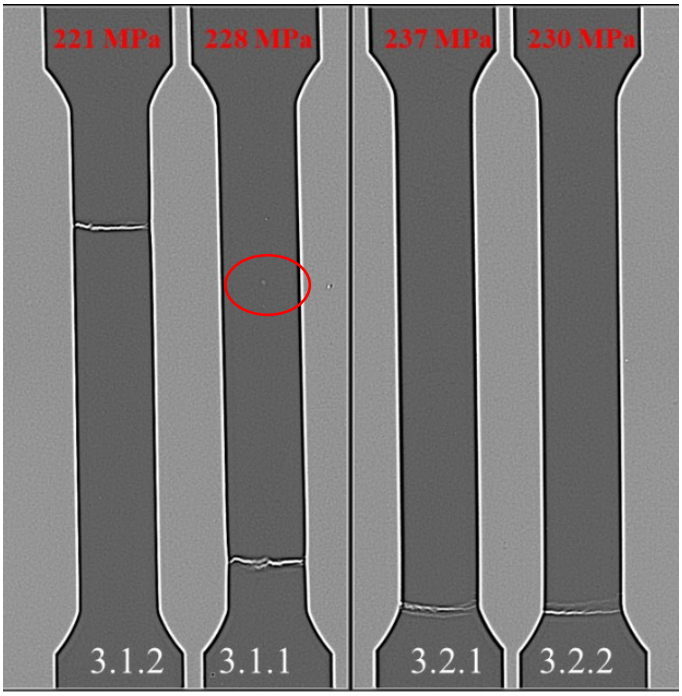

Figure 4.36: TAX3 casting (810 rpm, 150 bar, 2.5 m/s), with porosities in specimen 4.1.1.

4.5 Result discussions

4.5.1 Discussion of Method

The methodology used for this work started with the definition of the number of process parameter to change during casting and the number of cast parts to product and then evaluate. It was clear from the beginning that doing experimental design without any computer aided instrument was not possible, because there were several parameters and a vast range of values to choose in the mix.

Design Expert software was used to focus the attention on mix of settings that were interesting to assess in respect on the thesis purpose. The aim was to have a mix of very good but also a mix of potentially poor casting conditions to see big variety in the results. The variables to change and the range of variation was inserted in the software, which proposed a mix of settings. The procedure was iterated by the user until the output was believed to be good for the thesis purpose. The software gave in output 19 different casting conditions, divided in 10 for one cleaning method of the melt (holding) and 9 for the other (transportation). In every setting there were three changing variables, and with this method was possible to choose the range for every variable, in a way to have certain conditions with extreme values of each variable, in both low and high values.

The main weakness of this methodology was that the setting proposed were extremely precise in the amount of pressure and velocities supposed to be insert in the real machine. Although precision is good for experimental work, in the practical world is hard (or even not possible) to set the machines in high precision values, so most of the times the values proposed in the software was adapted to the real capabilities of machine and operators. For example, initially it was decided to evaluate a 3 m/s second phase speed, which could have been an interesting value in the mix. However, the high pressure die casting machine at disposal could not reach this value of speed, therefore the machine was setted with the highest value available: 2.5 m/s. The mix of settings which was used were respectful of the work's purpose, however the two advantages introduced by the software (precision of the values and high automation) was partially lost at the expense of the operators, which in most cases had to change and adapt the values manually.

The cast process was conducted following the process flowchart in Figure 3.1. It started with the material preparation from 70 % secondary ingots and 30 % reused scrap metal. The material preparation was successful: the check in the chemical composition done with a mass spectrometer confirmed that the alloy obtained was the 42000, which was the alloy chosen for the analysis.

The process was then articulated in the melt preparation (by doing two different routes with different cleaning procedures); the slurry making process; and the casting process.

The casting process turned out successful because the casted parts were completed on time and most of them presented no visive defects.

In some of the samples with a 1 m/s second phase speed there was a partial filling in the feedstock system, as showed in Figure 4.37. This didn't represent a problem because the feedstock was not meant to be used for examination in this work, and the plates itself presented no un-filled regions.

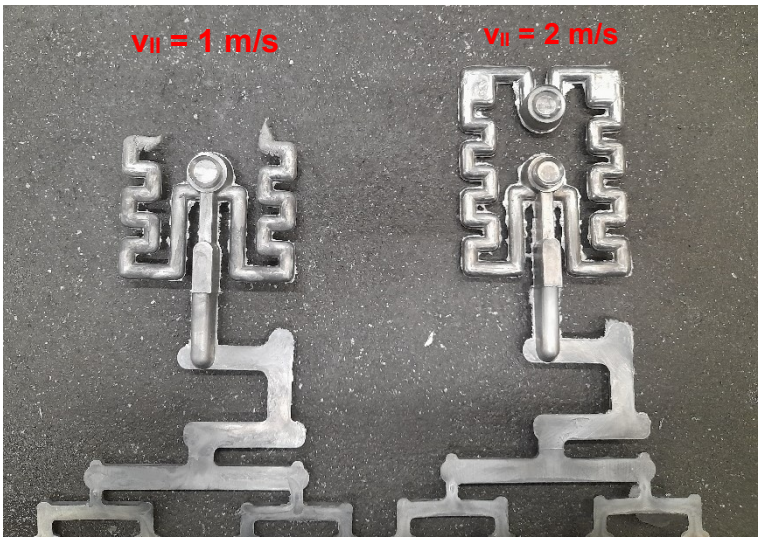

Figure 4.37: Missing feedstock system in a sample injected with 1 m/s (left) compared to a sample without filling defects and 2 m/s second phase speed (right).

The real downside of the casting process was discovered after the process. The cast part had two plates useful for experiments, where the tensile tests were cutted. The samples from the two different plates were distinguished from samples taken from left and from right plates. During the tensile tests it was clear that the specimens coming from the two different plates, which were supposed to be equal as the cast part is symmetric, had different mechanical proprieties. This caused to study separately the specimens coming from the left and from the right plates during the process parameter analysis and the correlation finding.

The method used for cutting the tensile tests was CNC cutting with an automated machine. This stage presented no problems, it was conducted and controlled by experienced personal, and the tensile bars obtained in the process were all respecting the dimensions and the tolerances imposed by the normative EN ISO 6892-1. The successful making of the specimens for the tensile tests were positive for the tensile tests itself. Also, the tensile tests were conducted successfully: there was no specimen that presented problems during the tensile test.

The calculation of aRMS was done with two different methods of evaluation, which ended up in similar results in the acceleration values, and most importantly in very similar correlation indexes. The only critical part of both methods of estimation was low variation in the results. For the method of Fiorese and Bonollo there were only three different accelerations, because the results only depended on the three different second phase speeds, the only variable in the settings (the first phase speed and the switching point where constants). The method of Jarfors was using the intensification pressure in the calculation, so more variation of data was achieved. The different values of stirring speed could not be taken in consideration, because both methods didn't depend on that variable.

Two variables included in both methods of estimation were: the first phase speed, and the position of the switching point between the first and the second phase of injection. In this work, these two values were always the same through the settings. An opportunity to add more variation in RMS acceleration values is to create parameter settings which variates the first phase speed and the switching point, rather than variate the stirring speed which is not included in the calculation.

4.5.2 Discussion of Findings

- Mechanical characterization and tensile test proprieties. How are the proprieties of the alloy through the changing parameter conditions?

As seen in Table 4.1 for holding cleaning and Table 4.2 for transportation cleaning, the 42000-aluminum alloy used for the work have stable Young modulus (average of 75 GPa for both holding and transportation cleaning) and stable values of yield strength (average of 115 MPa for holding and 116 MPa for transportation). Young modulus is a propriety not influenced by the change in process parameters, so it's correct that the values are stable trough the settings and in the two cleaning methods. The yield strength is mostly related to cooling conditions of the cast, which were constant for all the settings during the process. The stability of these two mechanical proprieties indicates that the tensile tests conducted were reliable and representative of the true condition of the alloy.

As suggested by the literature [10,11,12] the tensile strength and the fracture elongation changes when different parameter settings are used. This affirmation has been confirmed, as the value of tensile strength changes from 225 to 250 MPa and the elongation varies in a range from 3.5 to 6.5 % through the settings.

While doing the tensile tests, differences from left and right plates of casting has been noted. The young modulus and yield strength stays stable from left to right samples, but the values of tensile strength and elongation showed big variation (some settings were differing in 20 MPa for tensile strength and 2 % in elongation). The right plate specimens seem to have better mechanical proprieties than the specimens from left plate. The difference may be caused by the presence of defects inside the melt during the casting process: despite the symmetric mold (which should lead to symmetric fillings and therefore symmetric mechanical proprieties) there may be a concentration of melt impurities, oxides, porosities in the left plates which could be a reason of un-symmetric proprieties from left to right samples.

Looking at table 4.4 and 4.5 regarding the differences in the mechanical proprieties, it has been noted that the samples with higher second phase speed (2 and 2.5 m/s) tend to have the biggest differences from left to right plate samples. Higher speeds cause higher turbulence during the filling of the mold: this may have a relationship with the difference in defect concentration inside the casting plates.

- Two different estimations of aRMS. Which one leads to the best correlation with mechanical proprieties?

This study was conducted using two methods of estimation of the root-mean-square acceleration. The two methods, one proposed by the work of Fiorese [15] and the other proposed by Jarfors [17], calculates the same parameter but with two different basic principles. The method proposed by Fiorese calculates the root mean square acceleration from the times and the speeds involved in the HPDC process, effectively reconstructing a shot curve of the high pressure die casting process. The method proposed by Jarfors bases on a balance of pressures during the plunger motion in second phase of HPDC. Thus, the method includes the intensification pressure and the speeds involved in the casting process.

The two methods are very different in the basic principle, but in all the charts investigated in the correlation finding, the two methods seem to give similar results in all the conditions examined. The differences in terms of R-square values in the correlation charts are very limited.

- Different cleaning methods of the melt. Are there differences in the mechanical proprieties? Is there one method to prefer?

The two different cleaning method chosen for this work differs in the procedure, as one is done while transporting the melt from the shaft furnace to the holding furnace (Transportation method) and the other cleans the aluminum melt directly into the holding furnace after the transportation of the molten metal (Holding method). Despite this difference, the two procedures share the same degassing procedure, so the expected difference in mechanical proprieties was little.

To characterize the difference in mechanical proprieties caused by the different cleaning method, three distinct settings was chosen for each cleaning method, one with high values of process parameters, one with low values and one intermediate. The compared settings had similar values of stirring speed, intensification pressure and second phase speeds, so that the cleaning method was the only real variable in this investigation.

In terms of fracture elongation, there seems to be a difference in proprieties in favor of holding cleaning samples. The elongation difference is around 0.5 % in advantage of holding samples in most of the settings taken in consideration, with a variation that goes from 1.0 % to one case with no difference in elongation values.

The most relevant difference between the two methods were noted during the correlation finding with the root mean square acceleration: the correlation indexes are constantly higher in the holding cleaning samples. This may indicate that the quality of the casting achieved with holding cleaning method is higher, therefore this method should be preferred to use in further investigations with the same purpose.

- Investigation in the process parameters. Which influence the most the mechanical proprieties? Are there optimal casting conditions to achieve better static proprieties?

There are several process parameters involved in a high pressure die cast that influences the material proprieties and the quality of the casting. In this study was chosen to variate the stirring speed of the slurry making process, the second phase speed of injection and the intensification pressure of the third phase of injection. Moreover, two different procedures of melt cleaning were used.

To see the influence in mechanical proprieties, every parameter was compared with the fracture elongation obtained in each setting, with dispersion charts.

The stirring speed doesn't seem to have a big influence the mechanical proprieties, as suggested by the charts in Figure 4.1 and Figure 4.2: the trend lines appear flat when the speed is increased.

The trends of intensification pressure and second phase speed are more defined, and generally higher pressure and injection speeds results in better fracture elongation of the alloy, as shown in Figure 4.3, 4.4, 4.5 and 4.6. This confirms the results discussed in previous works [11, 12], which were pointing out an increase in mechanical proprieties for higher intensification pressures and higher second phase speeds.

The second phase speed is critical to successful fill the mold, as discussed in the method in reference to Figure 4.21: some samples with 1 m/s speed were found with the missing feedstock system (the last part in the cast, which is used as a terminal section to discard). The second phase speed appears to be the parameter which influences the most the mechanical performances: the trend lines presented in the dispersion charts (Figure 4.7 and 4.8) have the highest slope compared to the charts which investigated the stirring speed and the intensification pressure. Also, the higher values of correlation indexes with fracture elongation seems to confirm this assertion.

The proposed optimal casting condition are a mix of high intensification pressure, second phase speed. The influence of stirring speed appears to be uncertain to the mechanical proprieties of the shot settings.

- Correlation finding. Process parameters and mechanical proprieties have a 1:1 correlation? Could the correlation indexes be improved?

The correlation finding was the final and the most important investigation conducted in this study. The correlations charts were constructed comparing three distinct mechanical proprieties with the root mean square acceleration.

The correlation charts are dispersion type, and for each was considered the R square value (note as the correlation index) and the trend of the fitting line. Fiorese compared RMS acceleration with yield strength and tensile strength, while this work investigated fracture elongation, hardening rate index, and fracture energy: despite different mechanical proprieties used for the evaluations, similar results was achieved [15]. The highest values of correlation indexes were reached in holding cleaning samples, especially the samples taken from the right plates: the correlation indexes in this specific case reached 0.88 (for fracture elongation chart), and 0.87 (for fracture energy and hardening rate index charts). The left plates showed poor correlation with aRMS, as the correlation indexes were close to zero in most cases. In all charts from holding, the trend line presented better values of mechanical proprieties with the increasing root mean square acceleration; this result matches what has been suggested in the work of Fiorese [15,16].

As regards transportation cleaning, the correlation indexes appeared to be lower compared to what achieved with holding cleaning method. The samples coming from right plates showed a R-square value of 0.64 (for fracture elongation chart), 0.72 (for hardening rate index chart), and 0.61 (for fracture energy chart). Although the indexes are lower than holding, the trend is still indicating higher proprieties as RMS acceleration grows.

As regards the samples coming from left plate, the correlation indexes are close to zero in most cases, which suggest poor correlation with RMS acceleration. Also, the trend lines in the charts do not follow what suggested by Fiorese, who pointed out that higher root mean square accelerations means higher static mechanical proprieties [15]: in the samples from left plates the fitting lines are showing the opposite trend.

To sum up, the closest case to a 1:1 correlation is represented by holding samples from the specimens taken from the right plate of the cast. The samples from the left plates are decreasing the average values of correlation indexes: this could mean that the quality of the casted parts influences the value of correlations. The calculations for the root-mean-square-acceleration, in fact, doesn't consider the presence of defects in the cast, so the RMS acceleration value stays the same from left to right plate specimens, even if there are possible defects that can contributes to decrease the mechanical proprieties. This could be the reason why left plate specimens (suspected to have more defects for the lower mechanical proprieties, in comparison with samples from the right plates) have poor correlations with RMS acceleration.

- Investigations on the microstructure of the alloy. Does the microstructure changes through the parameter settings? Are there defects inside the cast that could explain the reason of left and right difference in mechanical proprieties?

In the samples chosen for the analysis the microstructure didn't appear to change despite the different process settings used and two different cleaning method. The solid fraction analysis is suggesting that there is a small decrease in solid fraction quantity when the stirring speed is increased, but this doesn't seem to influence the mechanical proprieties of the alloy. The fracture surface and x-ray image analysis suggested that one reason of the differences between the left and right plaque samples are due to defects within the castings. The defects were most frequently founded inside the left plate samples, and they porosities; inclusions of undesired elements such as sulfur, molybdenum, and copper; and oxide bifilms. These defects could have led to early fractures in the left plate samples, explaining why these samples had differences with right plate samples. However, not in all the samples were found evident defects despite the difference in proprieties, so the presence of defects could not be the only reason to the encountered difference.

5 Conclusions and future work

5.1 Conclusions

The results from this work can be concluded with the following main points:

- The results from the tensile tests appeared to be representative of the mechanical proprieties of the alloy through the different settings studied: the values of Young modulus and Yield strength are stable in all conditions, as it was expected. The results from the tensile tests highlighted a difference in mechanical characterization between the samples coming from the two different plates of the cast.
- The dispersion charts studied to verify the influence of the process settings in fracture elongation are suggesting that the best combination to achieve higher mechanical proprieties and higher values of root-mean-square acceleration are high intensification pressure and high second phase speed. The value of stirring speed of the Enthalpy Exchange Material seems to not have a big influence in the studied conditions.
- The two different cleaning methods used in the casting process seems to give similar mechanical proprieties with a gap in terms of fracture elongation of 0.5 % in favor of holding cleaning procedure. There seems to be more difference with the correlation with RMS acceleration, as holding samples showed better correlation indexes in all the conditions examined.
- The correlation charts indicate an increase in static mechanical proprieties when higher values of root-mean-square accelerations are used in a high pressure die casting process. The correlation indexes, if all the samples are taken in consideration, don't reach the 1:1 correlation as wished by the research purpose, however in the samples taken from the right plates for holding cleaning method the correlation index reaches a value of 0.87 in comparison with all the three mechanical proprieties examined: fracture elongation, fracture energy and hardening rate index.
- Analysis of the fracture surfaces suggested that part of the differences between the left and right plaque samples are due to defects within the castings: in almost all the fracture surfaces of the left samples chosen for the analysis were found porosities, inclusions, and oxide films. These defects generate local stress intensification leading to early fractures, and thus negatively affect the mechanical properties of the samples from the left plates.

5.2 Future work

What has been achieved still has room for improvements. For future works, some suggestions are summarized below:

- A possible way to improve the correlation, would be to include in the RMS acceleration values some coefficient to count the quality of the castings: the high number of defects inside a tensile test specimen affect its mechanical proprieties, but the value of RMS acceleration stays the same to a specimen with less defects and higher mechanical proprieties (with the same process parameter conditions). To do this, the quality of the castings should be first assessed, and then some coefficients shall be applied when the RMS acceleration is determined.
- The defects founded inside the cast are part of the reason of the big difference in mechanical proprieties between left and right samples. To explain better the cause of the differences, an investigation in the injection system of the HPDC machine could be conducted, to assess if there are filling asymmetries that could induce to uneven filling in the two plates.

6 References

[1] Asm International Handbook Committee, "Proprieties and selection: Nonferrous alloys and special-purpose materials", ASM Metals Handbook, 2017, vol. 2.

[2] John Gilbert Kaufman, Elwin L. Rooy "Aluminum Alloy Castings: Properties, Processes, and Applications", ASM International, December 2004.

[3] Asm International Handbook Committee, "Casting", ASM Metals Handbook, 2017, vol. 15.

[4] Asm International Handbook Committee, "Aluminum Casting Alloys and Casting Processes" ASM Metals Handbook, 2018, vol. 2A.

[5] Bonollo F, Gramegna N, Timelli G, "High-pressure die-casting: contradictions and challenges" JOM 67(5):901–908, 2015.

[6] Z.Fan, "Semisolid metal processing", International Materials Reviews, 18 Jul 2013.

[7] G. Timelli, F. Bonollo, "Quality mapping of aluminium alloy die-castings", Metallurgical Science and Technology Vol. 26-1 - Ed. 2008.

[8] P. Alena, B. Marianna, B. Dana (2013), "Quality control in foundry - Analysis of casting defects", Business, Materials Science.

[9] S. Janudom, J. Wannasin, J. Basem, S. Wisutmethangoon, "Characterization of flow behavior of semi-solid slurries containing low solid fractions in high-pressure die casting.", Acta Materialia 61 (2013) 6267–6275.

[10] S. W. Choi, Y. C. Kim, J. I. Cho & C. S. Kang (2008), "Influence of die casting process parameters on castability and properties of thin-walled aluminium housings", International Journal of Cast Metals Research, 21:1-4, 330-333.

[11] L. Arnberg, G. Timelli, E. Fiorese, F. Bonollo, A. Adamane, "Influence of Injection Parameters on the Porosity and Tensile Properties of High-Pressure Die Cast Al-Si Alloys: A Review", International Journal of Metalcasting, Volume 9, Issue 1, March 2015.

[12] Karban, R., "The Effects of Intensification Pressure, Gate Velocity, and Intermediate Shot Velocity on the Internal Quality of Aluminum Die Castings", PhD thesis, Purdue University, West Lafayette, IN, USA (2000).

[13] Afsaridis Kimon, "Investigation of residual stresses generation in aluminium flywheel", Tekniska Högskolan I Jönköping, June 2010.

[14] Hans J. Thamhain (2014), "Assessing the Effectiveness of Quantitative and Qualitative Methods for R&D Project Proposal Evaluations", Engineering Management Journal, 26:3, 3-12, DOI: 10.1080/10429247.2014.11432015

[15] E. Fiorese, D. Richiedei, F. Bonollo, "Improving the quality of die castings through optimal plunger motion planning: analytical computation and experimental validation", Int J Adv Manuf Technol (2017) 88:1475–1484.

[16] E. Fiorese, F. Bonollo, "Simultaneous Effect of Plunger Motion Profile, Pressure, and Temperature on the Quality of High-Pressure Die-Cast Aluminum Alloys", The Minerals, Metals & Materials Society and ASM International 2016, VOLUME 47A, DECEMBER 2016—6453.

[17] A. E. W. Jarfors, A. Du, J. Zhou, J. Zheng, G. Yu, "On the In-Die Conditions and Process Parameter Settings in Indirect Squeeze Casting", Technologies 2022, 10, 29. https://doi.org/10.3390/technologies10010029

[18] Fiorese E, Bonollo F, Timelli G, Arnberg L, Gariboldi E, "New classification of defects and imperfections for aluminum alloy castings", Int J Met 9(1):55–66, 2015.

[19] M. Sahoo, S. Sahu, "Principles of Metal Casting", Third Edition, Mc Graw-Hill Education, 2014.

[20] F. Bonollo, "Transformation processes for Aluminum Alloys", Metallurgical industrial applications, 4 May 2020.

[21] E. Felix, "Marketing Challenges of Satisfying Consumers Changing Expectations and Preferences in a Competitive Market", October 2015, International Journal of Marketing Studies, DOI: 10.5539/ijms.v7n5p41.

[22] Zamora R, Faura F, López J, Hernández J (2007), "Experimental verification of numerical predictions for the optimum plunger speed in the slow stage of a high-pressure die casting machine.", Int J Adv Manuf Technol 33(3-4):266–276.

[23] Nikroo AJ, Akhlaghi M, Najafabadi MA (2009) "Simulation and analysis of flow in the injection chamber of die casting machine during the slow shot stage.", Int J Adv Manuf Technol 41(1-2): 31–41.

[24] Jian, X., Wu, G., "An Experimental Investigation on the Flow Behavior of Liquid Aluminium Inside Pressure Die-casting Dies Using High-Speed Photography," SPIE Proceedings, vol. 1358, 19th International Congress on High-Speed Photography and Photonics, pp. 1237-1244 (1990).

[25] S. Kalpakjian; S. R. Schmidt, "Tecnologia Meccanica", Pearson, 2nd edition, ISBN-13: 978-8865183748

[26] D. B. Spencer: PhD thesis, MIT, Cambridge, MA, 1971.

[27] Asm International Handbook Committee, "Semisolid metal casting", ASM Metals Handbook, 2018, vol. 2A.

[28] M. S. Salleh, M. Z. Omar, J. Syarif, and M. N. Mohammed, "An Overview of Semisolid Processing of Aluminium Alloys" Department of Mechanical and Materials Engineering, Faculty of Engineering and Built Environment, Universiti Kebangsaan Malaysia, 19 December 2012.

[29] E. Bernardo, L. Biasetto, G. Scarinci, "Introduction to Polymeric Materials, Proprieties and Structure", Department of Management and Engineering (Vicenza), September 2019.

[30] Anders EW Jarfors, "Semisolid Casting of Metallic Parts and Structures", Jönköping University, Jönköping, Sweden, 2022 Elsevier Inc.

[31] Magnus Wessén and Haiping Cao, "The RSF Technology – A possible breakthrough for semi-solid casting processes", Jönköping University, Div Component Technology.

[32] J. Wannasin, M. Fuchs, J. Lee, C. Lee, N. Rao, M. C. Flemings, "GISS Technology: Principle and Applications in Die Casting", Massachusetts Institute of Technology, Cambridge, MA, USA.

[33] A. E. W. Jarfors, J. Zheng, L. Chen, J. Yang, "Recent advances in commercial application of the rheometal process in china and europe", Jönköping University, School of Engineering, Department of Materials and Manufacturing, Jönköping, Sweden.

[34] M. Reisi, B. Niroumand, "Effects of stirring parameters on rheocast structure of Al–7.1wt.%Si alloy", Journal of Alloys and Compounds 470 (2009) 413–419.

[35] R. Gupta, A. Sharma, U. Pandel, L. Ratke, "Effect of stirring speed on microstructure of A356 alloy cast through rheometal process", Department of Metallurgical and Materials Engineering, Malaviya National Inst. Of Technology, Jaipur-302017, India.

[36] M. Saeedipour, S. Schneiderbauer, S. Pirker, "A Numerical and Experimental Study of Flow Behavior in High Pressure Die Casting", TMS (The Minerals, Metals & Materials Society), January 2014.

7 Appendices

Complete results from the tensile tests:

HOLDING							
Cast code	Stirring speed [rpm]	vII [m/s]	Ip [bar]	**Young Modulus [GPa]**	**Yield Strenght [MPa]**	**Tensile Strenght [MPa]**	**Elongation at fracture [%]**
HAX	765	2,5	160	75 ± 1	116 ± 2	244 ± 10	5,6 ± 1,1
HAY	765	2	120	75 ± 1	117 ± 1	243 ± 9	4,8 ± 1,0
HAZ	765	1	150	75 ± 2	116 ± 2	235 ± 7	4,5 ± 0,7
HAU	765	2	130	75 ± 1	117 ± 2	246 ± 8	5,2 ± 1,0
HBX	650	2,5	145	76 ± 2	114 ± 2	244 ± 5	5,8 ± 0,6
HBY	650	1	120	75 ± 1	114 ± 1	236 ± 6	4,4 ± 0,6
HBZ	650	2	184	75 ± 1	116 ± 2	231 ± 14	4,4 ± 1,6
HCX	1100	1	150	76 ± 2	115 ± 3	236 ± 9	4,4 ± 0,7
HCY	1100	2	120	74 ± 1	114 ± 2	236 ± 17	4,6 ± 1,4
HCZ	1100	2,5	180	74 ± 2	115 ± 3	239 ± 12	5,4 ± 1,4

Table 7.1 Complete data from tensile test results for holding cleaning method.

TRANSPORTATION							
Cast code	Stirring speed [rpm]	vII [m/s]	Ip [bar]	**Young Modulus [GPa]**	**Yield Strenght [MPa]**	**Tensile Strenght [MPa]**	**Elongation at fracture [%]**
TAX	810	2	180	75 ± 2	116 ± 2	238 ± 12	5,6 ± 1,1
TAY	810	1	180	76 ± 2	113 ± 3	229 ± 10	4,8 ± 1,0
TBX	940	2.5	150	75 ± 1	118 ± 2	240 ± 10	5,1 ± 1,2
TCX	1100	1	120	75 ± 1	117 ± 2	238 ± 8	4,1 ± 0,8
TCY	1100	2	180	75 ± 1	116 ± 2	244 ± 5	5,3 ± 0,7
TDX	650	2	150	75 ± 1	118 ± 2	245 ± 4	5,2 ± 0,7
TDY	650	2.5	180	75 ± 1	116 ± 2	228 ± 13	4,0 ± 1,4
TDZ	650	2.5	120	75 ± 1	114 ± 2	231 ± 12	4,2 ± 1,1
TDU	650	1	150	76 ± 1	117 ± 2	230 ± 12	3,8 ± 0,8

Table 7.2: Complete data from tensile test results for transportation cleaning method.

Differences between left and right plates: hardening rate index and fracture energy (Holding and Transportation).

Holding	Hardening rate index [MPa]			Fracture energy [MJ/m^3]		
	ALL	LEFT	RIGHT	ALL	LEFT	RIGHT
HAX	24	24	23	1007	1008	1032
HAY	28	31	25	858	729	1007
HAZ	28	28	27	790	778	805
HAU	26	29	24	939	811	1070
HBX	23	23	23	1043	1016	1076
HBY	29	30	29	761	725	798
HBZ	27	36	23	770	507	1050
HCX	29	29	29	770	803	729
HCY	28	30	26	800	713	912
HCZ	24	26	22	960	828	1096

Table 7.3: Difference between specimens from left and right plates in hardening rate index and fracture energy (Holding).

Transp.	Hardening rate index [MPa]			Fracture energy [MJ/m^3]		
	ALL	LEFT	RIGHT	ALL	LEFT	RIGHT
TAX	27	32	24	823	687	996
TAY	29	29	28	728	712	748
TBX	25	29	22	909	725	1148
TCX	31	32	30	733	697	775
TCY	25	26	24	955	907	998
TDU	31	30	32	665	701	621
TDX	26	26	26	935	915	955
TDY	29	34	25	695	553	879
TDZ	29	32	26	731	609	857

Table 7.4: Difference between specimens from left and right plates in hardening rate index and fracture energy (Transportation).

Root mean square calculation datas, Fiorese-Bonollo-Richiedei method.

Cast code	First phase speed [m/s]	Second phase speed [m/s]	Plunger travel [mm]	Switching point [mm]	T1 [s]	T2 [s]	**$aRMS_{Fiorese}$ [m/s²]**
HAX	0,35	2,5	430	360	1,03	0,05	**96,5**
HAY	0,35	2	435	360	1,03	0,07	**56,1**
HAZ	0,35	1	445	360	1,03	0,14	**10,2**
HAU	0,35	2	435	360	1,03	0,07	**56,1**
HBX	0,35	2,5	430	360	1,03	0,05	**96,5**
HBY	0,35	1	445	360	1,03	0,14	**10,2**
HBZ	0,35	2	435	360	1,03	0,07	**56,1**
HCX	0,35	1	445	360	1,03	0,14	**10,2**
HCY	0,35	2	435	360	1,03	0,07	**56,1**
HCZ	0,35	2,5	430	360	1,03	0,05	**96,5**

Table 7.5: Complete data for RMS acceleration estimations, Fiorese method, holding.

Cast code	First phase speed [m/s]	Second phase speed [m/s]	Plunger travel [mm]	Switching point [mm]	T1 [s]	T2 [s]	**$aRMS_{Fiorese}$ [m/s^2]**
TAX	0,35	2	435	360	1,03	0,07	**56,1**
TAY	0,35	1	445	360	1,03	0,14	**10,2**
TBX	0,35	2,5	430	360	1,03	0,05	**96,5**
TCX	0,35	1	445	360	1,03	0,14	**10,2**
TCY	0,35	2	435	360	1,03	0,07	**56,1**
TDU	0,35	1	445	360	1,03	0,14	**10,2**
TDX	0,35	2	435	360	1,03	0,07	**56,1**
TDY	0,35	2,5	430	360	1,03	0,05	**96,5**
TDZ	0,35	2,5	430	360	1,03	0,05	**96,5**

Table 7.6: Complete data for RMS acceleration estimations, Fiorese method, transportation.

Root mean square calculation datas, Jarfors et al. method.

Cast code	First phase speed [m/s]	Second phase speed [m/s]	Plunger travel [mm]	Switching point [mm]	Ip [bar]	$M_{melt+plunger}$ [Kg]	**$aRMS_{Jarfors}$ [m/s^2]**
HAX	0,35	2,5	430	360	160	17,95	**106,0**
HAY	0,35	2	435	360	120	17,95	**61,2**
HAZ	0,35	1	445	360	150	17,95	**10,9**
HAU	0,35	2	435	360	130	17,95	**58,8**
HBX	0,35	2,5	430	360	145	17,95	**111,4**
HBY	0,35	1	445	360	120	17,95	**12,2**
HBZ	0,35	2	435	360	184	17,95	**49,4**
HCX	0,35	1	445	360	150	17,95	**10,9**
HCY	0,35	2	435	360	120	17,95	**61,2**
HCZ	0,35	2,5	430	360	180	17,95	**100,0**

Table 7.7: Complete data for RMS acceleration estimations, Jarfors method, holding.

Cast code	First phase speed [m/s]	Second phase speed [m/s]	Plunger travel [mm]	Switching point [mm]	Ip [bar]	$M_{melt+plunger}$ [Kg]	**$aRMS_{Fiorese}$ [m/s^2]**
TAX	0,35	2	435	360	180	17,95	**50,0**
TAY	0,35	1	445	360	180	17,95	**10,0**
TBX	0,35	2,5	430	360	150	17,95	**109,5**
TCX	0,35	1	445	360	120	17,95	**12,2**
TCY	0,35	2	435	360	180	17,95	**50,0**
TDU	0,35	1	445	360	150	17,95	**10,9**
TDX	0,35	2	435	360	150	17,95	**54,7**
TDY	0,35	2,5	430	360	180	17,95	**100,0**
TDZ	0,35	2,5	430	360	180	17,95	**122,4**

Table 7.8: Complete data for RMS acceleration estimations, Jarfors method, transportation.

Correlation charts data: fracture elongation vs RMS acceleration.

	ALL PLATES	LEFT PLATES	RIGHT PLATES		
Holding	**Elf [%]**	**Elf [%]**	**Elf [%]**	**$aRMS_{Fiorese}$ [m/s^2]**	**$aRMS_{Jarfors}$ [m/s^2]**
HAX	5,6	5,6	5,7	96,5	105,4
HAY	4,8	4,1	5,5	56,1	60,9
HAZ	4,5	4,4	4,6	10,2	10,9
HAU	5,2	4,5	5,8	56,1	58,5
HBX	5,8	5,7	6,0	96,5	110,7
HBY	4,4	4,2	4,5	10,2	12,2
HBZ	4,4	3,0	5,8	56,1	49,1
HCX	4,4	4,5	4,2	10,2	10,9
HCY	4,6	4,1	5,1	56,1	60,9
HCZ	5,4	4,7	6,1	96,5	99,4
	ALL PLATES	LEFT PLATES	RIGHT PLATES		
Transportation	**Elf [%]**	**Elf [%]**	**Elf [%]**	**$aRMS_{Fiorese}$ [m/s^2]**	**$aRMS_{Jarfors}$ [m/s^2]**
TAX	4,6	3,9	5,6	56,1	49,7
TAY	4,3	4,2	4,4	10,2	9,9
TBX	5,1	4,1	6,2	96,5	108,9
TCX	4,1	3,9	4,3	10,2	12,2
TCY	5,3	5,0	5,5	56,1	49,7
TDU	3,8	4,0	3,6	10,2	10,9
TDX	5,2	5,1	5,2	56,1	54,4
TDY	4,0	3,3	5,0	96,5	99,4
TDZ	4,2	3,6	4,9	96,5	121,7

Table 7.9: Data inserted in the dispertion charts of fracture elongation vs. RMS acceleration.

Correlation charts data: hardening rate index vs RMS acceleration.

	ALL PLATES	LEFT PLATES	RIGHT PLATES		
Holding	**Δσ/Δε [MPa]**	**Δσ/Δε [MPa]**	**Δσ/Δε [MPa]**	**$aRMS_{Fiorese}$ [m/s^2]**	**$aRMS_{Jarfors}$ [m/s^2]**
HAX	24	24	23	96,5	105,4
HAY	28	31	25	56,1	60,9
HAZ	28	28	27	10,2	10,9
HAU	26	29	24	56,1	58,5
HBX	23	23	23	96,5	110,7
HBY	29	30	29	10,2	12,2
HBZ	27	36	23	56,1	49,1
HCX	29	29	29	10,2	10,9
HCY	28	30	26	56,1	60,9
HCZ	24	26	22	96,5	99,4
	ALL PLATES	LEFT PLATES	RIGHT PLATES		
Transportation	**Δσ/Δε [MPa]**	**Δσ/Δε [MPa]**	**Δσ/Δε [MPa]**	**$aRMS_{Fiorese}$ [m/s^2]**	**$aRMS_{Jarfors}$ [m/s^2]**
TAX	27	32	24	56,1	49,7
TAY	29	29	28	10,2	9,9
TBX	25	29	22	96,5	108,9
TCX	31	32	30	10,2	12,2
TCY	25	26	24	56,1	49,7
TDU	31	30	32	10,2	10,9
TDX	26	26	26	56,1	54,4
TDY	29	34	25	96,5	99,4
TDZ	29	32	26	96,5	121,7

Table 7.10: Data inserted in the dispertion charts of hardening rate index vs. RMS acceleration.

Correlation charts data: fracture energy vs RMS acceleration.

	ALL PLATES	LEFT PLATES	RIGHT PLATES		
Holding	**Ψ [MJ/m3]**	**Ψ [MJ/m3]**	**Ψ [MJ/m3]**	**$aRMS_{Fiorese}$ [m/s^2]**	**$aRMS_{Jarfors}$ [m/s^2]**
HAX	1007	1008	1032	96,5	105,4
HAY	858	729	1006	56,1	60,9
HAZ	790	778	805	10,2	10,9
HAU	939	811	1070	56,1	58,5
HBX	1043	1016	1076	96,5	110,7
HBY	761	724	798	10,2	12,2
HBZ	770	507	1050	56,1	49,1
HCX	770	803	729	10,2	10,9
HCY	800	713	912	56,1	60,9
HCZ	960	828	1096	96,5	99,4
	ALL PLATES	LEFT PLATES	RIGHT PLATES		
Transportation	**Ψ [MJ/m3]**	**Ψ [MJ/m3]**	**Ψ [MJ/m3]**	**$aRMS_{Fiorese}$ [m/s^2]**	**$aRMS_{Jarfors}$ [m/s^2]**
TAX	823	687	996	56,1	49,7
TAY	728	712	748	10,2	9,9
TBX	909	725	1148	96,5	108,9
TCX	733	697	775	10,2	12,2
TCY	955	907	998	56,1	49,7
TDU	665	701	621	10,2	10,9
TDX	935	915	955	56,1	54,4
TDY	695	553	879	96,5	99,4
TDZ	731	609	857	96,5	121,7

Table 7.11: Data inserted in the dispertion charts of fracture energy vs. RMS acceleration.